BEHAVIOR OF SEVERAL AMPHIPHILIC COPOLYMERS AT THE AIR-WATER INTERFACE

By

SOPHIE BERNARD

A DISSERTATION PRESENTED TO THE GRADUATE SCHOOL
OF THE UNIVERSITY OF FLORIDA IN PARTIAL FULFILLMENT
OF THE REQUIREMENTS FOR THE DEGREE OF
DOCTOR OF PHILOSOPHY

UNIVERSITY OF FLORIDA

2007

To my parents Françoise and Guy and my brothers Romain and Mathieu

for their constant love and support

ACKNOWLEDGMENTS

I would first and foremost like to thank my advisor Dr Randolph S. Duran for making this experience possible. Throughout my entire PhD, he has been supporting in the good and bad times and I could not be more thankful. His presence and advices made my stay at the University of Florida, an experience I will never forget.

I also like to give a special thanks to Dr John Reynolds and Dr Ken Wagener. Without their support and their caring attention, they made my experience on the polymer floor really enjoyable. I would also like to show appreciation to the rest of my committee members, Dr Daniel Talham, Dr Valeria Kleiman, Dr Eric Enholm, and Dr Richard B. Dickinson. Their constructive criticism and their trust in me did not go unnoticed, and for that I could not be more grateful.

A special thank you goes to Denise Sharbaugh for all her precious help and patience.

There are a lot of past and present members of the polymer floor that made my work environment so enjoyable and I will never forget all those times inside and outside the lab. So for that thank you Florence Courchay, Merve Ertas, Piotr Matloka, Aubrey Dyer, Emilie Galand, Tim Steckler, and Genay Jones.

None of that could have been possible without the support of the entire Duran's group, Jorge Chàvez, Henk Keiser, Brian Dorvel, Danyell Wilson, Dr Martin Andersson, Dr Maria Stjerndahl, Dr. Firouzeh Sabri, Eric Greeley, Kristina Denoncourt and Aleksa Jovanović. A special thank goes to Dr Thomas Joncheray and Dr Jennifer Logan for all their support and constructive conversations during my whole PhD.

Some people were always here in good and bad times. Thank you Vicky for those wonderful five years that you definitely made interesting. Thanks to.Jordan, Neil, Eric and Brent for all those times spent at number 23. Thank you to Jamie, Austin and Kristen for all those late

Friday nights. I would also like to acknowledge my classmates, Lisa, Richard and Lindsay for going through those five years with me. Special thanks goes to Roxy, David, Nicolas and Ashlee for being the best support a person could ask for during the writing process. Everyone made my life as a graduate student so much easier and I will never forget all those times spent at GC. I love them all and will miss them immensely.

Finally, probably the most important, I want to thank my parents Françoise and Guy as well as my brothers Romain and Mathieu, who without even being aware of it, have made this experience possible. Their love and support was the constant in my life that kept me going and got me through some rough times.

TABLE OF CONTENTS

page

LIST OF TABLES

LIST OF FIGURES

LIST OF ACRONYMS

AFM	Atomic Force Microscopy
TEM	Transmission Electron Microscopy
STM	Scanning Tunneling Microscopy
BAM	Brewster Angle Microscopy
ATRP	Atom Transfer Radical Polymerization
RAFT	Reversible Addition Fragmentation Chain transfer
TR	Transfer Ratio
LB	Langmuir Blodgett
LC	Liquid Crystalline
CMC	Critical Micellar Concentration
EO	Ethylene Oxide
*t*BA	*tert*-butyl acrylate
St	Styrene
PEO	Poly(ethylene oxide)
P*t*BA	Poly(*tert*-butyl acrylate)
PCL	Polycaprolactone
PS	Polystyrene
PS-*b*-PEO	Polystyrene-*block*-Poly(ethylene oxide)
PS-*b*-PtBA	Polystyrene-*block*-Poly(tert-butyl acrylate)
PEO-*b*-PCL	Poly(ethylene oxide)-*block*-Polycaprolactone

Abstract of Dissertation Presented to the Graduate School
of the University of Florida in Partial Fulfillment of the
Requirements for the Degree of Doctor of Philosophy

BEHAVIOR OF SEVERAL AMPHIPHILIC COPOLYMERS AT THE AIR-WATER INTERFACE

By

Sophie Bernard

December 2007

Chair: Randolph S. Duran
Major: Chemistry

The two-dimensional structure of amphiphilic copolymers is studied at the air-water interface using Langmuir-Blodgett methods, atomic force microscopy (AFM), and Brewster angle microscopy (BAM). Measurements are made for several block copolymers containing polystyrene (PS), poly(ethylene oxide) (PEO), poly(*tert*-butylacrylate) (P*t*BA) and polycaprolactone (PCL).

Measurements are also made for blends of the PS-b-PEO copolymer with both a PS and a PEO homopolymer. When increasing the amount of PS homopolymer, the isotherms do not show any change in the high surface area region. However, a linear dependence of the condensed area is observed. An increase in the PEO ratio has an effect on the biphasic region of the isotherms but no change is detected for the condensed area. The AFM data indicate a significant effect of the homopolymers on the monolayer structure. In fact depending on the homopolymer added, a change in the chaining behavior of the copolymer is observed. Also, when introducing more PEO, a phase separation between the layer of PEO and clusters of two-dimensional micelles is detected.

The PS-*b*-PtBA copolymers investigated are star-shaped copolymers with a polystyrene (PS) core and a poly(*tert*-butylacrylate) (P*t*BA) corona. They were prepared with a constant PS

block and three different P*t*BA block lengths. A transition can be observed for the three copolymers with a plateau's length depending on the PtBA composition. The images obtained by AFM are in agreement with the isotherms showing the evidence of a phase transition around 24mN/m. In fact for the three copolymers, below the plateau only single domains are observed whereas for pressures higher than 24mN/m, aggregates can be detected. Transfer experiments were performed after several equilibration times. The structure of the film formed seems to be dependant on the time waited before performing the transfer, showing more compact films when the time waited was longer.

Poly(ethylene oxide)-*block*-Polycaprolactone (PEO-*b*-PCL) copolymers are also studied in this work. Their behavior and the PCL crystallization process at the air-water interface is investigated using BAM. The formation of crystals directly on the water subphase is illustrated and compared to the pictures obtained by AFM.

CHAPTER 1
INTRODUCTION

1.1 Scope of the Dissertation

The aim of this project is to find fundamental information on a novel series of polymers by understanding their behavior at the air/water interface. Chapter 2 describes the different techniques used throughout my doctoral research. A review of these techniques as well as their multiple applications is given. Chapter 3 and 4 go over the investigation of several amphiphilic copolymers at the air-water interface as well as their ability to form more complex architectures when blended with one of their corresponding homopolymers. Atomic Force Microscopy (AFM) is used as a tool to observe the formation of the morphology once the copolymer solutions are spread onto an interface and transferred to solids. Chapter 5 describes the behavior of a polystyrene-*b*-polycaprolactone (PS-*b*-PCL) linear copolymer and a PS-*b*-PCL star-shaped copolymer. In this investigation, Brewster angle microscopy (BAM) is used in order to understand the copolymer crystallization process. The goal of Chapter 5 was to obtain a better understanding about the formation of polycaprolactone crystals when a solution is spread onto a water subphase.

The reminder of this chapter is a literature review on the behavior of block copolymers in the bulk and at an interface.

1.2 Block Copolymers in the bulk

Self-assembling copolymer materials are interesting because of their multiple commercial applications such as thermoplastic elastomers and compatibilizers in polymer blends. In the past decades, interest in the behavior of block copolymers has grown due to many further potential applications in nanoscale lithography [1] or electronics.[2-4] The emergence of controlled polymerization techniques such as such as living anionic polymerization,[5] ATRP (atom transfer

radical polymerization),[6] or RAFT (reversible addition fragmentation chain transfer)[7] has allowed the formation of more complex architectures leading to a wide range of properties.[8-10]

Block copolymers are composed of different polymer chains. Depending on the number of different blocks, their composition, and the way they are linked together, they can form a variety of ordered morphologies with characteristic lengths on the mesoscale .[11]

The simplest class of block copolymers is linear block copolymers composed of two immiscible blocks, A and B. This type of architecture can adopt several equilibrium morphologies depending on the composition of the two blocks: spheres (S), cylinders (C), double gyroid (G), lamellae (L), and the inverse structures (Figure 1-1).[11,12]

This phase behavior is dictated by the Flory-Huggins segment-segment interaction parameter ($\chi_{AB)}$, the degree of polymerization (N), and the composition (ϕ). The product $\chi_{AB}N$ gives us an idea on the phase segregation.[13] For small values ($\chi_{AB}N < 10$), the A and B blocks mix, resulting in a disordered phase. When $\chi_{AB}N$ is larger ($\chi_{AB}N > 10$), the enthalpic terms dominate, causing an order-disorder transition (ODT) where the A and B segments segregate into various microstructures.

When block copolymers are dissolved in a selective solvent that is good solvent for one of the block and precipitant for the other, the copolymer chains aggregate to form micelles.[5] Those reversible, well-defined micelles form above the critical micellar concentration (CMC). The CMC can be determined from plots of the surface tension as a function of the logarithm of the concentration. It is then defined as the concentration at which the surface tension stops decreasing and reaches a plateau value. For concentrations lower than the CMC, only single polymer chains are present in solution. Once the CMC is reached, the polymers chains aggregate into spherical aggregates as shown in Figure 1-2.

The aggregates observed are in conjunction with those seen for low molecular weight surfactant even if the values of the CMC are much lower in the case of block copolymers.

Depending on the composition of the starting block copolymer, two limiting structures can be observed: (1) "starlike" micelles with a small core compared to the corona and (2) crew-cut micelles with a large core and highly stretched coronal chains. Both situations are shown in Figure 1-3.

1.3 Block Copolymers at the Air-Water Interface

The morphologies described previously represent those formed in a three-dimensional system, but block copolymers also have the ability to self-assemble as two-dimensional structures. Such experiments are performed using a Langmuir apparatus, the setup of which will be further explained in chapter 2. In such case, the polymer solutions are spread onto a subphase and each block aligns in the phase for which it has an affinity. Amphiphilic diblock copolymers have been observed to self-assemble into numerous nanoscale and mesoscale structures when spread onto a water substrate, finding potential applications in coatings, microelectronics, stabilization, and lubrification.[15] Such copolymers are appropriate for surface pressure studies involving Langmuir troughs. This technique provides insight on the monolayer morphologies by controlling the surface density. The force acting on the molecules when spread onto a liquid is referred as the surface tension, γ, which is the measurement of the cohesive (excess) energy present at a gas/liquid interface. The molecules of a liquid attract each other; the interactions of a molecule in the bulk of a liquid are balanced by an equally attractive force in all directions. Molecules on the surface of a liquid experience an imbalance of forces as indicated in Figure 1-4.

The net effect of this situation is the presence of free energy at the surface. The excess energy called surface free energy can be quantified as a measurement of energy/area. For a constant temperature and pressure, surface free energy equals surface tension, which is quantified as a force/length measurement. The common units for surface tension are dynes/cm or mN/m. An analogous quantity is the line tension. From a mechanical point of view, line tension is defined as the operative force along the so-called three-phase line. A three-phase line is the intersection of three interfaces; for example, the periphery of the contact circle of a liquid drop that is placed on a solid surface and is surrounded by a vapor phase. Similar to surface tension, i.e., the tensile force encountered where two bulk phases meet, line tension is a well-defined thermodynamic property. However, unlike surface tension, it is not a well-quantified property; experimental values in the literature range from 10^{-11} to 10^{-5} N.[16-30]

1.3.1 Polystyrene (PS) and Poly(ethylene oxide) (PEO) at the Air-Water Interface

Seo *et al.* [31] showed the formation of stabilized two-dimensional micelles using polystyrene-*b*-poly(methyl methacrylate) (PS-*b*-PMMA) diblock copolymers at the air-water interface. Once formed, those surface aggregates were kinetically stable, preventing any unimer-micelle exchange. Polystyrene-*b*-poly(ethylene oxide) (PS-*b*-PEO) diblock copolymers of various molecular weights and chemical compositions have also been extensively used to study their properties in both the bulk and in solution.

In addition, several groups have described their behavior at the air-water interface.[32-44] The choice of PEO as one of the blocks renders the copolymer both biocompatible as well as amphiphilic. The inclusion of PS provides an anchor at the air-water interface, preventing the PEO from eventually dissolving into the water subphase. As a result, PS-*b*-PEO films can be further compressed than a film composed simply of PEO homopolymer.

Without PS, PEO can still be spread at the air-water interface. Shuler and Zisman [45] studied the behavior of such a film. They observed a change in the film compressibility as surface density increases leading to a phase change reflecting in the film's structure. The lack of reversibility in the compression and expansion experiments is explained by a structural change in the polymer molecule. A modification in conformation was given to explain the different monomer area observed in the π-A isotherms. Kuzmenka and Granick [46] performed the same type of experiment for a wide range of PEO molecular weights. They determined that for PEO chains beyond molecular weights of 100,000g/mol, the film attains a constant equilibrium surface pressure. This behavior was explained by the difficulty of a high molecular weight PEO to pass into an aqueous substrate due to the amphiphilic character of the EO monomer. Lower molecular weight PEO, however, requires a more hydrophobic anchor in order to quantitatively remain at the air-water interface, generally partitioning between the subphase and the surface, analogous to soluble surfactants.

While PEO has been widely studied at the air-water interface, PS has only been studied by one group. Being hydrophobic, PS is not expected to form any type of morphology when spread onto a water subphase. However, Kumaki [47] detected a change in surface pressure when a dilute solution of PS (2.0×10^{-5}g/mL) was spread at the air-water interface. Even if in this case, the measured surface pressure mainly represented mechanical force due to the compression, this group found stable monomolecular particles were observed for molecular weights higher than 50,000g/mol. However this work remains controversial. In fact, despite its importance, this remains the only study on pure PS.

As a result, recent work has focused on the behavior of PS-*b*-PEO at the air-water or solid-water interface, demonstrating the formation of novel nanostructures. Gonçalves da Silva ***et al.***

[34,39] described the utility of diblock amphiphilic copolymers in testing the scaling properties of grafted polymers. They presented π-A isotherms that show several regions referred to as pancake, quasi-brush, and brush. Within these regions, different morphologies of surface micelles and further micellar aggregates were observed by transmission electron microscopy (TEM) and atomic force microscopy (AFM) depending on the balance between block sizes. At the air-water interface, copolymers behave similarly to copolymers in bulk dispersion. Static light scattering proved that PS-*b*-PEO copolymers aggregate spontaneously into micelles over the CMC. The isotherm regions compare to those observed for solution CMC values: (1) below the CMC, surface micellization is observed; (2) at the CMC, the PEO segments are pushed into the subphase in order to decrease the surface area per molecule; and (3) above the CMC, PS-rich regions exist in between spaces formed by the PEO chains.

Gonçalves da Silva *et al.* [34,39] also investigated the effect of the PEO block size on the copolymer behavior at the air-water interface. In this case, the short PS chains are only used as an anchor to prevent the PEO from dissolving completely into the water substrate. Upon compression, they observed a transition of the PEO blocks, from a two-dimensional structure floating on the water, to a three-dimensional structure when the PEO stretched into the water. The first structure is the one previously termed "pancake" whereas the second was identified as "brush" (Figure 1-5). The plateau displayed in the π-A isotherms is an indication of the transition between these two states with its span dependent on the relative sizes of the two blocks.

The importance of PEO in film behavior has been recognized by others. For example, Devereaux and Baker [43] conducted π-A isotherms experiments of PS-*b*-PEO copolymers with varying PEO chain lengths. One copolymer contained 15% of PEO whereas the other had only 7%. The copolymer with the longest PEO block displayed a plateau close to 10mN/m, indicating

that the copolymer spreads well at the interface. In contrast, the copolymer containing only 7% of PEO has no plateau, supporting the theory that PS chains interfere with the PEO blocks upon compression.

While most groups support the model of a transition from pancake to brush described previously, Cox *et al.* [41,42] provide a different model to explain the shape of the π-A isotherm for a PS-*b*-PEO copolymer. Whereas in the first model the PEO passes into the aqueous subphase, the Cox model suggests a dehydration of the PEO followed by a conformational change, similar to that previously described by Shuler and Zisman[40] for homopolymer PEO. As shown in Figure 1-6, conformation (a) (more flexible) is compressed into conformation (b) (more compact and sterically hindered). This transformation can be explained by an increase in the intramolecular forces in the second conformation.

While numerous studies detail the behavior of linear PS-*b*-PEO, advances in polymerization techniques within the past decade have allowed chemists to design new copolymer architectures. Logan,[48] Logan *et al.*,[49] and Francis *et al.*,[50,51] for example, investigated the behavior of several star amphiphilic copolymers at the air-water interface. Peleshanko *et al.*[42] observed formation of morphologies when spreading an amphiphilic heteroarm PEO-*b*-PS_m. The AFM images showed that the formation of different morphologies depends on the pressure used during the transfer. The unusual properties of those architectures allow the formation of more stable morphologies than those formed using regular linear copolymers.

1.3.2 Polyacrylates at the Air-Water Interface

Some copolymers, called stimuli-responsive systems, respond by a change of size or shape to a modification in temperature, ionic strength or pH.

For example, in the Armes group, the synthesis and solution properties of water-soluble copolymers were studied. The copolymers were composed of different alkyl methacrylates for the hydrophobic block and poly(2-dimethylamino) ethyl methacrylate, poly(sulfubetaine), poly(4-vinylbenzoate) and more for the hydrophilic block.[53,54,55] Block copolymers containing PS and poly(acrylic acid) (PAA) are another type of self-assembling copolymers.[56-59] Eisenberg *et al.*[57,59] synthesized PS-*b*-PAA copolymers by anionic polymerization and investigated their behavior at the air-water interface. They identified a wide range of structures like spheres, rods, bilayer and bicontinuous architectures, as well as inverted structures. All the aggregates observed possess a phase-separated insoluble core and a crew-cut soluble corona. The synthesis as well as the micellar properties in an aqueous media was studied for more complex architectures based on PS and PAA.[60-66] Even if numerous efforts have been done to study the interfacial behavior of PAA-based copolymer, Poly(*tert*-butylacrylate) (P*t*BA) -based copolymers studies remain rare. Our group was the first to publish results concerning PS and P*t*BA based copolymers at the air-water interface.[67,68]

1.3.3 Poly(ε-caprolactone) (PCL) at the Air-Water Interface

PCL is an interesting flexible polymer for monolayer studies. It is a hydrophobic and crystalline polyester with a glass transition around -60°C, a melting point around 55°C, good biocompatibility, and low toxicity. In the past decades, PCL-containing systems have been found potentially useful for applications such as controlled-release drug delivery and scaffolds for tissue engineering.[69-71] At the air-water interface, previous results indicate that PCL can form a "2D" close-packed monolayer with a collapse point around A ≈ 20 $Å^2$/monomer. We found that very little interest was given to studying the assembly of monolayers of PCL homopolymers and PCL-based copolymers. Leiva *et al.* were first to describe the behavior of PCL homopolymers at

the air-water interface.[72] Recently, Li *et al.*[73] studied their crystallization behavior using Brewster angle microscopy (BAM). The architectures formed are illustrated in Figure 1-7.[73]

1.3.4 Previous Studies on Polymer Blends

While different architectures can result in different surface film behavior, the synthesis of such systems can be difficult and time-consuming. In an effort to acquire new properties without the required synthesis, surface films of blended polymers have also been investigated. In the 1980s, the Gabrielli group[74-81] examined the behavior of numerous mixtures of polymers and low molecular weight materials as binary systems with different degrees of incompatibility. They also quantified the determination of the two-component monolayer miscibility by observing the π-A isotherms of their two-dimensional blend. Thibodeaux *et al.*[82] studied mixtures of a liquid crystalline copolymer with its corresponding monomer. The films formed by the blend monolayer appeared to be more condensed than the pure copolymer films, proving that two-dimensional mixtures of two or more polymers could enhance the interfacial behavior and enable the formation of more stable films.

In addition, such technique allows the blending of different polymer characteristics into a single film. Malzert *et al.*[83-85] developed a suitable model for understanding the interactions between polymers by mixing poly(ethylene glycol) (PEG) and poly(lactide-*co*-glycolide). The difference between the organization of the films resulting from a spreading of a mixture or a covalently linked copolymer gave the possibility to modulate and control the composition of the interfaces. Hottle *et al.*[86] studied blends of amphiphilic poly(dimethylsiloxane) and trisilanolisobutyl-POSS and observed the formation of uniform monolayers when adding up to 80wt% POSS. By adding poly(lactide-*co*-glycolide) to the PEG monolayer, Malzert *et al* were able to avoid the dissolution of the hydrophilic polymer and therefore control the composition of

the interface. More recently, Seo *et al.*[87] investigated the structures formed at the air-water interface by blending poly(styrene-*b*-ferrocenyl silane) (PS-*b*-FS) and poly(styrene-*b*-2-vinyl pyridine) (PS-*b*-P2VP). While neither of those copolymers assemble when spread separately at the air-water interface, their blends formed ordered structures which appear to be more versatile, a promising development in the fabrication of polymeric templates for lithography. Experiments were performed for several temperatures and showed that close to the Tg of one of the block, the formed micelles retained their surface mobility and could organize in equilibrium structures in response to changes in surface density or applied electric fields. In general, the surface behavior of amphiphilic diblock copolymers is readily examined through Langmuir techniques. Methods involving film compression and transfer provide both quantitative and qualitative results indicating how surfactant responds to pressure. PS-*b*-PEO proves to be particularly of interest due to the biocompatibility of PEO. While different architectures of this copolymer have been shown to demonstrate different properties than those of linear analogues, additional characteristics may yet be attained through blending, both with PS and PEO homopolymers.

While only a few preliminary studies of blending at the air-water interface exist, spin coated thin films of polymer blends have been investigated.[88-94] Mayes *et al*[88,89] studied the homopolymer distributions in ordered block copolymers. By blending a PS-*b*-PMMA diblock copolymer with PS and PMMA homopolymers, this group was able to illustrate the interactions between a homopolymer and its corresponding block. A similar system studied by Jeong *et al* [92-94], showed that the miscibility between PMMA homopolymer and PMMA block was higher in thin films than in the bulk.

The most commonly used technique to observe the morphologies formed by compressing a monolayer at a certain pressure is AFM. For soft samples such as polymer films, an appropriate

AFM technique is tapping mode. Here, the cantilever is excited to an oscillation near its resonance frequency. The interactions between the tip and the sample give a deviation in the oscillation amplitude, recording the changes in the sample. This mode has been employed for most polymer samples because of its ability to investigate soft materials without further staining and with little or no tip-induced damage or morphology changes. However, Knoll *et al.*[95] highlighted the limitations of this technique, finding that the appearance of artifacts was related to tip-sample interactions. Nevertheless, AFM provides valuable information on film morphology. Bodiguel *et al*.,[96] for example, introduced a method for determining the dependence of the phase signal on the thickness of the sample. They corroborated that the origin of the phase signal was adhesive and represented the local elastic properties of the sample. Garcia *et al.*[97] showed that phase shift measurements obtained by AFM in tapping mode could be converted into energy dissipation values. They suggested that the characterization of material properties is less sensitive to the interaction regime and more to the tip-surface interactions. For a completely different application, Dorvel *et al.*[98] used AFM to characterize the formation of tethered bilayer lipid membranes on gold substrates.

In the following chapters, three different polymer systems will be investigated. Several PS or PEO containing amphiphilic systems will be considered. Those copolymers were chosen for their interesting surface activities, making them good candidates for interfacial investigations. Those experiments will give us important fundamental information regarding the two-dimensional self-assembly of amphiphilic copolymers. The blending properties of a copolymer will also be given, allowing the formation of different morphologies by controlling the amount of each component. Moreover, the effect of the nature of the more hydrophobic block will be described using an amorphous (PS) and a crystalline (PCL) polymer.

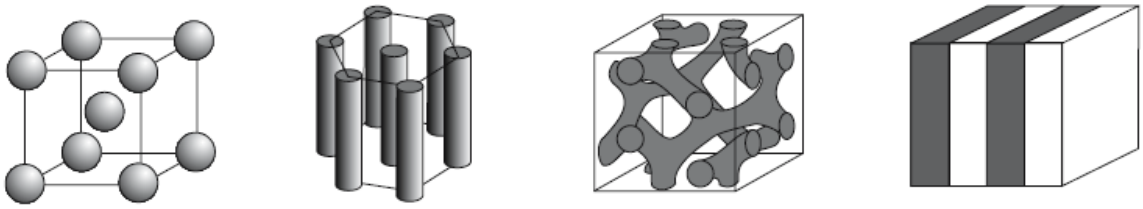

Figure 1-1. Morphologies of diblock copolymers: cubic packed spheres (*S*), hexagonal packed cylinders (*C* or *Hex*), double gyroid (*G* or *Gyr*), and lamellae (*L* or *Lam*) (Adapted from Reference 2).

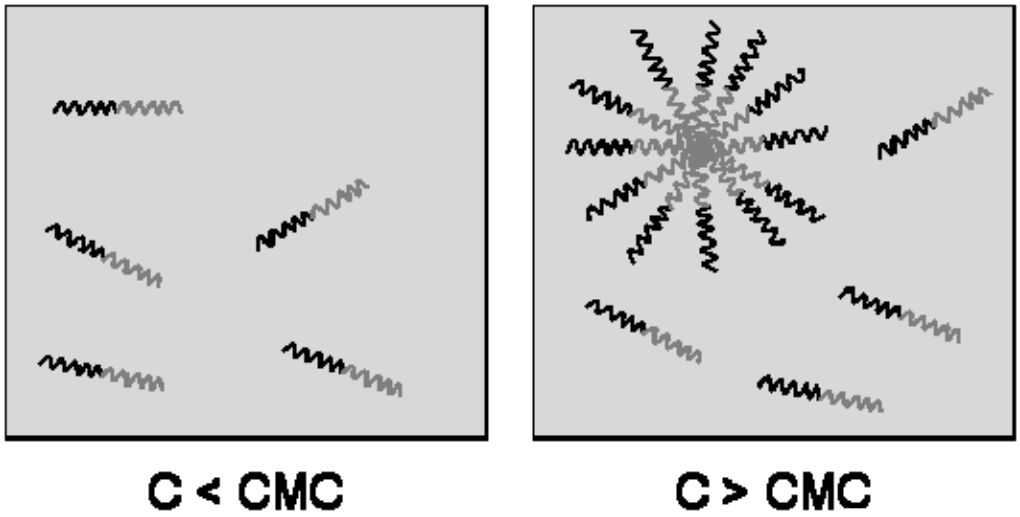

Figure 1-2. Solution states for an amphiphilic diblock copolymer for concentration below and above the CMC.

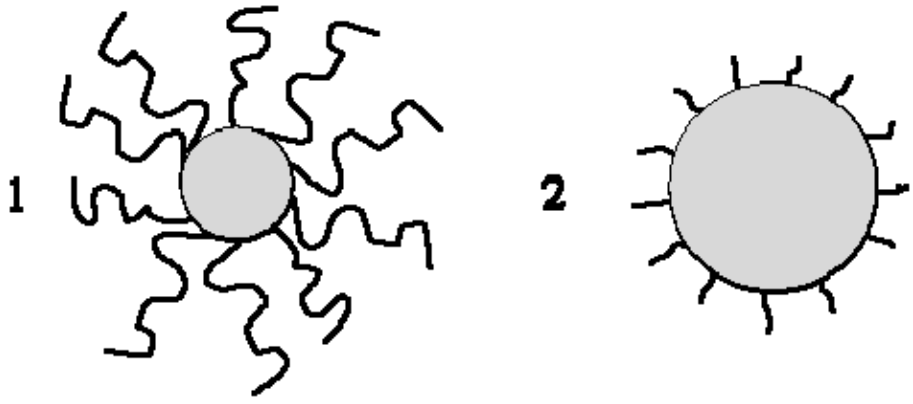

Figure 1-3. Schematic representation of a "starlike" (1) and a "crew-cut" (2) micelle.

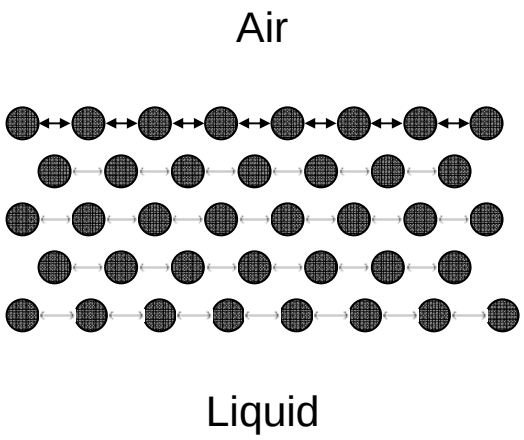

Figure 1-4. Description of Surface tension showing how the forces on surface molecules differ from those in the bulk

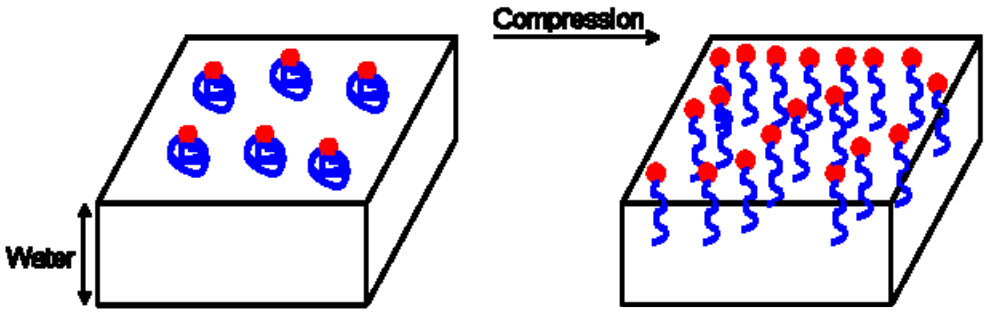

Figure 1-5. Schematic representation of the pancake to brush transition proposed by Goncalves da Silva *et al.*[34] for PS-*b*-PEO copolymers.

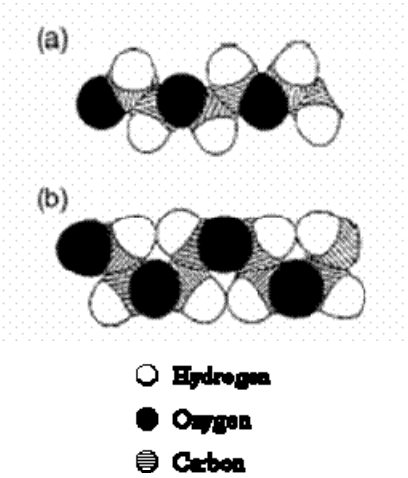

Figure 1-6. The two conformatins for PEO at the air-water interface proposed by Shuler and Zisman.[45] Conformation (a) is loose and flexible, but compressing it into the compact conformation (b) tends to lock the chain in one position resulting in a sterically hindered and more rigid structure

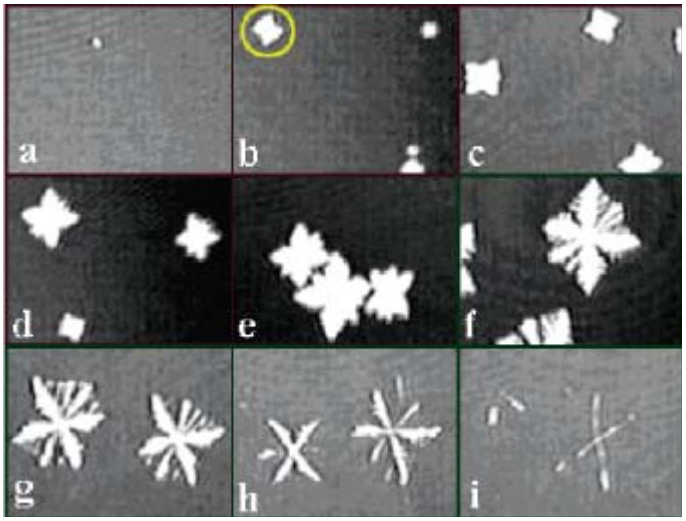

Figure 1-7. BAM images obtained during an hysteresis experiment at 22.5°C with a compression and expansion rate of ~ 0.010 $nm^2.monomer^{-1}.min^{-1}$ for a PCL homopolymer. Compression ($A/nm^{-1}.monomer^{-1}$): (a) 0.243, (b) 0.200, (c) 0.170, (d) 0.120, and (e) 0.080; Expansion ($A/nm^{-1}.monomer^{-1}$): (f) 0.082, (g) 0.173, (h) 0.272, and (i) 0.387. (Adapted from Li *et al.*[137])

CHAPTER 2
EXPERIMENTAL TECHNIQUES

Any study involving Langmuir monolayers requires the use of a Langmuir trough set-up for quantitative measurements and for the preparation of Langmuir-Blodgett films. Irving Langmuir was one of the principal scientists to observe the formation of monolayers when a surfactant is spread onto water, which lead to the development of the Langmuir trough technique (Figure 2-1).[99] With this apparatus, he studied floating monolayers on water in the late 1910s and early 1920s. Several years later, Katherine Blodgett gave the first detailed description of sequential monolayer transfer onto solid supports.[102]

2.1 Langmuir Trough

A typical Langmuir trough (Figure 2-2) is composed of the trough itself, one or two movable barriers, and a device for measuring surface pressure. The Wilhelmy technique is the most commonly used and consists of a wettable thin plate partially submerged in a subphase and suspended from a balance. The force acting on the plate is directly proportional to the surface tension of the liquid.

At equilibrium the surface tension can be described as:

$$\gamma = \left(\frac{\partial F}{\partial A}\right)_{T,V,n_i} = \left(\frac{\partial G}{\partial A}\right)_{T,P,n_i} \qquad 2\text{-}1$$

where F and G are the Helmholz and Gibbs free energies respectively, and A is the surface area. An analogous quantity, the line tension is defined as the free energy per unit length associated with the boundary between two phases on a surface. Because most Langmuir-Blodgett techniques involve using pure water or aqueous subphases, the surface tension of pure water is important. Its value at 25°C is 72mN/m.

The surface tension can be measured using a Wilhelmy plate technique as shown in Figure 2-1. The plate is usually very thin and made of platinum; however glass, quartz, mica, and filter paper can also be used. The net downward force is given by the equation:

$$F = \rho_P glwt + 2\gamma(t+w)\cos\vartheta - \rho_l gtwh \qquad 2\text{-}2$$

where ρ_p and ρ_l are the densities of the thin plate material and liquid, respectively, g represents the gravitational constant, γ is the subphase surface tension, and θ is the contact angle of the liquid on the solid plate. The plate is also described by its thickness (t), width (w), and length (l) (see Figure 2-3).

When measuring the change in h (height of the plate) for a constant applied force, the change in surface tension can be calculated using equation 2-3.

$$\rho_l gtw\Delta h = 2\Delta\gamma(t+w) \qquad 2\text{-}3$$

The 2D analogue of pressure at a surface is called surface pressure, π and is the difference between the surface tension of a film covered surface, γ, and a pure liquid subphase, γ_0. A decrease in the surface pressure will be observed when in presence of a film. This leads the interesting fact that the maximum surface pressure attainable at an air-water interface will be 72mN/m with pure water at T = 25°C.

Therefore surface pressure can be defined as:

$$\pi = \gamma_0 - \gamma \qquad 2\text{-}4$$

Since the surface pressure is defined as a negative change in surface tension, the surface pressure can then be determined using equation 2-5 when measuring the change in F for a stationary plate between a clean surface and the same surface with a monolayer present.

$$\pi = -\Delta\gamma = -\rho_l gtw\Delta h 2(t+w) \qquad 2\text{-}5$$

If the plate is completely wetted by the liquid ($\cos\theta = 1$), the surface pressure is then obtained from the following equations:

$$\Delta F = 2\Delta\gamma(t + w) \quad \text{2-6}$$

$$\pi = -\Delta\gamma = -\frac{\Delta F}{2(t + w)} \quad \text{2-7}$$

For the Wilhelmy method, the thickness of the plate used is small, leading to $t << w$ and the equation 2-8.

$$\pi = -\frac{\Delta F}{2w} \quad \text{2-8}$$

Nowadays, electrobalances allow very little change in the plate's movement, improving sensitivity (5×10^{-2} mN.m^{-1}).

2.2 Equilibrium Spreading Pressure

Surfactants in general are simply molecules that migrate to the air-water interface and form a film. Molecules are spontaneously inserted into the film only up to a certain surface pressure, known as the equilibrium spreading pressure (ESP). Surface pressure can be thought of as the repulsive force resulting from molecules in a film being in close proximity with each other. At equilibrium spreading pressure, the molecules are too close to each other to easily allow more material to be inserted. However, if the surface area of the film is increased, more molecules from the subphase are inserted into the film to maintain the equilibrium spreading pressure. For polymers, a way to measure the ESP is to place a solid polymer onto the water subphase. The polymer chains are inserted in the monolayer up to a certain surface pressure representing the ESP.

2.3 Langmuir Trough Experiments

Measuring the surface pressure as a function of the area of water surface available to each molecule provides insight into monolayer properties. Such experiments are carried out at constant temperature using a heat exchanger and are known as isotherm experiments. The data are recorded by compressing the film at a constant rate while monitoring the surface pressure (Figure 2-4).

In a manner analogous to bulk materials, distinct regions can be observed at surfaces, defining the different phases of the monolayer. These different monolayer states can be observed, depending on the hydrocarbon chain length, nature of the head group, conditions, and other factors; for example, an increase in chain length increases the interactions between the chains in classical low molecular weight amphiphiles, leading to a more condensed π-A isotherm. For a minimal compression, and areas typically in the hundreds or thousand of $Å^2$ and pressures of only a small fraction of 1mN/m, the monolayer exists in the gaseous phase (G). While compressing, the monolayer undergoes phase transitions to one or more of the following phases: liquid-expanded state (L1), followed by the liquid-condensed state (L2), and finally one or more solid state phases that we will group together with the symbol (S) for simplicity. There also exists a series of liquid crystalline phases in the L2 region that are important for certain low molecular weight systems and in particular for biological properties of membrane amphiphiles. The various LC and solid phases are not relevant to the polymers discussed in this work so we will not further discuss them. Another important detail is that the sequence of phases observed, like in the case of cooling bulk 3D materials, does not need to show all the potential phases possible, though the phases always proceed in such a way that more and more ordered phases are observed as the pressure increases. If the monolayer is compressed beyond the solid phase, it will

collapse into three-dimensional structures. A way to better observe the different transitions observed on a surface pressure-MMA (where MMA is the mean molecular area representing the available area per molecule) plot is to calculate the compressibility of the monolayer using equation 2-9 (where K is the compressibility and π the surface pressure).

$$K = -\frac{1}{MMA}\frac{d(MMA)}{d(\pi)} \qquad 2\text{-}9$$

d(MMA)/d(π) represents the slope of the surface pressure-MMA isotherm plot. In these experiments, this value was calculated using for each point on the isotherm by calculating the instantaneous slope over 2000 points. It is important to note that the MMA does not take into account the polydispersity of the sample and is based on the number average molecular weight. Therefore, the area occupied by one polymer chain of average molecular weight is only calculated.

While the regions described above can often be found in small surfactant molecules, diblock copolymers typically have fewer regions as noted above. An example is shown in Figure 2-5. Here, extrapolations of selected regions of the isotherm to zero pressure quantify the isotherm in such a way that the surface behavior of different copolymers and their blends to be compared independent of differences in pressure. It should also be noted that the surface area in experiments involving polymers is often expressed in area per repeat unit. This is calculated by dividing the MMA by the number of repeat units present in one polymer chain. This allows interpretations and comparisons with low molecular weight standards. Similarly, for block copolymers the area can be expressed in area per repeat unit in one of the blocks which can be calculated by dividing the MMA by the total number of repeat units of one of the block in one copolymer chain. This simplifies comparisons between copolymers consisting of different segments of varying molecular weights and even different architectures.

In addition to the classic isotherm experiment, numerous experiments such as isobars, isochores or compression-expansion hysteresis, can be done using the Langmuir trough. In the isobaric experiment, the monolayer is compressed to a specific target pressure. The pressure is then maintained constant while the MMA is recorded over time. Isobars provide the ratio of the current monolayer area to its initial area. The change in area can be correlated with film properties such as creep. In the isochoric experiment, the monolayer is compressed to a specific target pressure. Once that pressure is reached, the compression is stopped and the surface pressure is recorded versus time.

The compression-expansion experiment measures the ability of the monolayer to relax to its initial expanded state after compression. If upon expansion, the monolayer relaxes following the same pressure-MMA curve, no hysteresis is detected. If however, the second compression produces a new curve, the hysteresis can be detected to quantify the amount of irreversibility of the film formed. Those experiments can give us information about the stability of the film formed. In fact, for high surface pressures, numerous block copolymers form metastable films, metastability being described as the ability of a non-equilibrium chemical state to persist for a long period of time. For example, for PCL homopolymers, Li *et al* reported the formation of metastable crystals during the compression cycle with the crystal sizes being dependent on the compression rate.[73] During the expansion cycle, those crystals were re-adsorbed (melted) onto the water subphase.

Unless otherwise noted, surface pressure measurements were performed using a Teflon Langmuir trough system (W = 160 mm, L = 650 mm; KSV Ltd., Finland) equipped with two movable barriers and a Wilhelmy plate Between runs, the trough was cleaned with ethanol and rinsed several times with millipore filtered water (resistivity ≥ 18.2 MΩ.cm). The samples were

typically prepared by dissolving approximately 1 mg of polymer in 1 mL of chloroform. Volumes ranging from 10 to 30 μL were spread dropwise on a Millipore filtered water subphase with a gastight Hamilton syringe. The chloroform was allowed to evaporate for 30 min to ensure no residual solvent remained. When not in use, the volumetric flasks containing the polymer solutions were wrapped with Teflon tape followed by Parafilm and stored at 10 °C in order to prevent changes in concentration due to chloroform evaporation. In all the experiments, subphase temperature and barrier speed were kept constant at 25 °C and 5 mm/min, respectively.

2.4 Langmuir-Blodgett Films

Besides Langmuir monolayers, a common application of the Langmuir trough is the transfer of monolayer onto a solid substrate. This is accomplished by dipping the substrate into the subphase, allowing the adsorption of the monolayer. The surface pressure is maintained constant by a computer controlled feedback system between the electrobalance measuring the surface pressure and the barrier moving mechanism. Depending on the number of dippings, successive monolayers, from several to hundreds, can be deposited onto the solid substrate.

Numerous substrates have been used. For analytical work involving subsequent imaging, mica is commonly preferred in LB film transfer due to its low cost, easy cleaning, and easy preparation. However, mica possesses a water layer that may affect the film transfer. Other substrates such as silicon wafers can be used; treatment with chromic sulfuric acid renders them highly hydrophilic. Still other materials can be used as hydrophobic substrates, including graphite, polymer films, and silanized silicon dioxide.

LB films can be formed either by pulling out or dipping the substrate into the subphase. Pulling or the upward pass of the substrate through the subphase is also known as an upstroke while the downward dipping refers to the downstroke. Three different types of deposition can exist (Figure 2-6). The X-type deposition can be done by a downstroke whereas Z-type occurs

during the upstroke. The Y-type, the most common, is characterized by deposition on both an upstroke and a downstroke. Intermediate structures can sometimes be observed for some LB multilayers and are often referred to as XY-type multilayers.

Once transferred, these films can be studied by different surface analysis techniques, such as optical spectroscopy, X-ray diffraction, as well as atomic force microscopy (AFM) or transmission electron microscopy (TEM).

The quantity and quality of the deposited monolayer on a solid support are measured by a so called transfer ratio, TR. This is defined as the ratio between the decrease in monolayer area during a deposition stroke, Al, and the area of the substrate, As. For ideal transfer the TR is equal to 1. However, experimentally the TR often varies significantly. Low transfer ratios indicate a that the polymer chains transferred on the substrate are less dense than those on the water subphase. For transfer ratios greater than 1, the polymer chains on the solid substrate are more densely packed than those at the air-water interface. Another type of transfer ratio can also be calculated and recorded in typical LB experiments. The instantaneous transfer ratio is the amount of monolayer transferred versus the amount of substrate pulled out at a specific time. This type of transfer ratio gives information on the uniformity of the film transferred. In our experiments, all the instantaneous transfer ratios observed were homogeneous indicating a good transfer of the monolayer onto the mica substrate.

2.5 Atomic Force Microscopy

2.5.1 Instrument Parameters

Contrary to its precursor, scanning tunneling microscopy (STM), which only allows the study of electrically conductive samples, AFM can be applied to both conductors and insulators. The instrument consists of a tip at the end of a cantilever, which bends in response to the force between the tip and the sample (Figure 2-7).

Since the cantilever obeys Hooke's law for small displacements, the interaction force between the tip and the sample can be found:

$$F = -k\,x \qquad 2\text{-}10$$

where *x* is the cantilever deflection and k the spring constant.

In the early stages of AFM, contact mode was used. This method consists of a tip in close contact with the surface. The deflection of the cantilever is sensed and compared to the desired value of deflection. The voltage needed to restore the desired value of deflection is a measure of height of features on the sample surface. This mode was quickly forgotten for polymer studies because of excessive tracking forces applied by the probe to the sample.

To remove these drawbacks, a non-contact mode was developed. In this case, the tip hovers 50-150 Angstrom above the sample surface. The attractive Van der Waals forces acting between the tip and the sample are detected, and topographic images are constructed by scanning the tip above the surface. This technique was also found to be inapplicable to polymer samples. In general, the fluid contaminant layer existing on the sample is substantially thicker than the range of the Van der Waals force gradient and, therefore, all attempts to image the true surface with non-contact AFM fail as the oscillating probe becomes trapped in the fluid layer.

Later, a third method was developed in order to study softer samples (Figure 2-8). This mode, called tapping mode, consists of alternately placing the tip in contact with the surface to provide high resolution and then lifting the tip off the surface to avoid dragging the tip across the surface. As the oscillating cantilever begins to intermittently touch the surface, the cantilever oscillation is necessarily reduced due to energy loss caused by the tip contacting the surface. The reduction in oscillation amplitude is used to identify and measure surface features.

AFM involves scanners made from piezoelectric material, a substance which proportionally contracts and expands, depending on an applied voltage. If a positive voltage elongates the scanner, a negative voltage contracts it. The scanner is made of a piezoelectric material surrounded by electrodes which control the applied voltage. As scanning occurs in three dimensions, a scanner tube contains three piezo electrodes for the X, Y, and Z directions (Figure 2-9). Piezoelectric ceramics are capable of moving a probe very small distances. However, when a linear voltage ramp is applied, they move in a non-linear motion (Figure 2-10). All AFM must therefore be calibrated in the X-Y axis so that the images presented on the computer screen are accurate. Height measurements require that the piezoelectric ceramics in the Z axis of the microscope be both linear and calibrated. Often the microscope is calibrated at only one height; however, if the relationship between the measured and the actual Z height is not linear, the measurements will not be correct.

The studies described in this work utilize a Digital Instruments Nanoscope system. Several different scanners can be used depending on the sample studied. They differ on the scanning size and resolution. For example the J-scanners can scan images up to 125 μm, whereas E-scanners scan smaller sizes of 10 μm or less. In these experiments, the x-y range was calibrated monthly using a calibration grid with known periodicity. Likewise, z calibration was performed bi-annually, using standards of different heights. In our case, the standard used is a silicon calibration grating with a step height of 18.5±1nm (close to the height of our samples).

2.5.2 Limitations

Some limitations exist when using AFM. The tip can easily be damaged and the formation of debris can lead to dullness of the tip. A blunt tip can not detect narrow valleys or higher peaks

and will therefore create a blurry image. Resolution in AFM images consists of lateral (X,Y) and vertical (Z) components with the lateral resolution dependent on the tip radius of curvature.[101]

However the fabrication technique of the AFM probes leads to the formation of tip possessing flat, rectangular ends. This reduces the sharpness and therefore the resolution of the images as shown in Figure 2-11.

Polymer thin films can thus be characterized through a combination of Langmuir and AFM techniques. Such methods allow the easy control of surface density as well as the easy transfer of surface films onto solid substrates. The results of such analysis will be presented in the subsequent chapters.

2.5.3 Parameters Used

Surface films of the copolymers were transferred onto freshly cleaved mica at various pressures (25°C). The desired surface pressure was attained at rates of ±10 mm·min^{-1}. Once the film had equilibrated at a constant π for 30 minutes, the mica was then pulled out at a rate of 1 mm·min^{-1}. The transfer ratios are noted in the chapters and unless specifically noted, the transfer ratio remained constant over the transfer and even transfer can be assumed. The transferred film was air-dried in a dust-free environment for 24 hours and subsequently scanned in tapping mode with a Nanoscope III AFM (Digital Instruments, Inc., Santa Barbara, CA) using silicon probes (Nanosensor dimensions: T = 3.8-4.5 μm, W = 26-27 μm, L = 128 μm). Experiments were redone after a few weeks in order to observe if any change occurred in the film structure after transfer. No difference was detected, indicating the stability of our samples once transferred onto the solid substrate. Tapping mode was used, giving a better image of a polymer sample without damaging the surface by dragging the tip. This mode consists of a tip vibrating at its resonance frequency in tapping the surface. As the tip encounters a surface feature, its amplitude of

oscillation is decreased from its set-point value. This decrease is noted by the sensor and the tip is moved up away from the sample to re-attain the set-point amplitude. A similar behavior happens when the tip moves past the feature. A topographical map of the sample can then be recorded.

2.5.4 Image Analysis

A program designed by Yves Heckel, an undergraduate student from Paris, France, allowed us to define the characteristics of the aggregates observed in the AFM images. Parameters such as the number of domains as well as the size of those domains were determined in order to better understand the aggregation behavior of the copolymers. This program allows a domain size range to be chosen in which the values of the minimum and the maximum can be varied (Figure 2-12).

The image on the left of the screen allows the user to adapt the area range limits using a visual aid. Another attribute of this program, is that it counts the number of domains present in one chain as opposed to considering the chain as a single domain. If such a mistake is made, however, the program can be manually manipulated by the user to define domain separation and number. While this feature gives a better approximation of the shape and number of domains, the resulting disadvantage is lower user efficiency, but significantly higher accuracy.

Once all the domains are counted, the computer gives a computed image representing all the domains present with the different chaining and angles for each domain (Figure 2-13). Computer errors can occur, giving wrong angles and poorly defined aggregates, in which case the user can, by clicking on the domain, redo the separations and redefine the domain (Figure 2-14). The software allows domain populations to be chosen and analysis error to be manually corrected, permitting the analysis of images with more than one domain population, as in the case of the images observed for the blends.

Additional image analysis was performed with software from Nanoscope instrument. Notably, this software allowed calculation of domain size and domain height. For this reason, the calibrations described above are very important in order to obtain absolute values. Precise height values can be obtained by cross-section analysis. This is done by drawing a line across the domains of interest, giving a cross-sectional trace of the topography – an example is given in Figure 3-13.

2.6 Brewster Angle Microscopy

The AFM necessitates, as seen previously, appropriate modification (notably transfer to a solid substrate) in order to study monolayer films, therefore there is an uncertainty of whether the system under study is in its original state or not. The Brewster angle microscope is a non-invasive technique that allows the characterization of floating monolayers at the air-water interface. Ultra thin films on air-water interface or on dielectric substrates can therefore be directly observed.

For a beam of p-polarized light, there is an angle of incidence θ at which no reflection occurs. This is called the "Brewster angle" and is denoted by equation 2-11 where n is the refractive index of the corresponding phase.

$$\tan\theta = \frac{n_{Subphase}}{n_{air}} \qquad 2\text{-}11$$

Introducing a thin film in between the two phases changes the optical properties of the system so that a small amount of the incident intensity is reflected (Figure 2-15).

The principle behind the Brewster Angle Microscope (BAM) makes use of the zero reflectance of an air-water interface for vertically linearly polarized light at the Brewster Angle of incidence. As stated in equation 2-11, the Brewster angle is calculated from the refractive indexes of the two substrates involved (for example, the critical angle of the air-water interface is

53). When a condensed phase of a monolayer with different refractive index is spread or deposited on the interface of interest a measurable change in reflectivity will occur. The reflected light can then be used to form a high contrast image of the lateral morphology of the spread or deposited layer. For example, a monolayer spread on an air-water interface is extremely thin, approximately 0.5 % of the wavelength of visible light. The relative effect on the electric field reflected from a water surface is therefore very small and the monolayer is under normal conditions quite invisible. However, if the water surface is illuminated with pure vertically linearly polarized light at the Brewster angle before spreading the monolayer at the air-water interface, there is no reflection from the water surface and the monolayer itself is much more easily visualized. One of the drawbacks to this method is that due to the use of a small aperture (the entire interface is not scanned) the lateral resolution is low compare to the AFM: a typical resolution is only about 2μm.

The BAM consists of an opto-mechanical, an electronic control unit and a personal computer (Figure 2-16). The Z lift of the BAM is a linear stage with around 30mm to travel. To avoid any damage, the vertical distance between the sample and the objective should be such that there is some space left if the Z lift is in its lowest position.

A crystal polarizer allows to produce p-polarized laser beam. To obtain optimal results, both the angle of incidence and the state of polarization of the incident beam must be set to their optimal values (Brewster angle and p-polarization).

The BAM also contains a scanner that consists of an objective and a mechanical unit. The objective has typically a nominal 10× magnification that images the sample surface onto the CCD chip and provides a diffraction limited resolution of approx. 2μm. For optically anisotropic

materials, the reflected light shows both s- and p-polarized components. This anisotropy can be detected by the analyzer in front of the CCD camera.

All our BAM experiments were performed using a Nanofilm Technologie GmbH (Goettingen, Germany) BAM2plus system. A polarized Nd:YAG laser (532 nm, 50 mW) was used with a CCD camera (572 x 768 pixels). The instrument is equipped with a scanner that allows an objective of nominal magnification of 10x or 20x to be moved along the optical axis, producing a series of small focused image. X-y scanning and subsequent image reconstruction allows a larger focused image to be acquired. For the 10x objective a laser power of 50% and maximum gain is used. A shutter timing (ST) of 1/50 s, 1/120 s or 1/1000 s is used to obtain maximum contrast between the monolayer and the COM crystals. For the 20x objective a laser power of 80%, maximum gain and ST of 1/50 s are always used. The incident beam is set at the Brewster angle in order to obtain minimum signal before spreading the monolayer. A piece of black glass is placed at the bottom of the trough to absorb the refracted light beam that would otherwise cause stray light. The polarizer and analyzer are set at 0° for all experiments. The laser and camera are mounted on an x-y stage that allows examination of the monolayer at different regions. The reflected light is recorded into the CCD camera. Different systems can be studied using BAM. Isotropic (same reflection in all directions) or anisotropic (reflection in a preferential direction) monolayers can be observed. For typical anisotropic thin film systems such as crystalline monolayers, it is possible to invert the contrast between domains by rotation of the analyzer in the range of 70°-110°.

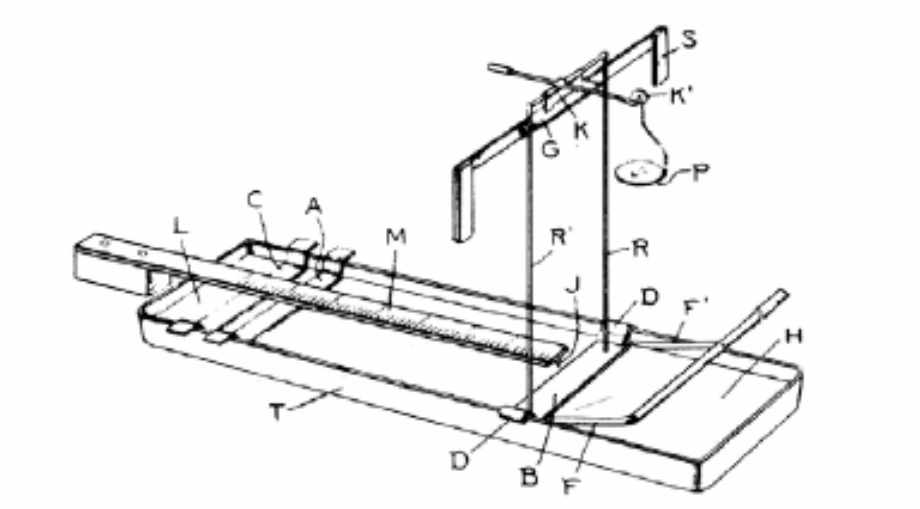

Figure 2-1. The original Langmuir balance as designed by I. Langmuir[76]

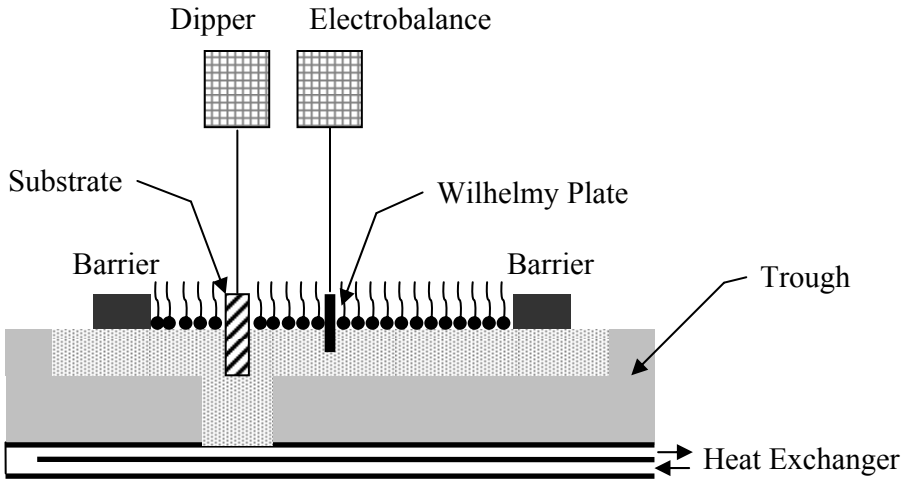

Figure 2-2. Set up of a typical Langmuir trough

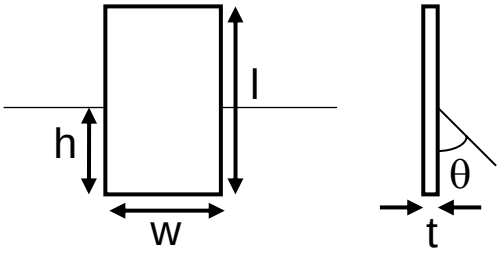

Figure 2-3. Schematic of the Wilhelmy plate

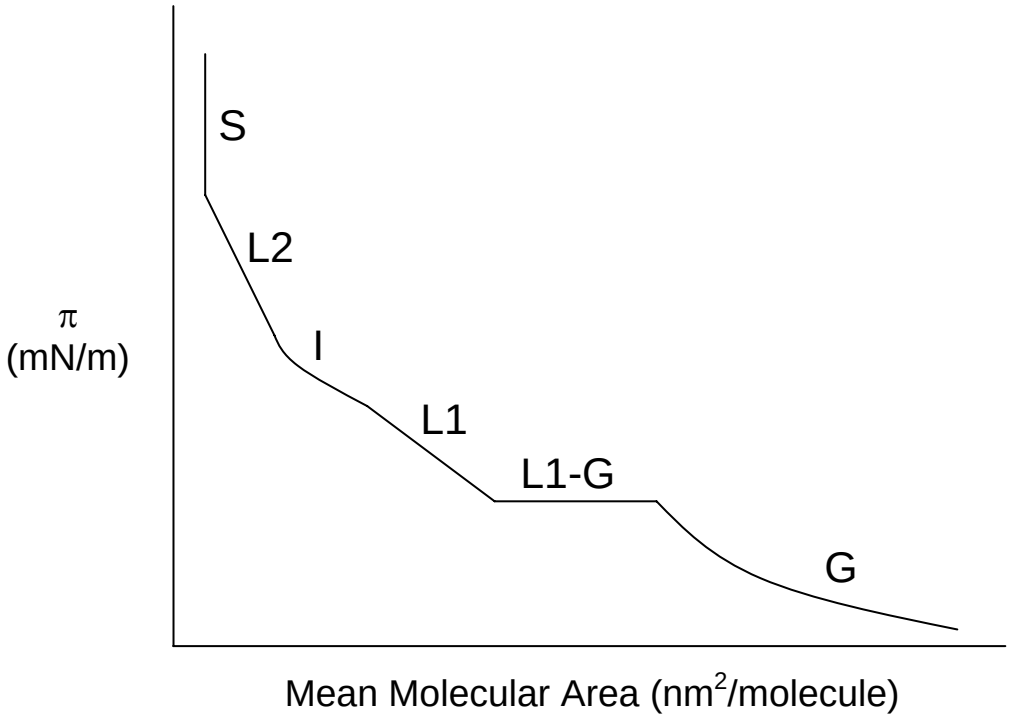

Figure 2-4. Schematic Surface pressure-MMA isotherm

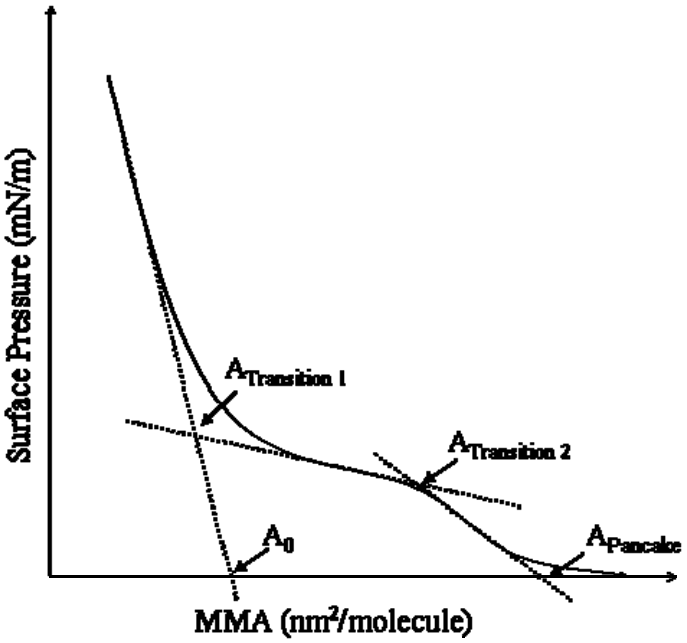

Figure 2-5. (a) Several representative isotherms are shown, depicting the dependence of surface pressure (π) on mean molecular area.

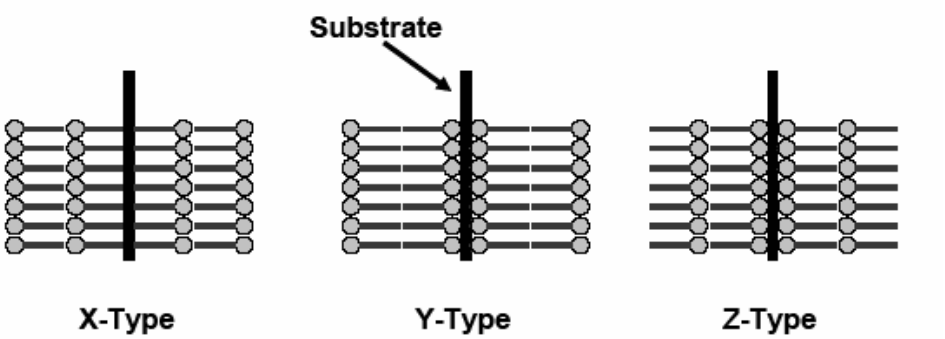

Figure 2-6 Different types of deposited LB films (borrowed from Jennifer Logan's dissertation[48])

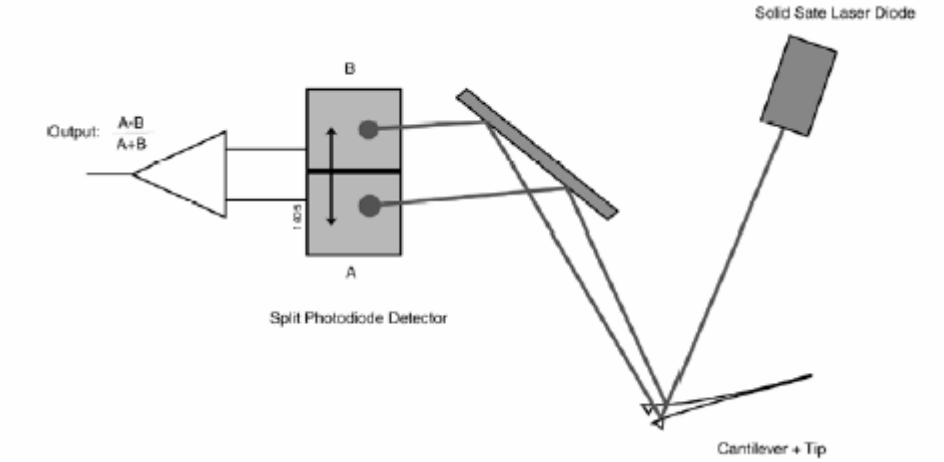

Figure 2-7. Optical system that detects cantilever deflection (Figure adapted from Digital Instruments' Training Notebook[103])

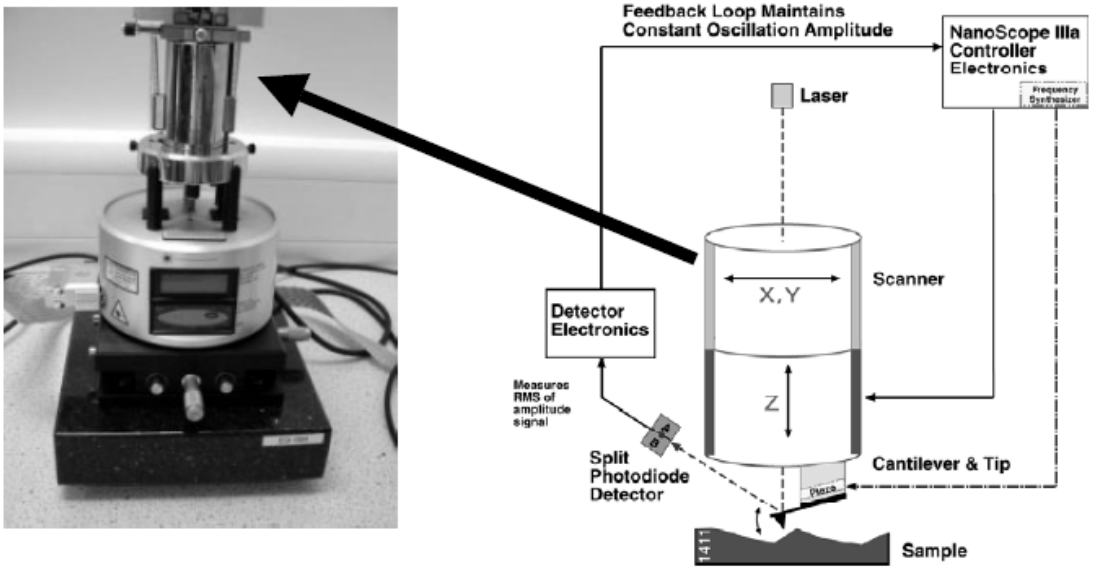

Figure 2-8. An atomic force microscope (AFM) (left) and the tapping mode electronic set-up (right) are shown (Figure adapted from Digital Instruments Training Notebook[103])

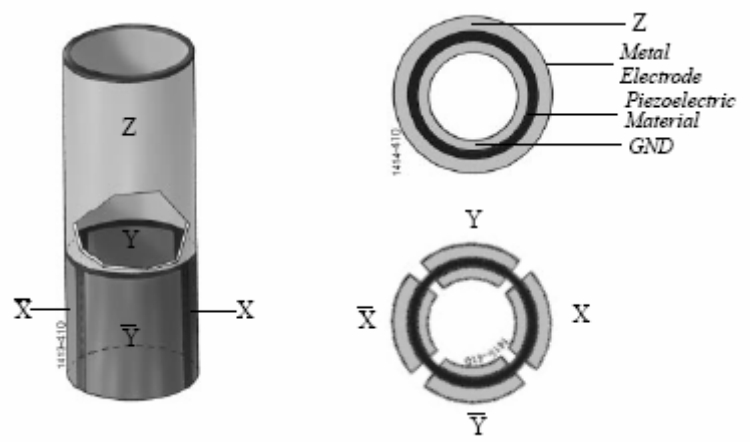

Figure 2-9. AFM scanner tube containing the piezoelectric material and metal electrode. The x, y, and z-directional components of the scanner are also indicated (Figure adapted from Digital Instruments' Training Notebook[103])

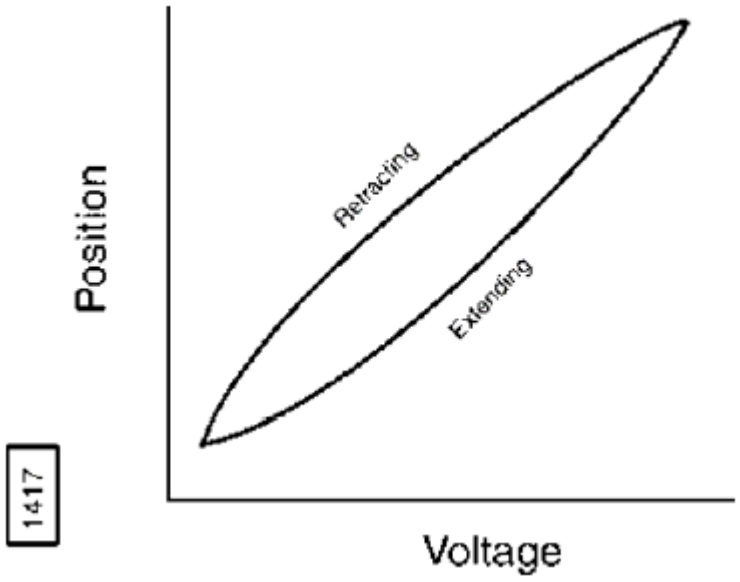

Figure 2-10. Dependance of the piezoelectric ceramic on voltage (Figure adapted from Digital Instruments' Training Notebook.[103])

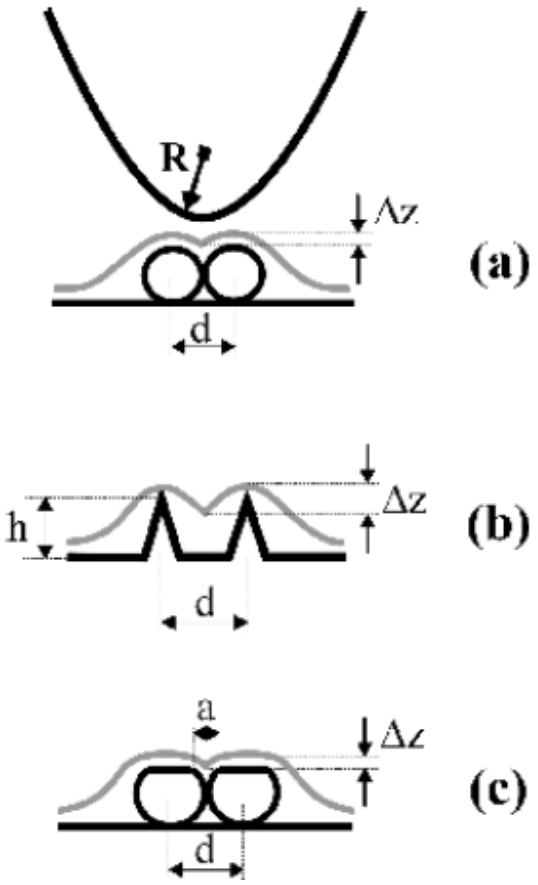

Figure 2-11. Imaging limitations in tip sharpness: Part (a) shows the dimple that results from two rigid spheres while (b) illustrates the imaging of two spikes. Part (c) resembles polymers in depicting two soft spheres that undergo slight deformation. (Figure adapted from Sheiko.[101])

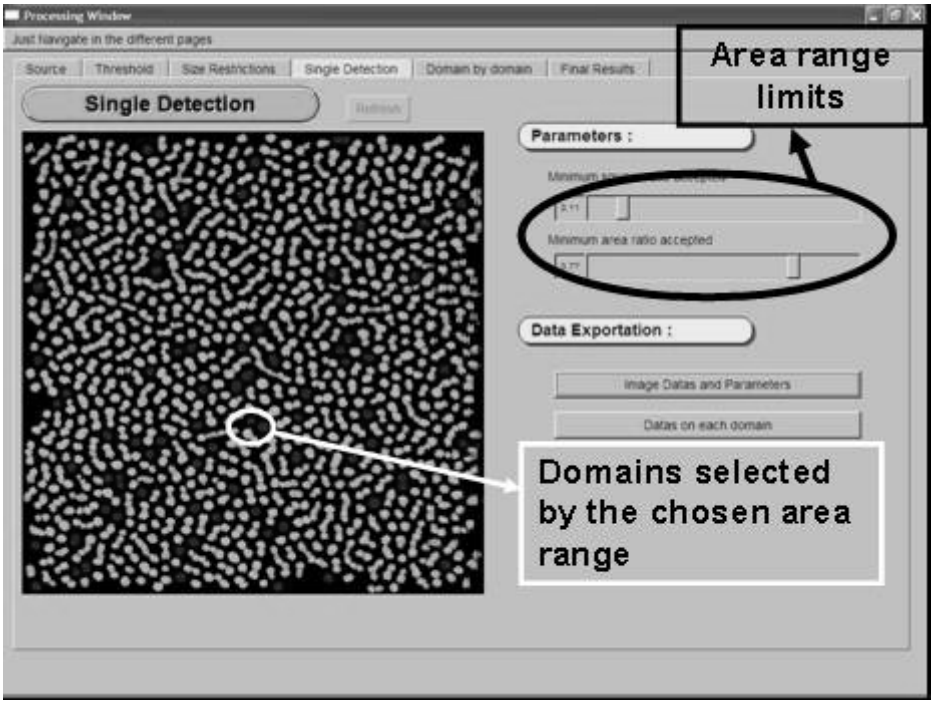

Figure 2-12. The software allows choosing a domain range by varying the minimum and maximum areas

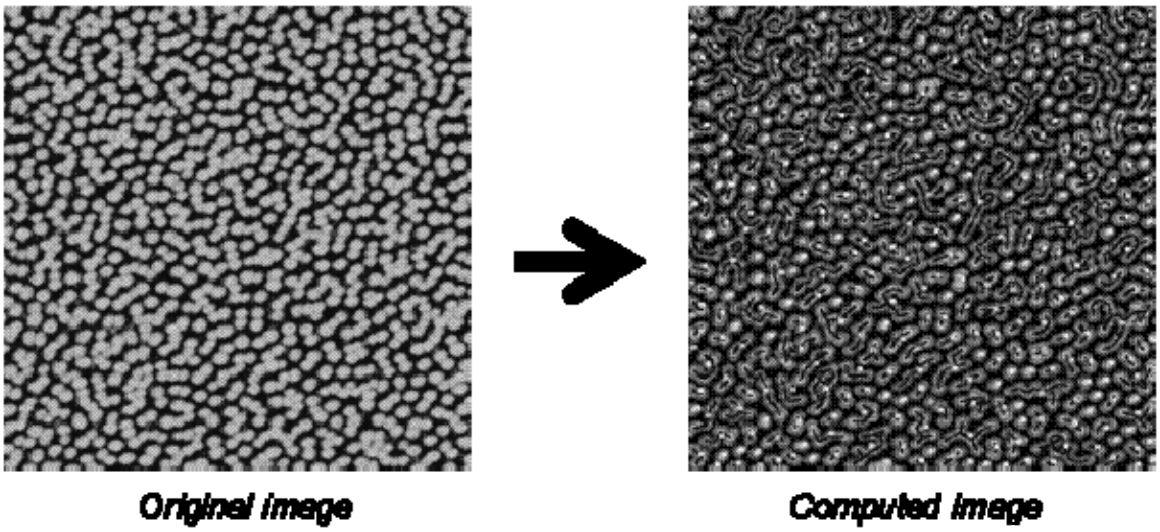

Figure 2-13. The software gives you a computed image representing the different domains and the possible angles between domains in the presence of chaining

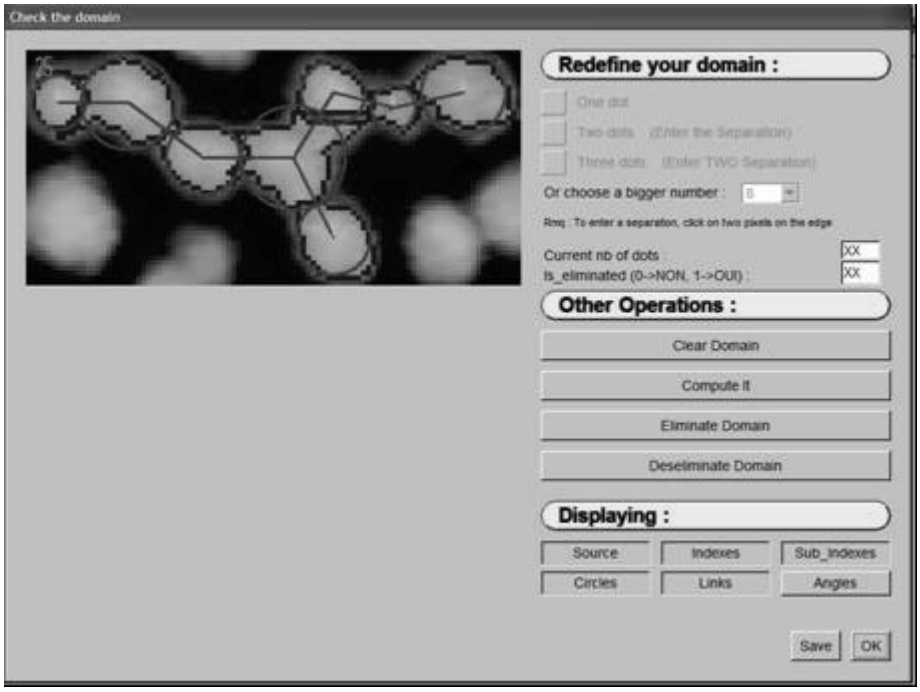

Figure 2-14. Error made by the computer can be corrected by the user

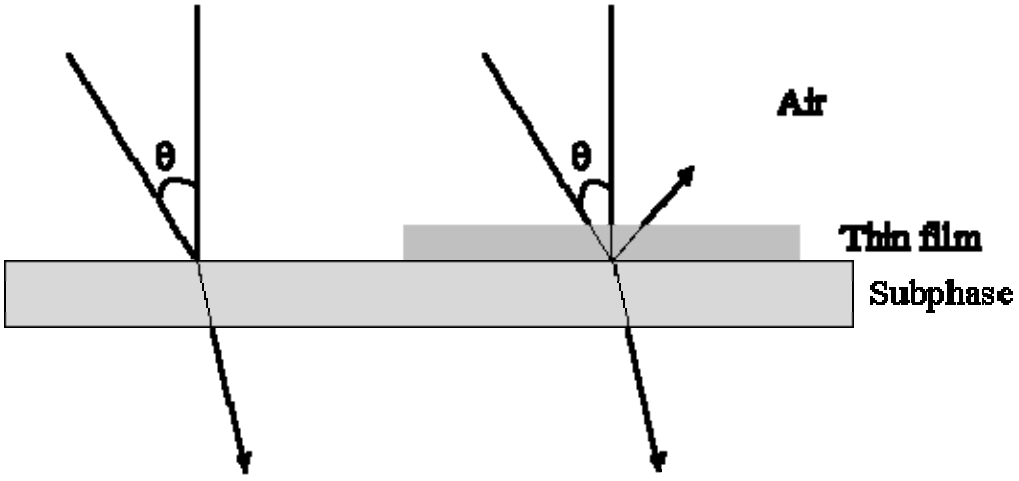

Figure 2-15. Scheme of the Brewster angle at the air-water interface and in presence of a thin film

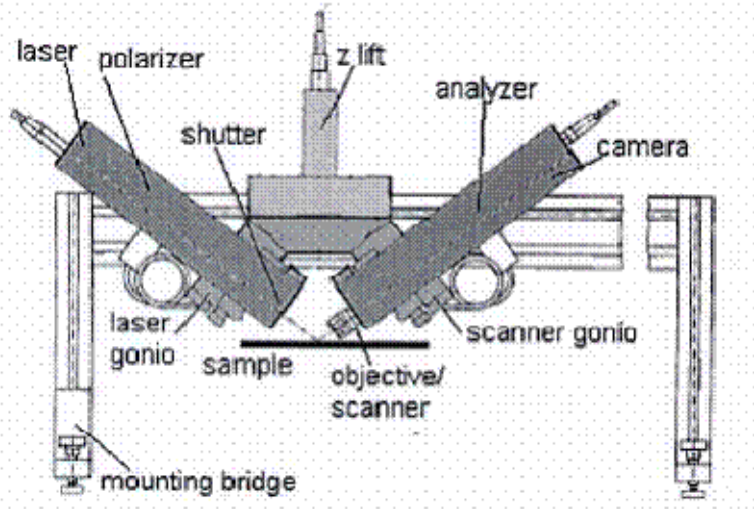

Figure 2-16. The different components of the BAM2 are shown (Borrowed from the Nanofilm Surface Analysis website)

CHAPTER 3
BLENDS OF A POLYSTYRENE-*BLOCK*-POLY(ETHYLENE OXIDE) COPOLYMER AND ITS CORRESPONDING HOMOPOLYMERS

3.1 Isotherm Experiment

3.1.1 PEO Homopolymer

As previously described [46], PEO homopolymers of sufficiently high molecular weight form thermodynamically stable Langmuir films at low surface pressures. The isotherm of a PEO homopolymer (Mn = 100,000g/mol) is given in Figure 3-1. Upon compression, the monolayers collapse, leading to the irreversible dissolution of the PEO chains into the water subphase. The collapse pressure value is highly molecular weight dependent[102] and reaches a maximum ~ 10mN/m for high molecular weight PEO.

3.1.2 Linear Polystyrene-*block*-Poly(ethylene oxide) (PS-*b*-PEO) Diblock Copolymer

Linear PS-*b*-PEO copolymers represent a convenient choice when studying the interfacial behavior of amphiphilic compounds, due to the biocompatibility of the PEO block and the low cost and availability of the PS block. Moreover, they have been widely studied and found to form stable, condensed surface films.[32-44]

The π-A isotherm for a 32,500 g/mol copolymer (see Table 3.1.) displays a pseudoplateau between 8 and 10mN/m and is shown in Figure 3-2. The observed pseudoplateau results from the hydrophilic part of the copolymer and appears over the same pressure range as the collapse pressure of a PEO homopolymer.[45]

The shape of the isotherm is independent of the copolymer solution concentration and the compression speed. In addition, multiple runs confirmed these experiments to be reproducible within $\pm 1.0 nm^2$. Within the isotherm, three distinct regions are observed. At large molecular areas, the surface film is expanded (Region I); this is usually called the “pancake” region due to the shape the PEO units form on the water surface.

As compression continues, a plateau appears (Region II) over the pressure range of 8 to 10 mN/m. Kuzmenka and Granick[46] studied the behavior of PEO homopolymers at the air-water interface with varying molecular weights. They observed a constant equilibrium spreading pressure for polymers having a molecular weight beyond 100,000g.mol^{-1}. The pseudoplateau detected in the case of our copolymer is in the same range of the collapse pressure of a PEO homopolymer and corresponds to the hydration and desorption of these chains from the surface and into the subphase.

The appearance of the pseudoplateau with an increasing amount of PEO in the copolymer was considered by Devereaux and Baker[43] They studied two PS-*b*-PEO copolymers containing different masses of PEO. The 7% PEO copolymer had no pseudoplateau whereas the 15% PEO did. This observation was explained by the long PS interfering with the PEO blocks, preventing the PEO from stretching into the aqueous subphase. Our results are in agreement with this interpretation showing a plateau for a copolymer containing 32% PEO.

Considering the affinity of PEO for water, at large molecular areas the films most likely exist as PEO films with globules of PS on top. Region II, however, represents a biphasic phase where aggregates and single polymer domains coexist. The fact that the pseudoplateau occurs within the same pressure range as the collapse region of PEO homopolymer illustrates the significant influence PEO has on the copolymer surface film. Bijsterbosh *et al.*[33] and Goncalves da Silva *et al.*[34,39] both demonstrated the existence of a pseudo first-order transition from a pancake-like structure to that of a brush upon compression of a series of PS-*b*-PEO copolymers containing a constant PS length and varying amounts of PEO. While this model is prevalent in the literature, Cox *et al.*[41,42] provided a new interpretation for the presence of the pseudoplateau assuming that the formation of brushes is not possible due to PEO's low surface energy. They

proposed that PEO instead undergoes a dehydration process and a conformational change upon compression. This observation is consistent with the one made by Shuler and Zisman[45] for a PEO homopolymer. They explained the lack of reversibility observed in their hysteresis experiments by a structural change in the polymer molecule during the compression cycle.

Contrary to PEO homopolymers, a third region (III) appears beyond the pseudoplateau and shows a sharp increase in surface pressure, indicating the formation of more rigid films. Here, the PS block serves as an anchor, keeping the PEO at the interface and allowing the films to be compressed to higher surface pressures. Without the PS, PEO would dissolve into the aqueous subphase at pressures beyond the plateau. In examining Region III, Bijsterbosh *et al*.[18] and Goncalves da Silva *et al.*[34,39] studied a series of copolymers with varying PEO lengths and a constant PS block. While Region III typically reflects PS, they found that the copolymer interfacial behavior at high pressures depends slightly on the size of the PEO block.

3.1.3 Blends of a PS-*b*-PEO diblock copolymer and a PS homopolymer

The same linear copolymer described in the previous section was used to study the effect of adding a homopolymer solution on its behavior at the air-water interface. The PS homopolymer used has a molecular weight of 20,000 g/mol, which corresponds to the molecular weight of the PS block in the copolymer. Different ratios of copolymer and homopolymer were studied in order to determine the impact on the formation of Langmuir monolayers.

The mixed monolayers were formed by separately spreading solutions of the PS and the PS-*b*-PEO block copolymer. After evaporation of the solvent, the floating monolayer was symmetrically compressed by the two movable barriers. π-A isotherms were recorded for several amount of added PS homopolymer (Table 3-2).

Figure 3-3 shows the isotherms data for different copolymer/homopolymer ratios. For all these blends as well as the pure linear copolymer isotherms, the three regions defined in the previous section were observed. This can be better detected on the compressibility plot where two different local maxima are observed (Figure 3-4). Each maximum corresponds to a phase transition and a rearrangement of the polymer chains in the monolayer. Increasing the amount of PS has only a small effect on the phase transitions observed, the local maxima in the compressibility plots show only a small increase when increasing the amount of PS homopolymer. This suggests the presence of PEO-related phase transitions independent of the PS content.

3.1.3.1 Pancake Region (I)

The first region, defined by low surface pressure and low surface density, can be quantified by its extrapolated area, A_P (Figure 2-5). The values for every blend remain constant while varying the amount of PS (average $A_P = 89.7$ nm^2). This is in agreement with a film of PEO with globules of PS on top of it where increasing the amount of PS will not change the area occupied at the interface by the PEO.

Fauré *et al.*[40] observed the same behavior for pure diblock copolymers at the air-water interface and showed that at low coverage, the interaction between the ethylene oxide (EO) monomers and the interface is attractive and therefore leads to the adsorption of the EO at the air-water interface. They assume the pressure to be only due to the total number of PEO segments in water. As a result, increasing the PS should have no effect on the behavior of this region. Logan,[48] Logan *et al.*,[51] and Francis *et al.*,[49,50] observed a similar trend for star copolymers of PS-*b*-PEO in which the pancake area did not depend on the number of PS segments. The pancake area per EO monomer (0.38 nm^2) is in reasonable agreement to the one found by Logan et al. for star copolymers (0.33 nm^2) and to the that determined for linear PS-*b*-

PEO by Gonçalves da Silva *et al.* (0.27 or 0.31 nm^2)[34,39] and Bijsterbosch *et al.*[18] (0.31 nm^2). The area observed in our case is a little higher; the addition of PS homopolymer increases the aggregation of the PS segments allowing the PEO blocks to spread more easily.

3.1.3.2 Pseudoplateau Region (II)

The pseudoplateau observed in Section 3-2 for a pure linear PS-*b*-PEO copolymer is observed for all blends and remains constant for different amount of PS. The width (ΔA_P) of the pseudoplateau can be estimated as the difference between $A_{Transition\ 1}$ and $A_{Transition\ 2}$ (Table 3-3, Figure 2-5). The value of ΔA_P remains constant for every blend (average ΔA_P = 21.9 nm^2). Region II is believed to represent a biphasic region. The phase transition is mostly due to the reorganization of the PEO chains from a pancake to a brush conformation and therefore a change in the amount of PS does not have any effect on the width of the pseudoplateau. In this region, the EO repeat unit occupies 9.2 $Å^2$ which is smaller than the value found by Logan *et al.*[48,51] (13.3 $Å^2$) for star copolymers. This difference can be explained by the fact that the PEO homopolymer is being dissolved in the subphase as the monolayer is compressed.

3.1.3.3 Condensed Region (III)

In Table 3-2, the theoretical area (A_0) that a compact surface film would occupy at zero pressure was determined for each blend. In agreement with our expectations, the area increases with an increasing mass of PS. The condensed area, representing mostly the behavior of the PS chains, varies linearly with the total mass of PS chains. This behavior can be compared to the behavior of copolymers presenting PS chains of high molecular weights. Cox *et al.*[41,42] studied several PS-*b*-PEO copolymers with varying PS molecular weights, observing a variation in the A_0 values. The increase of A_0 with increasing PS can be explained by the aggregation of the PS homopolymer with the PS chains of the copolymer.

To compare our results with those from copolymers of longer PS blocks, a normalization of the total number of styrene units was obtained by using the following equation.

$$N_{PS,TOT} = N_{PS,Diblock} + N_{PS,Homopolymer} \times \frac{n_{PS,Homopolymer}}{n_{PS,Diblocks}} \quad 3\text{-}1$$

With $N_{PS,Diblock}$ and $N_{PS,\ Homopolymer}$ being the number of styrene repeat units in the PS-*b*-PEO diblock copolymer and the PS homopolymer respectively. $n_{PS,\ Hompolymer}$ and $n_{PS,Diblocks}$ represent the number of moles of PS in the homopolymer and the copolymer. When plotting the condensed area per EO unit versus the apparent number of styrene units (Figure 3-5), a linear dependence can be observed ($R^2 = 0.9932$) with a trendline of $y = 0.0001\ x + 0.0753$.

The positive y-intercept shows us that even without any PS present in the monolayer, the PEO occupies 7.5 $Å^2$/EO units. This value is significantly smaller than the one observed for star copolymers by Logan *et al.* (16 $Å^2$/EO). [48,51] When PEO homopolymers are compressed at the air-water interface, no condensed area is observed. Without the presence of PS as an anchor, the PEO eventually dissolves in the aqueous subphase. In our case, while most of the PEO homopolymer remains aggregated to the PEO blocks of the copolymer, some of it could be dissolving in the water, explaining the smaller occupied area.

The collapse area plotted vs. the total number of styrene units follows the trendline $y = 0.0288\ x + 17.914$. The area per styrene unit obtained from the slope (2.9 $Å^2$) is smaller than the one J. Logan described for the behavior of star copolymers of PS-*b*-PEO at the air-water interface (ranging from 6.2-8.3$Å^2$, depending on architecture).[51] She reports the results for $(PEO_{26})_8$-$(PS_{42})_8$ (an 8 arm PS-*b*-PEO star copolymer with each arm containing 26 EO units and 42 Styrene units) which has a total of 336 repeat units of PS. For Blend 4 which has a total number of PS repeat units of 355, the PS homopolymer occupies an area equal to 5nm^2. This value is in the same range as the area per styrene value found in the literature for an atactic PS in

the bulk, calculated from the radius of gyration (38Å).[59] The PS, not covalently bound to the PEO, tends to adopt a random coil conformation less compact than the conformation produced by the PS segments of the copolymers. This copolymer can be compared to Blend 4 which presents a total of repeat units of 355 for the PS (using the formula described previously). J. Logan obtained a value of 28.6 nm^2 which is similar to the value obtained for Blend 4.

3.1.4 Blends of a PS-*b*-PEO diblock copolymer and PEO homopolymer

Contrary to PS, PEO is an amphiphilic polymer forming monolayers at the air-water interface. The addition of a PS block as an anchor keeps the PEO from going into the water subphase. This also allows the formation of more compact films by compressing at higher pressures. The effect that unencumbered PEO has on such films is examined in this part of the discussion where blends of the copolymer and homopolymer PEO were studied (Table 3-4).

Figure 3-7 shows the isotherm data for several blends of the 32,500$g.mol^{-1}$ PS-*b*-PEO copolymer and a 100,000 $g.mol^{-1}$ PEO homopolymer. The same transitions can be observed for all the copolymers independent on the amount of PEO added. When looking at the compressibility plots in Figure 3-8, one can see that when increasing PEO the local maximum present at 10mN/m increases. This suggests a PEO-related transition at 10mN/m.

3.1.4.1 Pancake Region (I)

Similar analysis was done for the homopolymer PEO blends as that seen for the PS ones. As with the pure copolymer, the resulting isotherms displayed all three regions. A_P was obtained for each blend and for the pure PS-*b*-PEO from the π-A isotherms (Table 3-5).

The pancake area depends linearly on the total number of ethylene oxide units (R^2 = 0.9968) with a trendline of y = 1.1297 x – 173.95. The area obtained from the slope (1.13 nm^2) is significantly higher than the one observed by Sauer *et al.*[81] for a PEO homopolymer (0.40-0.48 nm^2). Gonçalves da Silva *et al.*[34,39] recorded a smaller area for PS-*b*-PEO diblock copolymers

(0.27 and 0.31 nm^2). This can be explained by the fact that the PEO chains from the homopolymer pack less closely when in the presence of the PS-*b*-PEO diblock copolymer.

We can also observe a negative y-intercept indicating that all the EO units are not at the interface. In such a case, a pancake area equal to zero should correspond to zero EO units. Even with a negligible effect on the pancake area, the PS units may trap some of the PEO, leading to a lower apparent number of PEO units.

3.1.4.2 Pseudoplateau Region (II)

The addition of PEO, however, has an effect on the shape of the pseudoplateau observed for a pressure around 10mN/m. The more PEO is added to the monolayer, the longer the biphasic region becomes. To illustrate this point, $A_{Transition\ 2}$ (Figure 2-5) was recorded for each blend as well as for the pure diblock. The results are given in Table 3-6.

A graph of $A_{Transition\ 2}$ vs. the ratio of number of moles of homopolymer vs the number of moles of diblock shows a linear dependence ($R^2 = 0.994$) with a trendline of $y = 1082.9\ x + 47.532$ (Figure 3-9). To be able to compare those results to those published previously for pure diblocks or star copolymers, an identical formula as the one used in the previous part was developed. While $A_{Transition\ 1}$ remains constant for every blend, one can observe an increase in $A_{Transition\ 2}$ indicating the presence of a larger pseudoplateau area.

$$N_{PEO,TOT} = N_{PEO,Diblock} + N_{PEO,Homopolymer} \times \frac{n_{PEO,Homopolymer}}{n_{PEO,Diblock}} \qquad 3\text{-}2$$

The values calculated using this formula, are reported in Table 3-7.

A linear dependence ($R^2 = 0.9942$) was observed when the area for the second transition was plotted vs. the total number of repeat units of PEO, yielding a trendline of $y = 0.4769\ x - 66.032$ (Figure 3-10). This dependence is detected in the compressibility plots also showing a higher local maximum when increasing the amount of PEO (Figure 3-8).

These observations compare to those seen by Fauré *et al.*[40] They studied the phase transitions in monolayers of PS-*b*-PEO copolymer at the air-water interface for different PEO block sizes. Fauré *et al.* observed an increase in the length of the pseudoplateau as the number of PEO units increases. The transition from pancake to brush becomes more and more first order as they increase the PEO segment size.

In addition, one of the diblock copolymers they studied consisted of 31 repeat units of PS and 700 of PEO, a PEO amount similar to that of Blend 4. The Fauré copolymer demonstrates a π-A isotherm with an almost flat pseudoplateau, confirming the first order transition of the copolymer. Similarly, Blend 4 displays a pseudoplateau representing a strong indication of a first order transition. By adding PEO homopolymer to our monolayer, we have been able to broaden the range of the copolymer properties without going trough time-consuming synthetic techniques in order to increase the size of the PEO block.

3.1.4.3 Condensed Region (III)

This third region appears at higher surface pressures beyond the pseudoplateau. As demonstrated by Shuler and Zisman,[45] such a region does not exist for a PEO homopolymer, as no anchor exists to prevent PEO from completely immersing in the water subphase. This region depends only on the length of the PS blocks and not on PEO, as demonstrated by the π-A isotherms of the different blends in Figure 3-7. A_0 remains the same regardless of PEO added (23.7 nm^2).

By blending a PS-*b*-PEO diblock copolymer with its corresponding homopolymers, we were able to mimic linear chain behavior by manipulating PS and PEO quantities. On one hand, the addition of PS has proven to have the same effect on the copolymer behavior as increasing the PS block size. We see an increase in the condensed area while adding more PS homopolymer

to the system. On the other hand, raising the amount of PEO only had an effect on the biphasic region of the isotherm.

While this technique could be a good alternative to time-consuming synthetic techniques and expensive sample purchases, experiments still need to be performed with various molecular weight homopolymers as well as hysteresis data in order to better understand the aggregation behavior of those films.

Additional analysis continues in the next section in which the blends are transferred as Langmuir-Blodgett films and examined through atomic force microscopy (AFM).

3.2 Atomic Force Microscopy (AFM) Experiments

AFM is a technique that provides the opportunity to study surface morphology and structure at the submicron scale. By investigating transferred Langmuir-Blodgett films, AFM can give insight into the behavior of the copolymer blends at various pressures, providing both quantitative and qualitative results. Such data helps demonstrate the degree of interaction between the copolymer and homopolymers. The hydrophilicity of the substrate allows us to consider the hydrophilic PEO to be attached to the mica whereas the hydrophobic PS occupies a higher layer. By consequence in the AFM images, the PEO is represented by the darker (lower) areas whereas the PS exists as the brighter (higher) domains.

The AFM software contains several functions for image analysis. One method represents the three-dimensional surface plot of the imaged sample, as shown in Figure 3-12. The color shading is a representation of the height of the features on the sample (up to 7.3nm for Figure 3-12, for example).

Precise height data can be obtained for given domains through section analysis. This technique is illustrated in Figure 3-13. A line is traced across the domain region of interest, giving a cross-sectional view of the sample. In this example, the height difference between the

two marked domains is 1.2nm and the difference between the domain at the left and the PEO surface (brown) is 4.5nm.

3.2.1 Linear Polystyrene-*block*-Poly(ethylene oxide) (PS-*b*-PEO) Diblock Copolymer

AFM is a valuable technique for studying morphologies formed by spreading copolymer solutions at an aqueous subphase. Bodiguel *et al.* demonstrated the complementary nature of AFM and TEM in depicting phase separation of two distinct polymer blocks.[96] The technique assumes that the morphology of the transferred film represents that of the floating monolayer and that transfer is homogeneous. For pressures below the pseudoplateau pressure, transfer ratio (TR) were found to be close to unity (~1.10) implying a homogeneous transfer. However, once the pseudoplateau pressure is reached, a decrease in TR is observed (~0.40) suggesting that the films observed by AFM are less condensed than the floating monolayer. In the case of a TR equal to 1, the image observed for a pressure of 15mN/m should show a homogeneous layer of PS. However, we observed large domains surrounded by areas of PEO. The TR of 0.40 leads us to the conclusion that the monolayer expanded after transfer onto the mica substrate and does not represent the structure we would observe directly onto the water subphase. Langmuir-Blodgett (LB) films were prepared at several surface pressures and then studied using AFM in tapping mode. For each sample, an average of ten images was taken to ensure reproducibility.

The images shown in Figure 3-14 clearly demonstrate the formation of ordered structures in which the observed morphology depends on surface pressure. In fact, three distinct regions corresponding to those in the isotherm can be seen once again. For pressures of 4 and 7 mN/m (Region I of Figure 3-2.), images show a majority of single domains, typical of an expanded liquid. Two-dimensional micelles form at the air-water interface with a morphology depending on the ratio of the hydrophobic and hydrophilic block sizes. For pressures under 7mN/m, circular

micelles are observed like the one described by Potemkin *et al.*[105] (Figure 3-15) where one of the blocks is strongly adsorbed on a planar surface.

In the case of PS-*b*-PEO at the air-water interface, similar micelles are observed with the PEO extending more and more in the aqueous subphase as the concentration increases (Figure 3-16).

When compression continues and reaches the pseudoplateau range (Region II of Figure 3-2), chain formation is detected and continues until the collapse pressure is attained. The images also demonstrate the presence of intermediate stages in which the single domains begin to aggregate prior to chain formation.

Due to the hydrophilicity of the mica, we suppose PEO represents the bottom layer whereas PS occupies the top part of the LB film at a thickness of some nanometers, ranging from about 2 to 10 depending on the blend. In our images, the darker layer represents PEO and the bright domains show the PS blocks. Using a program described above, the number of domains per image was found, allowing the molecules per domain (or aggregation number) to be calculated.

For each given pressure, the aggregation number was determined using equation 3-3.

$$\Gamma = A/N_d.\sigma \qquad 3\text{-}3$$

where Γ refers to the number of molecules per domain, A the scanned area of the image, N_d the number of domains, and σ the mean molecular area during transfer. As shown in Figure 3-17, the number of molecules/domain depends strongly on the surface pressure. For pressures less than 10mN/m, the number of molecules/domain remains almost constant. However, once the pressure of the pseudoplateau is reached, an increase in aggregation number is observed.

As compression continues, aggregation increases and at the transition between Regions II and III, the aggregation number rises sharply. This behavior is another indication of the transition between the liquid expanded state and the liquid condensed state. Logan *et al.*[48,51] showed that compression-induced aggregation occurs when PEO is pushed into the aqueous subphase. However, at higher pressures, some PEO can remain at the interface and separate the PS domains. This situation represents two conflicting forces. The attraction between PEO and the water allows the polymer to spread on the surface, whereas the repulsion of PS with both water and PEO drives aggregation. Cox *et al.*[41,42], however, thought the relative interaction of the two blocks with the subphase and air is a more probable explanation for the existence of aggregation.

3.2.2 Blends of a PS-*b*-PEO diblock copolymer and a PS homopolymer

To observe the possible formation of aggregates between copolymer and homopolymer, the blends were studied by AFM for different transfer pressures. Transfers for pressures equal or below 10mN/m are considered homogeneous (TR~1.04) while transfers made for pressure above the pseudoplateau pressure (TR~0.40) indicate that the aggregates observed by AFM are less packed than those present at the air-water interface. In Figure 3-18, the AFM images for the pure diblock, Blend 2, and Blend 5 at several transfer pressures are given. As described previously, a chaining of the domains is observed for the pure PS-*b*-PEO when increasing the pressure. However, in the blend case, the addition of PS homopolymer seems to inhibit the formation of these chains. In Figure 3-19, the histograms of the domain area are given for both films at a transfer pressure of 10 mN/m. The pure diblock exhibits larger domain areas whereas the blend seems to exhibit the formation of big and small domains.

In the pancake region, the pure diblock exhibits local hexagonal packing with six neighbors for each domain, showing that even at low pressure, the copolymers arrange into

surface micelles. In the case of the blends, the addition of PS to the monolayer disrupts this packing by increasing the size of only some of the domains and enabling a population of smaller domains to form (Figure 3-19). The PS homopolymer aggregates with some of the PS blocks from the copolymer increasing the size of the domains observed by AFM. The addition of PS in the domains increases their attractive forces on the free PS.

This behavior can be compared to that described by Logan,[48] Logan *et al.*,[51] and Francis *et al.*,[49,50] for PS-*b*-PEO star copolymers of various hydrophobicity. For both stars and linear chains in the literature (particularly Devereaux and Baker[43]), increased PS results in nonuniform films with a greater variety of morphology. As pressure increases, no chaining is observed in the case of the blend. In fact instead of chaining, an augmentation in population of the bigger domains compared to the small domains can be observed. This phenomenon can be shown by using the computer program designed by Yves Heckel. Histograms of the domain areas are given in Figure 3-20.

In the pure diblock, formation of large chains that resemble pearl necklace-like strings occurs as the transfer pressure is increased. This phenomenon starts with the formation of domain "dimers" or "trimers" at a pressure of about 7mN/m that then keep on chaining with increased pressure. When PS is added to the monolayer, no such domains are observed. An increase in the size of the circular domains is observed, indicating the aggregation of the PS homopolymer within the PS chains of the copolymer (Figure 3-21).

3.2.3 Blends of a PS-*b*-PEO diblock copolymer and a PEO homopolymer

In a similar way, blends of the copolymer and a PEO homopolymer were transferred homogeneously onto a mica substrate (TR~1.07) in order to study the evolution of the morphologies depending on the amount of PEO added. Results are shown in Figure 3-22.

At low pressure, we can observe the disappearance of the hexagonal packing when increasing the amount of PEO. This behavior can be compared to that of PS-*b*-PEO star copolymers studied by Logan,[48] and Francis *et al.*,[49,50] By increasing the hydrophilicity of the stars, they observed a decrease in the number of domains and an increase in the distance between each domain. While less uniform, this same effect appears in the blends as a result of PEO homopolymer aggregation to the PEO chains of the diblock copolymer. To remove the artifacts than could have been formed by spreading successively the pure copolymer and the homopolymer, a mixed solution was made and this was spread as a comparison. The proportions were the same as the one used for Blend 2 and the film was transferred at a pressure of 9mN/m. The AFM images are shown in Figure 3-23.

Those experiments show that independent of the spreading technique, an increase in PEO composition results in the formation of longer chains than for the pure copolymer sample. A second effect of increased PEO content is the apparition of a phase separation between pure layers of PEO surrounding clusters of micelles.

In addition, the addition of a copolymer to a PEO homopolymer monolayer increases its stability and allows the formation of films at higher pressures than that of a pure PEO monolayer which collapses at 10mN/m.[45] The difference between the morphologies at high pressure for the pure diblock and for the blends shows that the PEO homopolymer aggregates with the copolymer instead of dissolving into the aqueous subphase.

3.3 Conclusions

When adding the homopolymers to the pure diblock copolymer at the air-water interface, reproducible isotherms were obtained and displayed the three regions present in a pure diblock copolymer (pancake, pseudoplateau, and brush). While the increase in the PS amount had an effect only on the condensed area (varies linearly with the amount of PS added), by combining

PEO and the copolymer, no change was observed in the condensed region of the isotherms. The length of the pseudoplateau representing the biphasic region increases as the amount of PEO gets more important. This behavior has also been observed for pure diblocks as well as for star copolymers when increasing the size of the PEO block.[48,51] AFM images were taken and were consistent with the isotherms showing the three regions described previously. On one hand, the addition of PS to the copolymer monolayer inhibited the chaining of the copolymer domains and enhanced the hydrophobic properties of the Langmuir-Blodgett film. On the other hand, combining the PS-b-PEO diblock copolymer with the PEO homopolymer also had an effect on the film morphology, increasing the chaining of the domains as well as favoring the phase separation between clusters of micelles and pure layer of PEO.

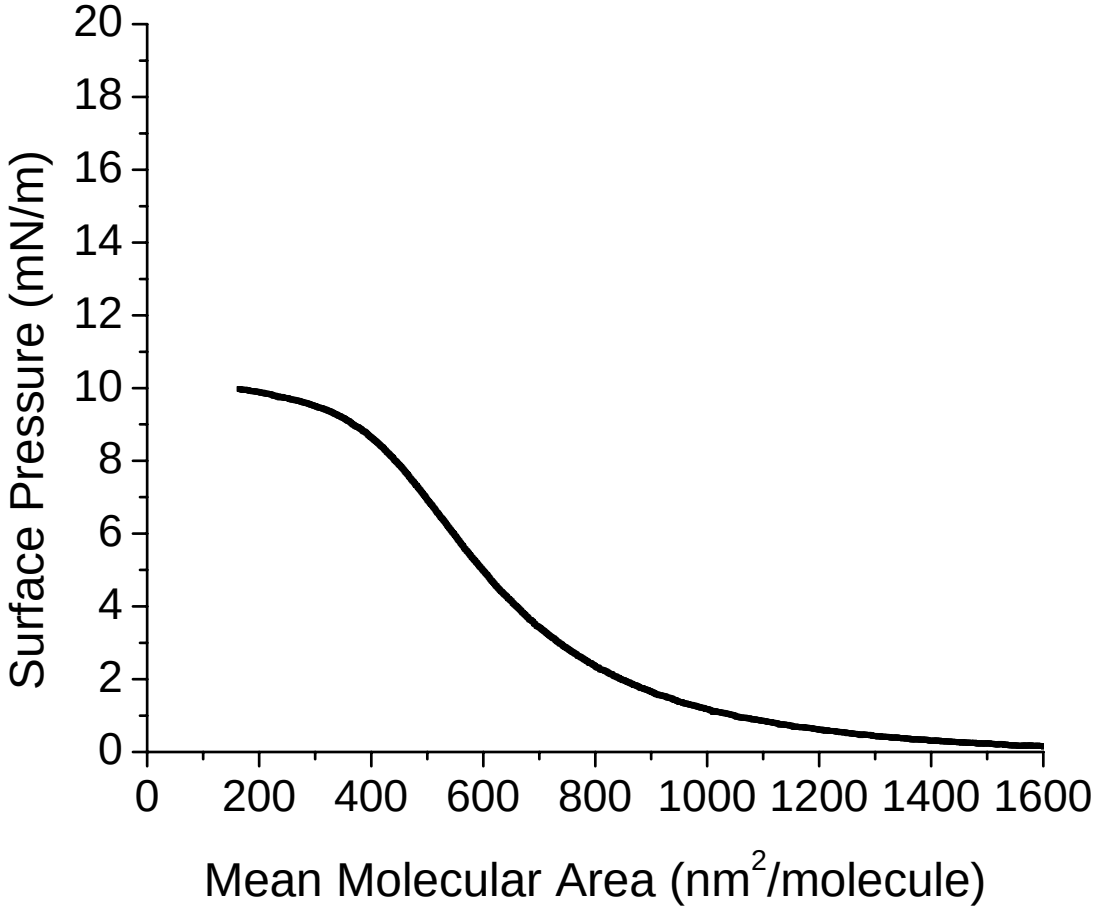

Figure 3-1. Surface pressure-MMA isotherm for the PEO homopolymer (Mn = 100,000g/mol) recorded for a compression speed of 5mm/min

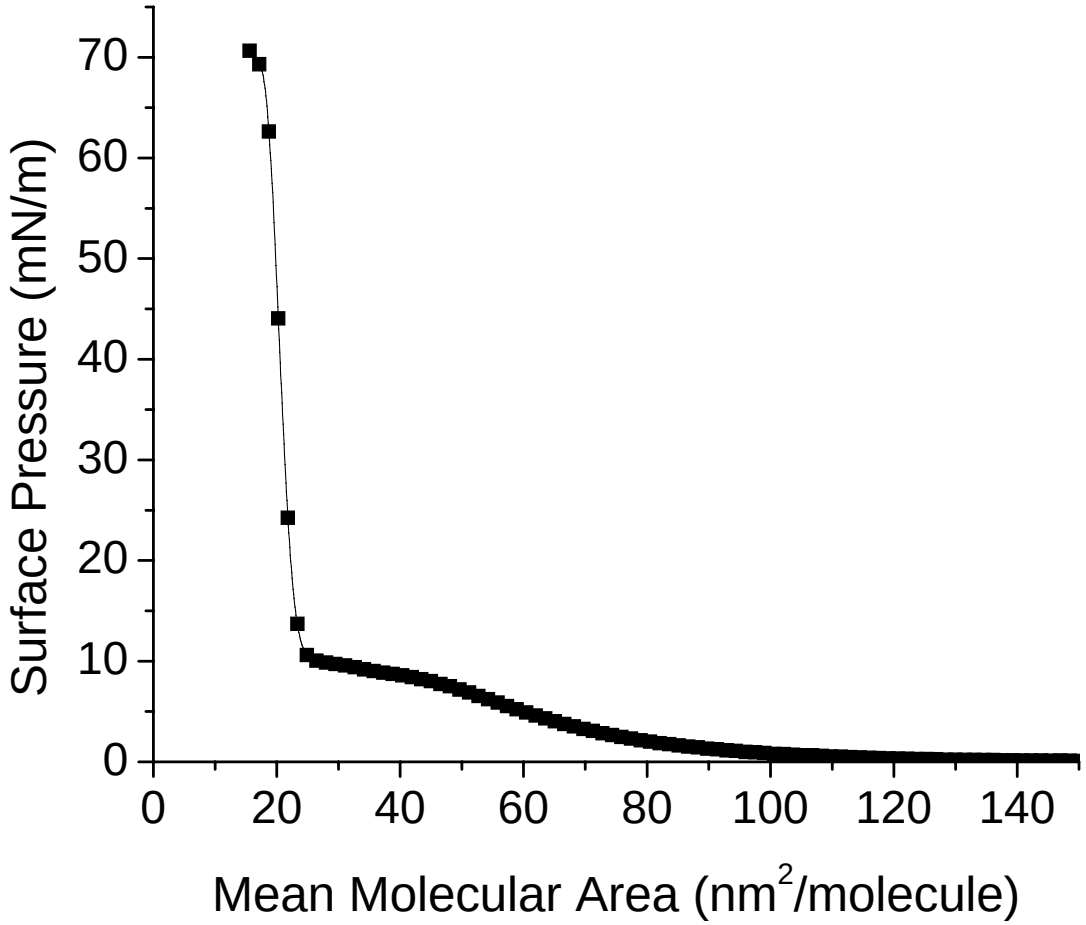

Figure 3-2. Surface pressure-MMA isotherm for the 32,500 g·mol^{-1} PS-*b*-PEO copolymer recorded for a compression speed of 5mm/min

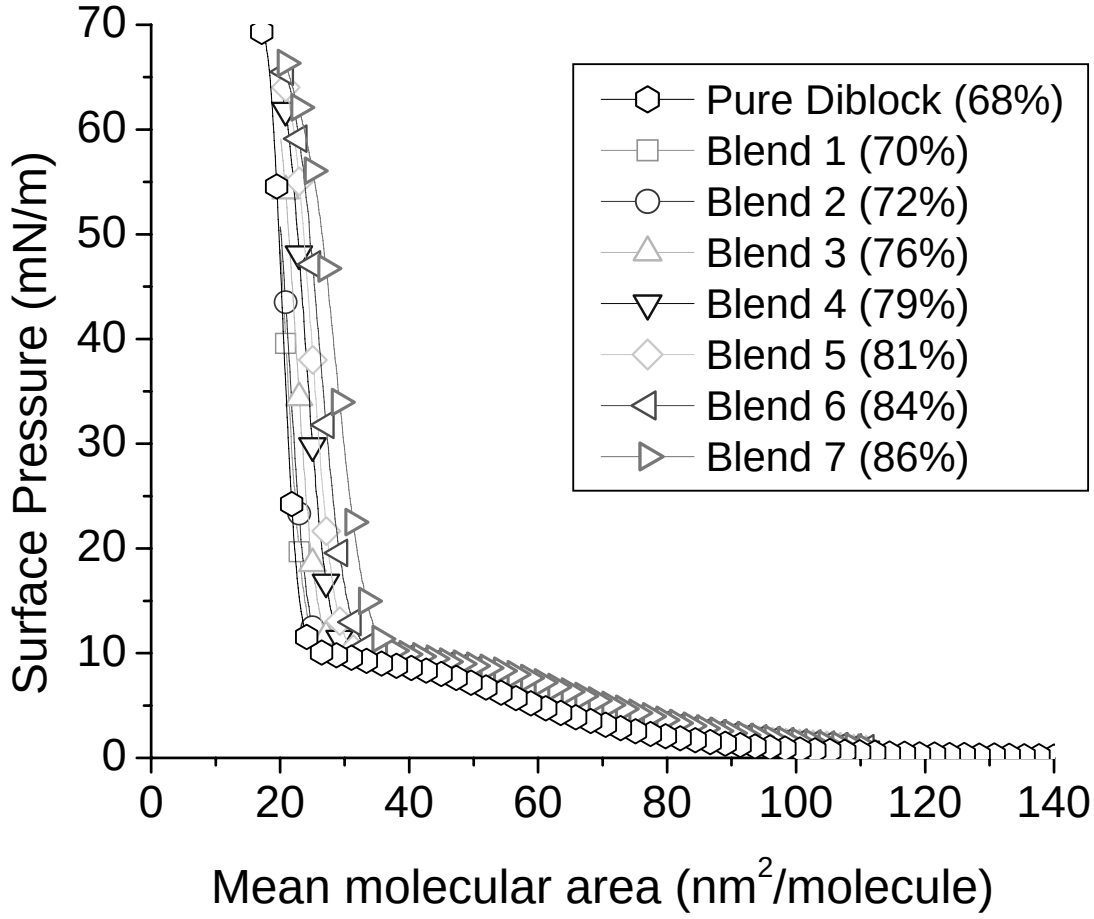

Figure 3-3. Several surface pressure-MMA isotherms are shown, indicating the dependence of surface pressure on the mean molecular area for different blend ratios. All the isotherm experiments were performed using a compression speed of 5mm/m

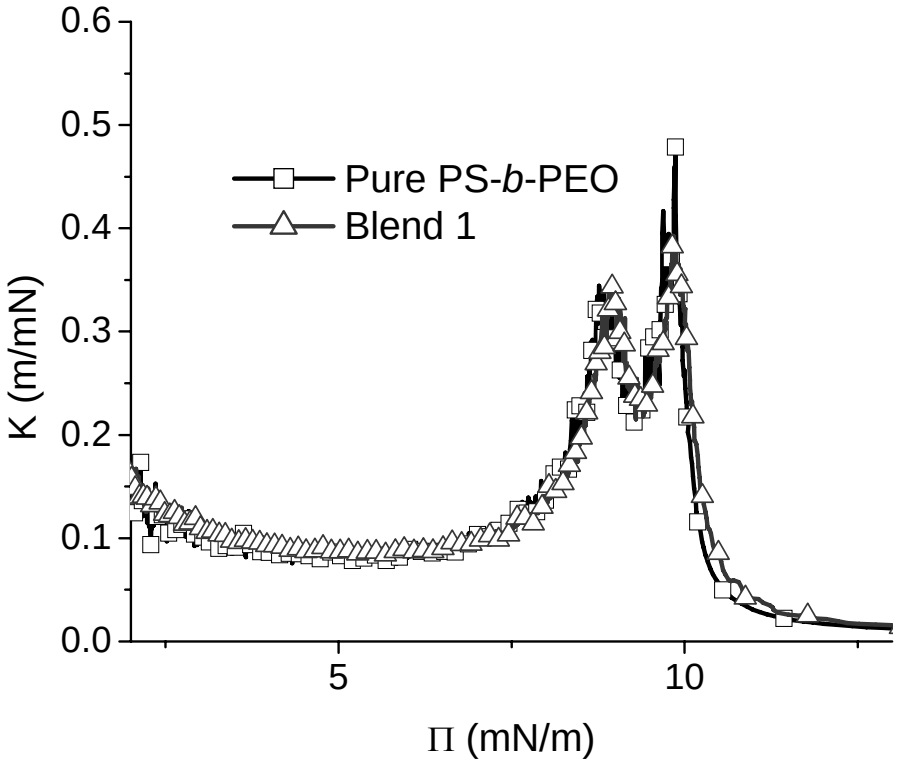

Figure 3-4. Monolayer compressibility plot for the PS-*b*-PEO copolymer and blend 1

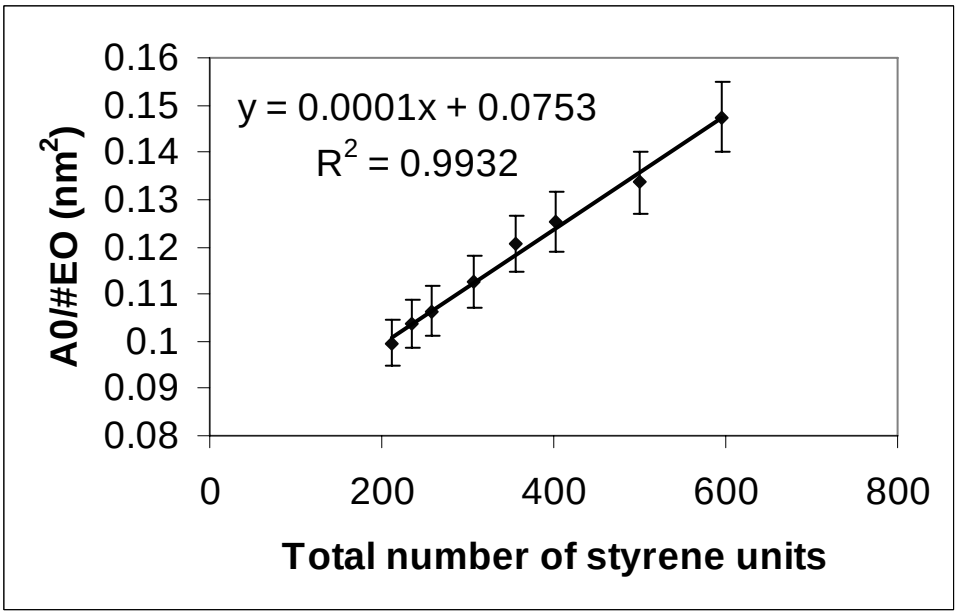

Figure 3-5. The condensed area per EO unit (A_0/EO) varies linearly with the number of styrene units present in the blends

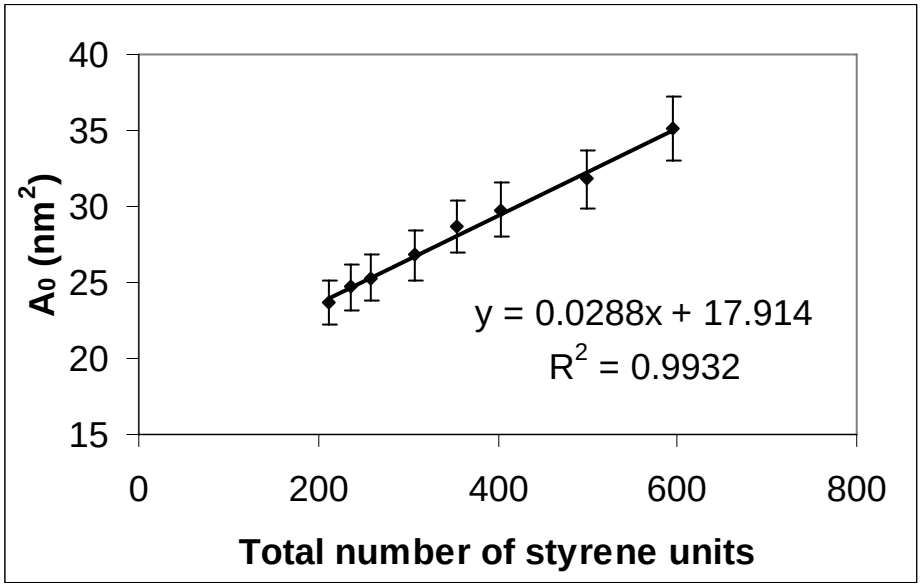

Figure 3-6. The condensed area (A_0) varies linearly with the total number of styrene units present in the blends

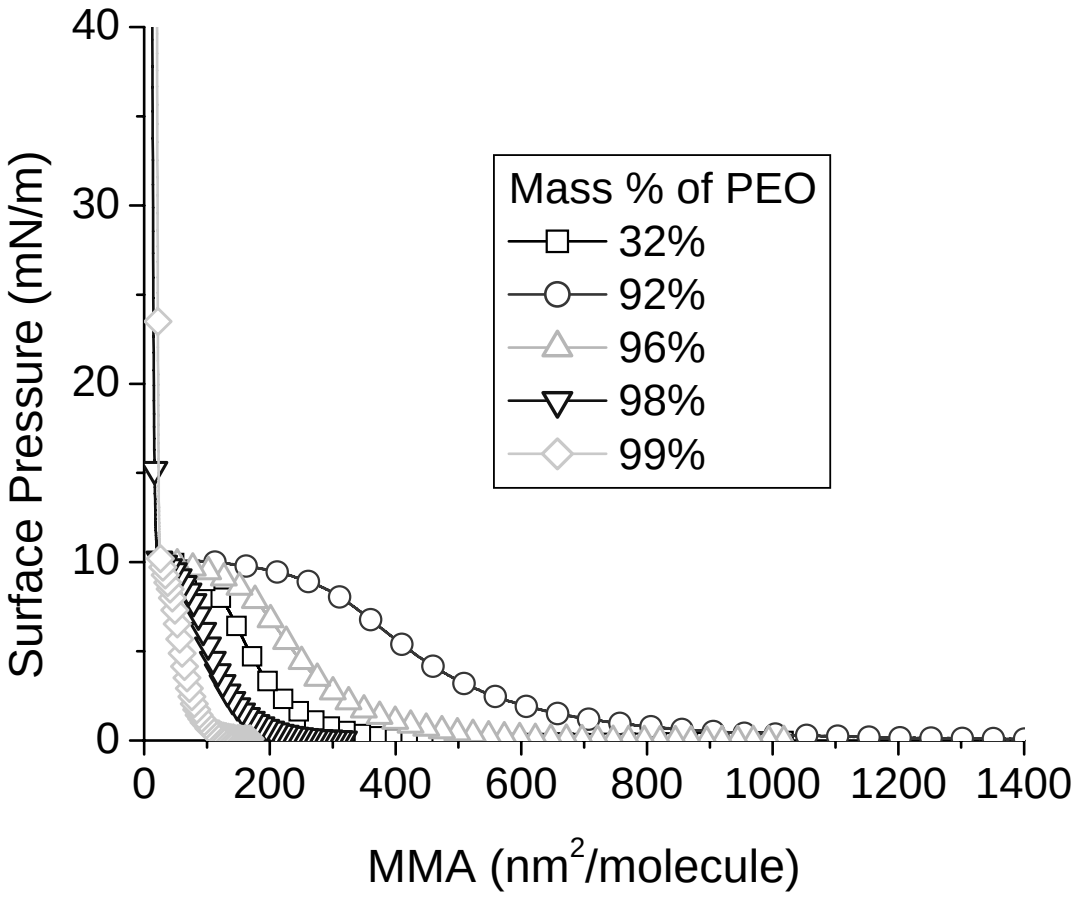

Figure 3-7. Several surface pressure-MMA isotherms are shown, showing the dependence of surface pressure on the mean molecular area for different amounts of PEO. All the isotherm experiments were performed using a compression speed of 5mm/min

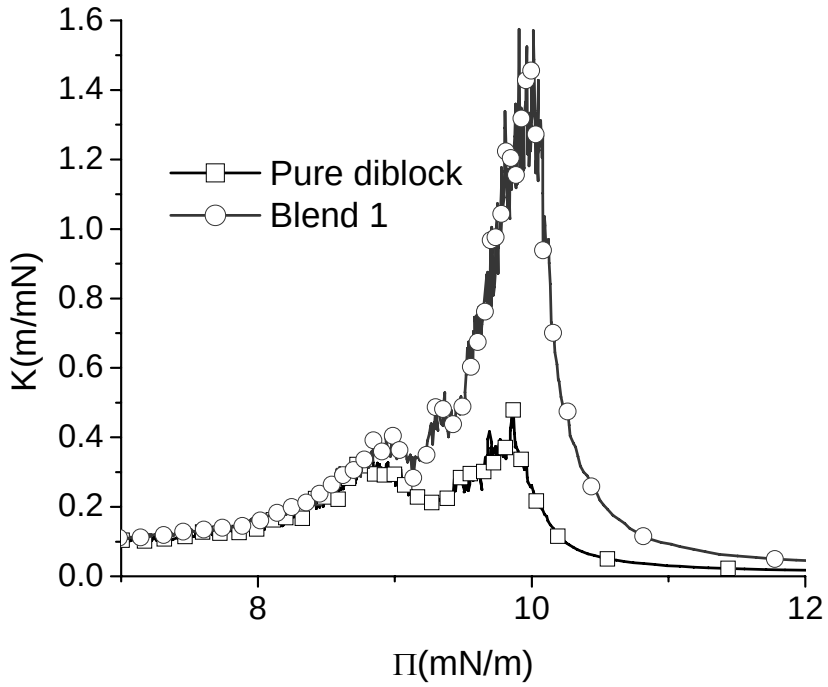

Figure 3-8. Monolayer compressibility plots for the PS-*b*-PEO diblock copolymer and blend 1

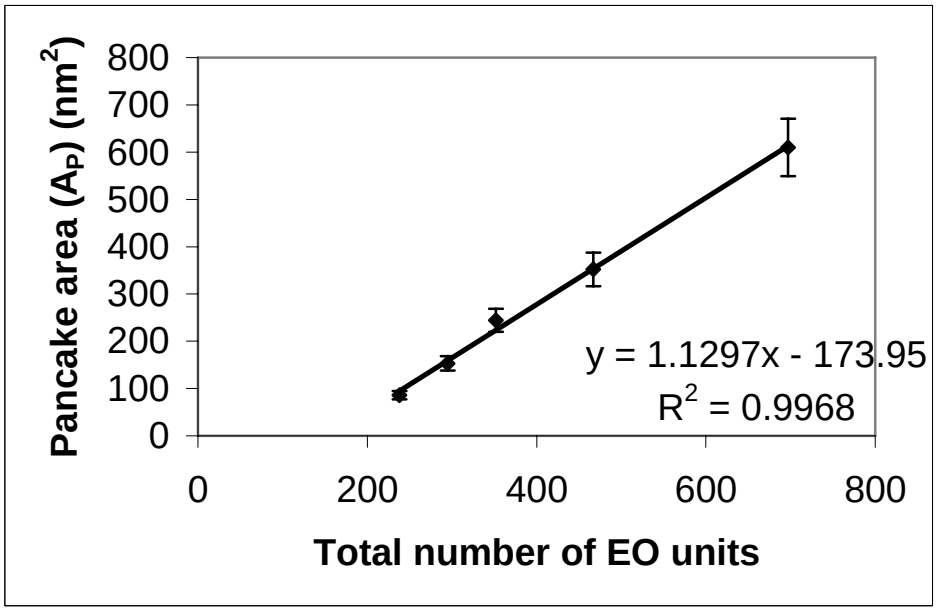

Figure 3-9. The pancake area (A_P) varies linearly with the total number of EO units present in the blends

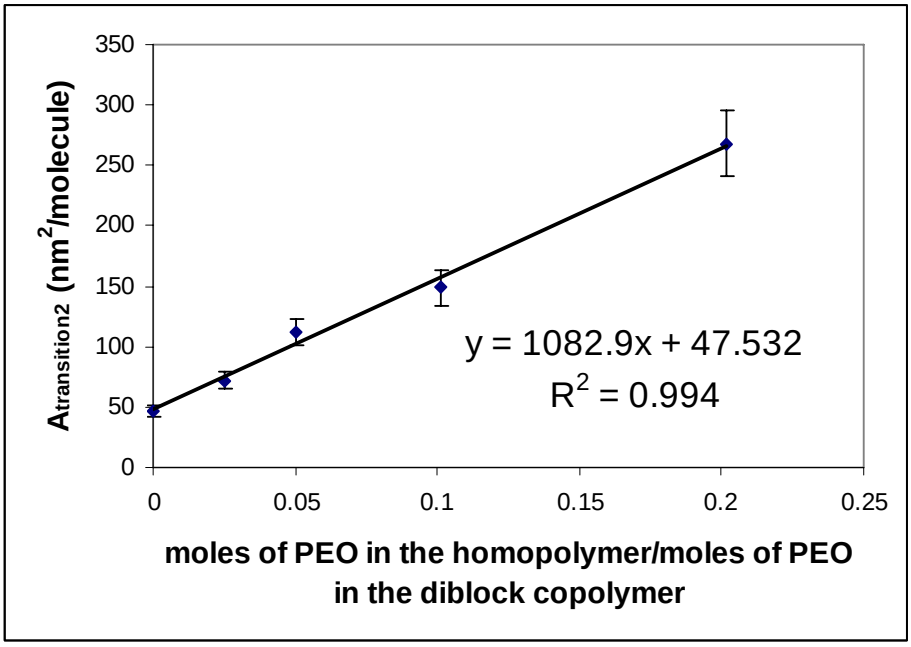

Figure 3-10. The area for the second transition depends linearly on the mole ratio of PEO from the homopolymer over PEO from the PS-*b*-PEO

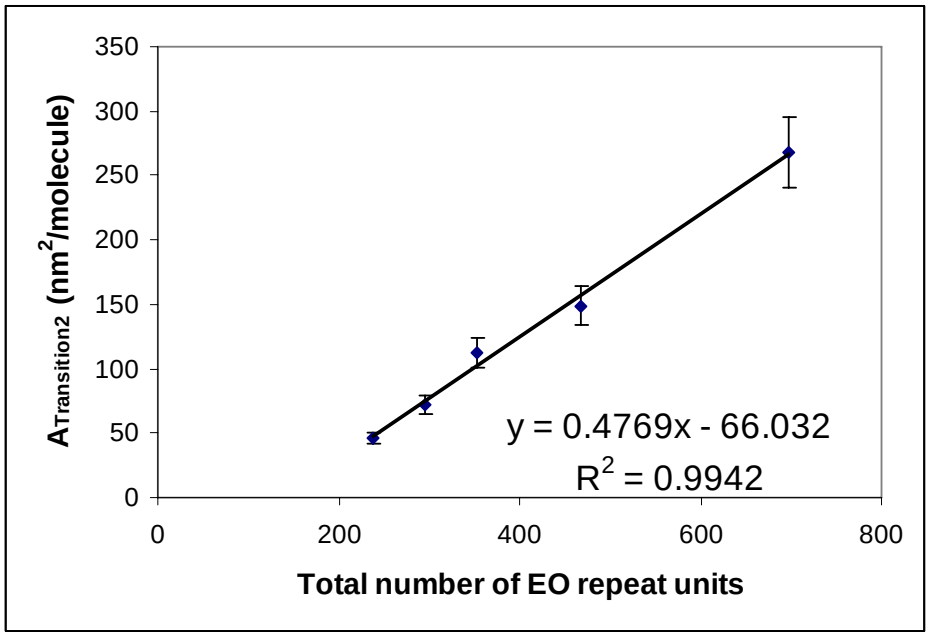

Figure 3-11. The area for the second transition depends linearly on the apparent total number of EO repeat units

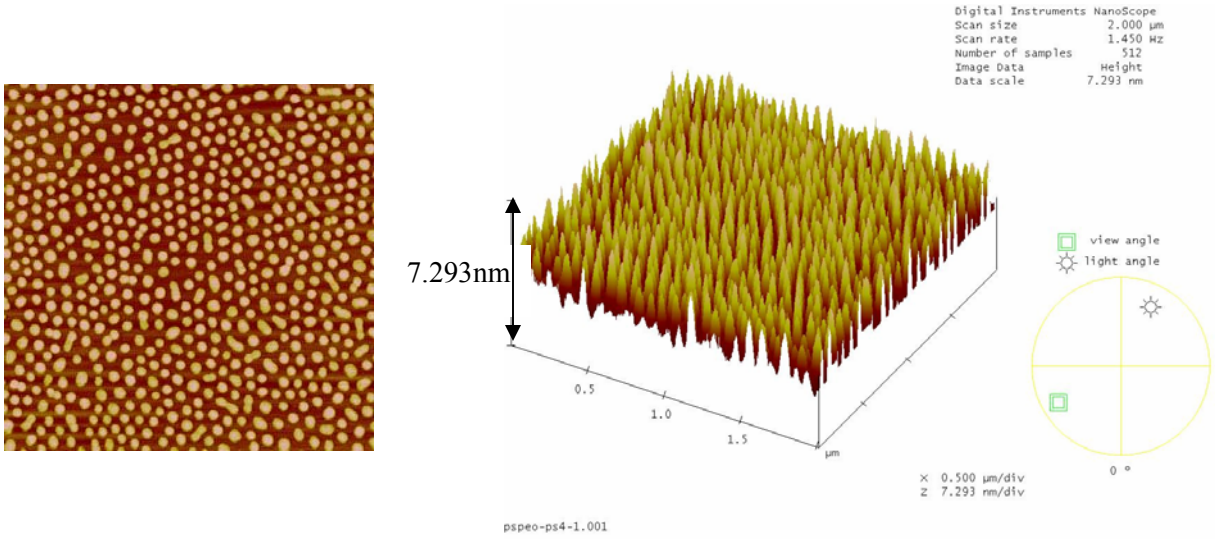

Figure 3-12. Example of a sample height image and surface plot (scan area shown is 2×2 µm)

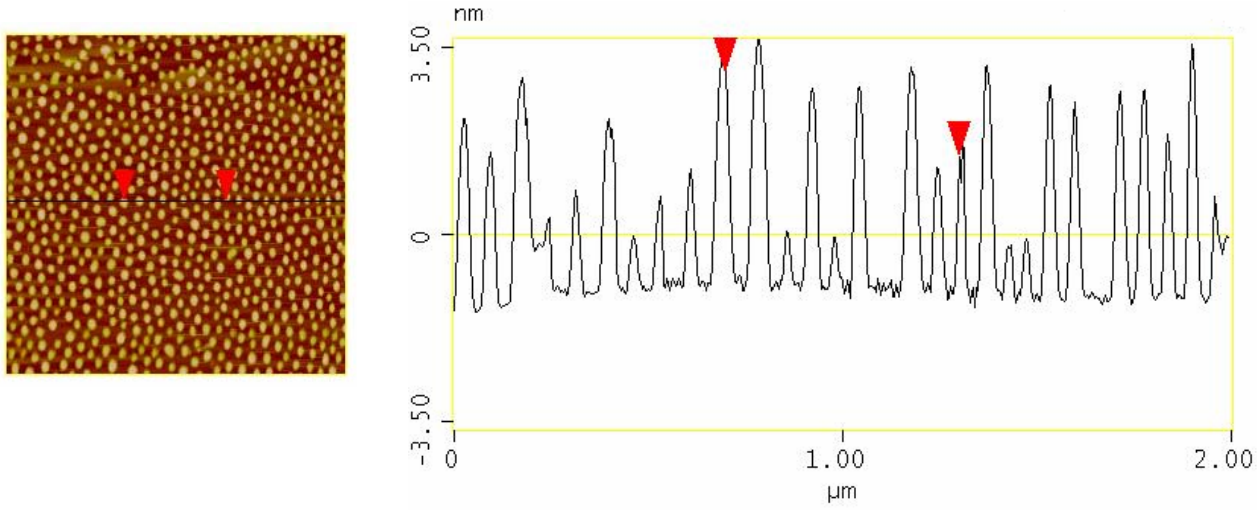

Figure 3-13. Example of a sample section image (2×2 µm)

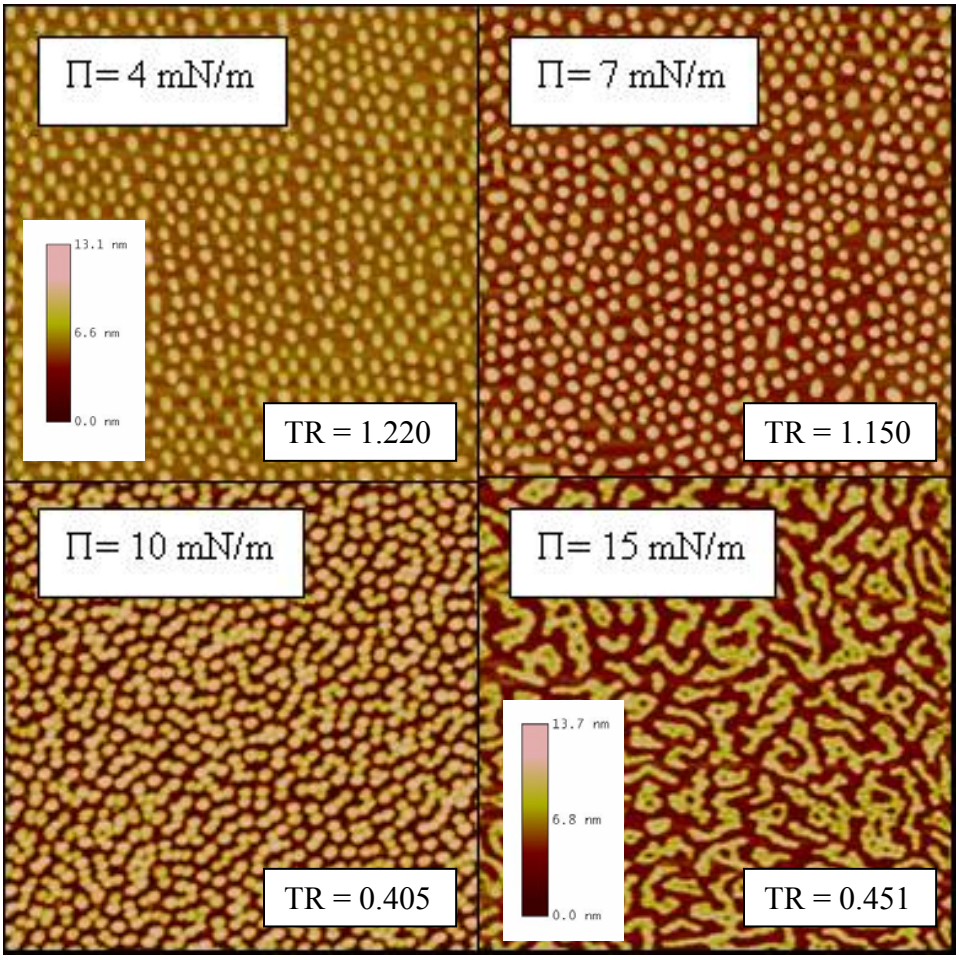

Figure 3-14. Height AFM images from tapping mode of the pure PS-*b*-PEO for several transfer pressures (scale 2×2μm). The transfer ratios are also given for each images.

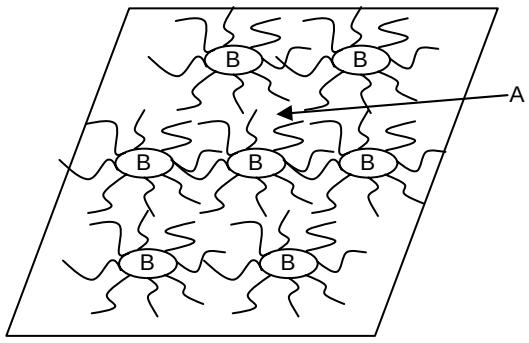

Figure 3-15. Schematic representation of surface micelles formed by A-b-B diblock copolymers with A strongly adsorbed to the surface (adapted from Potemkin *et al.*[105])

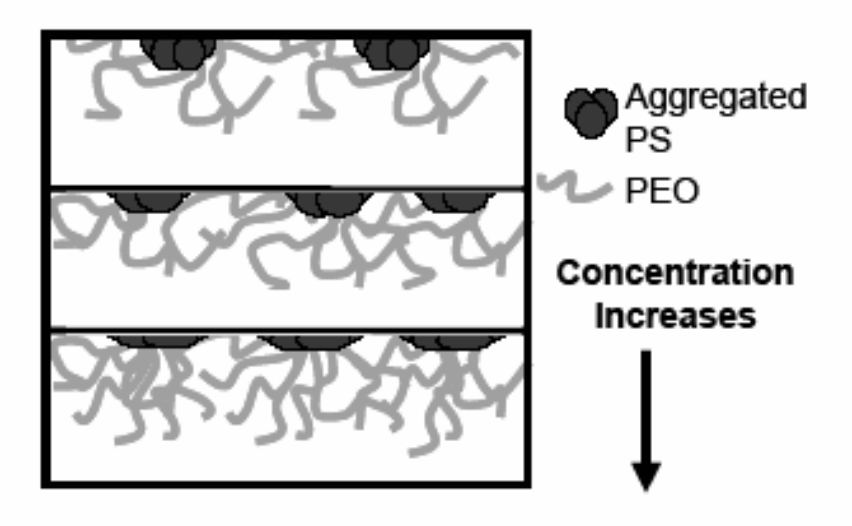

Figure 3-16. Model of PS-*b*-PEO absorbing at the air-water interface (Adapted from Dewhurst *et al.*[37])

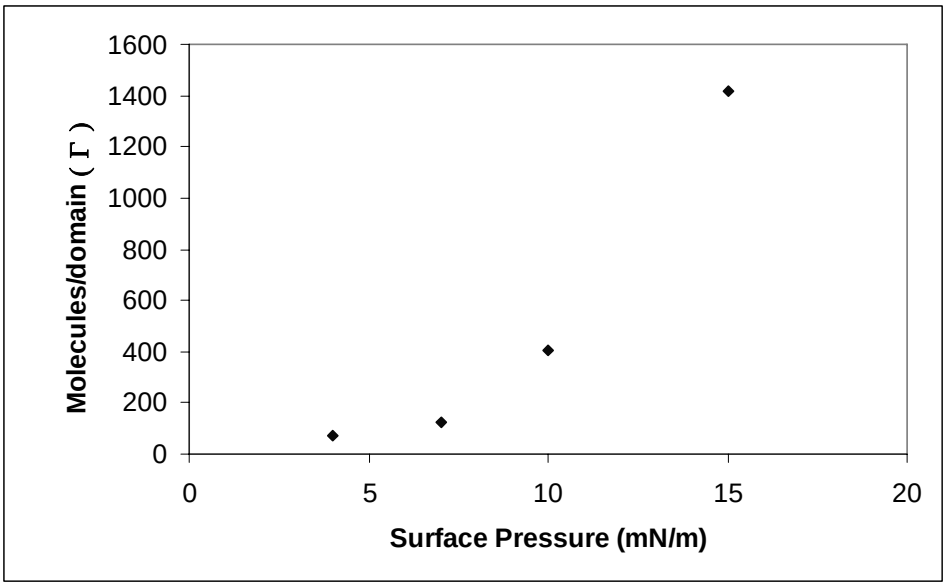

Figure 3-17. Dependence of the number of molecules per domain on pressure

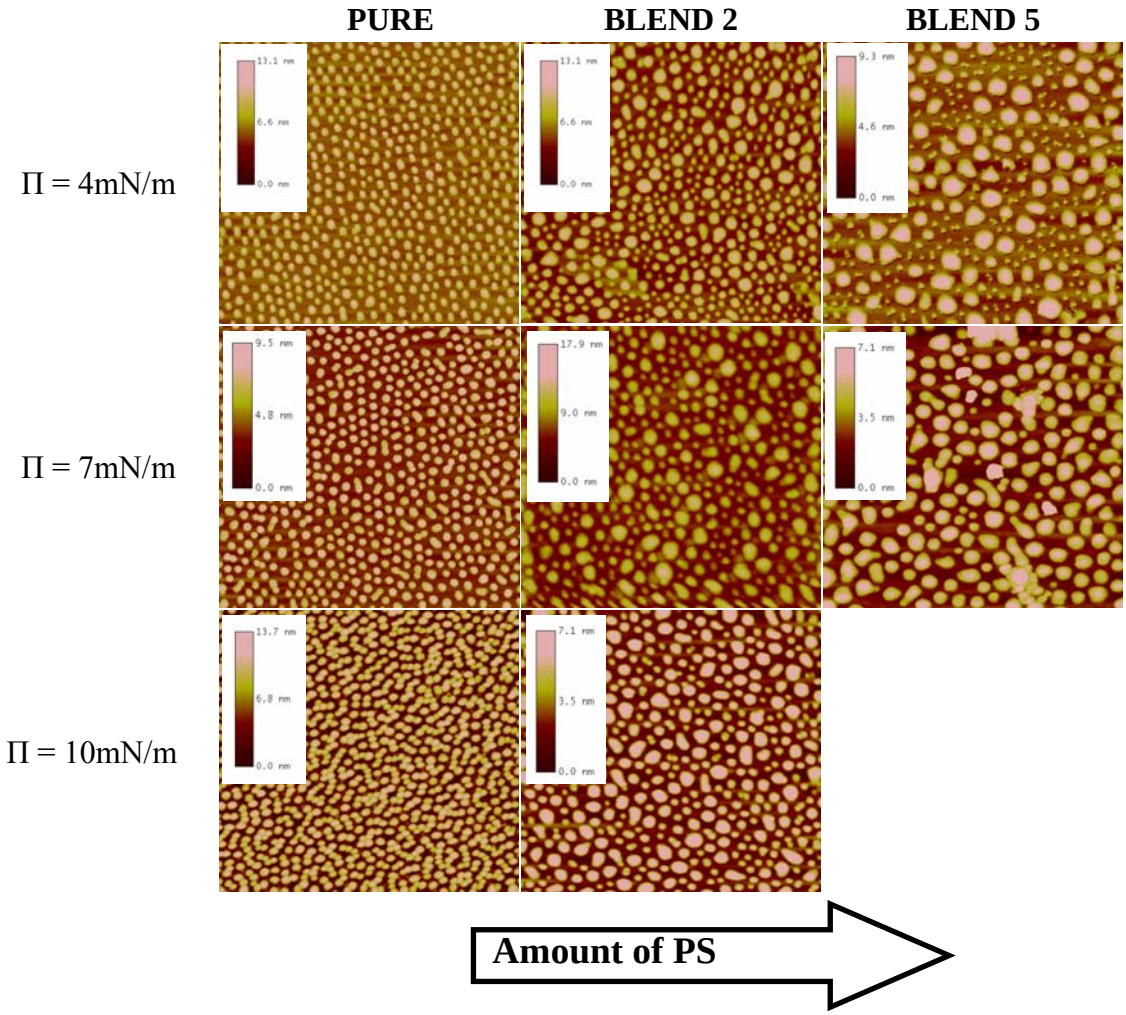

Figure 3-18. Height AFM images from tapping mode of the pure PS-*b*-PEO diblock copolymer as well as two of the blends for several transfer pressures (scale 2×2μm)

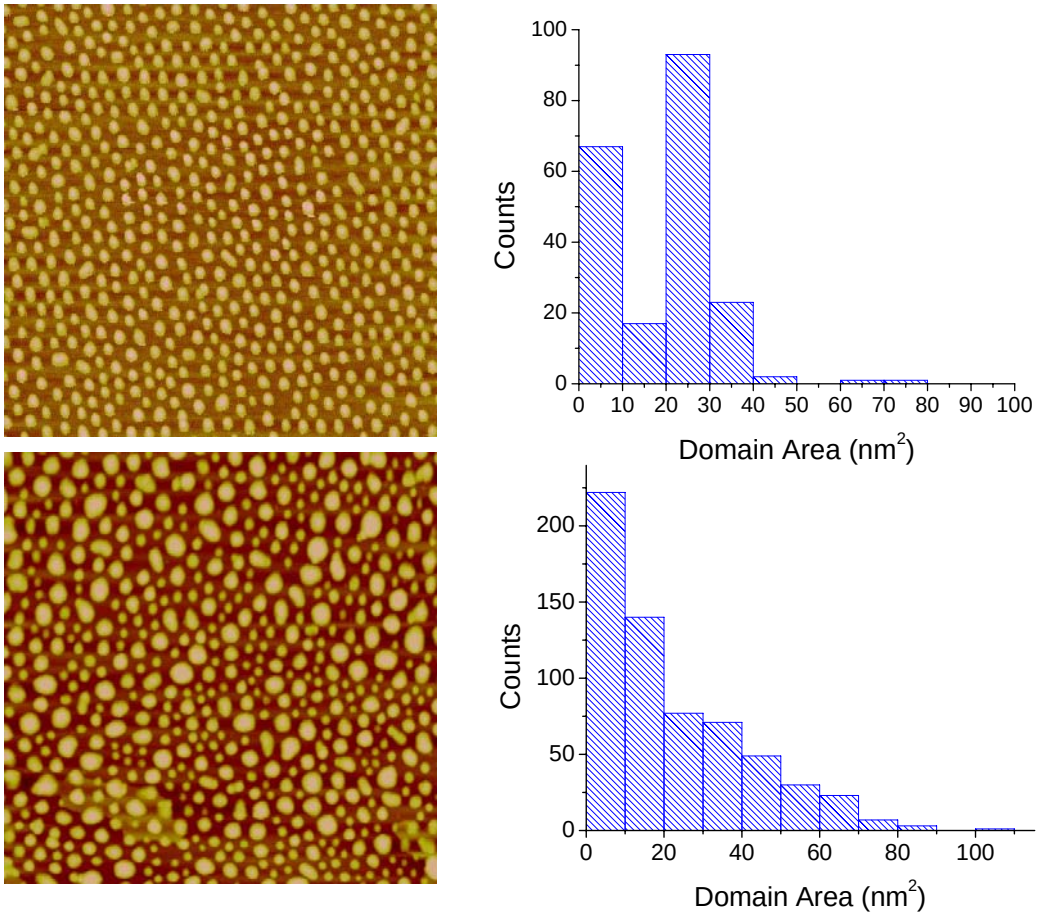

Figure 3-19. Height AFM images (scale 2×2μm) for the pure PS-*b*-PEO diblock copolymer and Blend 2 (transfer pressure of 4mN/m) as well as the distribution of the domain areas

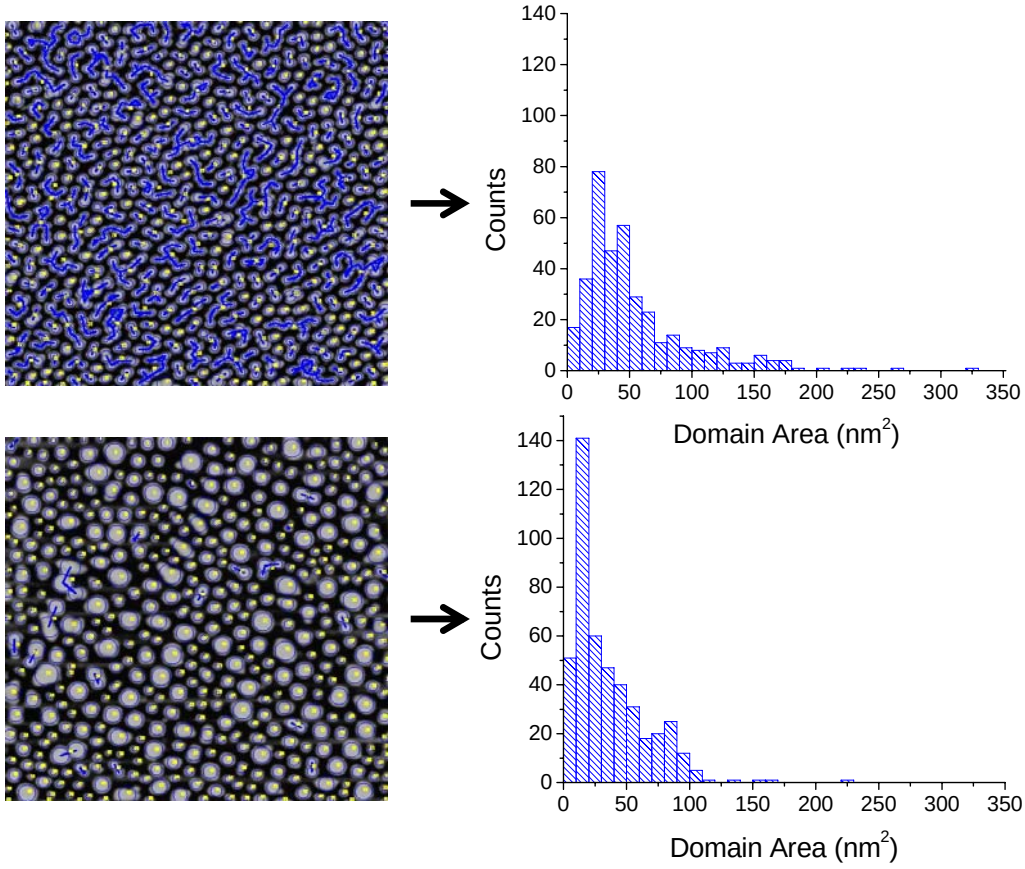

Figure 3-20. Computed images for the pure PS-*b*-PEO diblock copolymer and Blend 2 (transfer pressure of 10mN/m) as well as the distribution of the domain areas

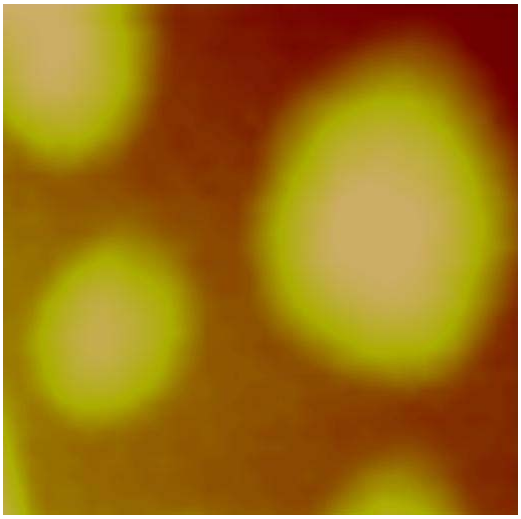

Figure 3-21. Magnification of a single domain formed for Blend 2 for a transfer pressure of 10mN/m (scale 150×150nm)

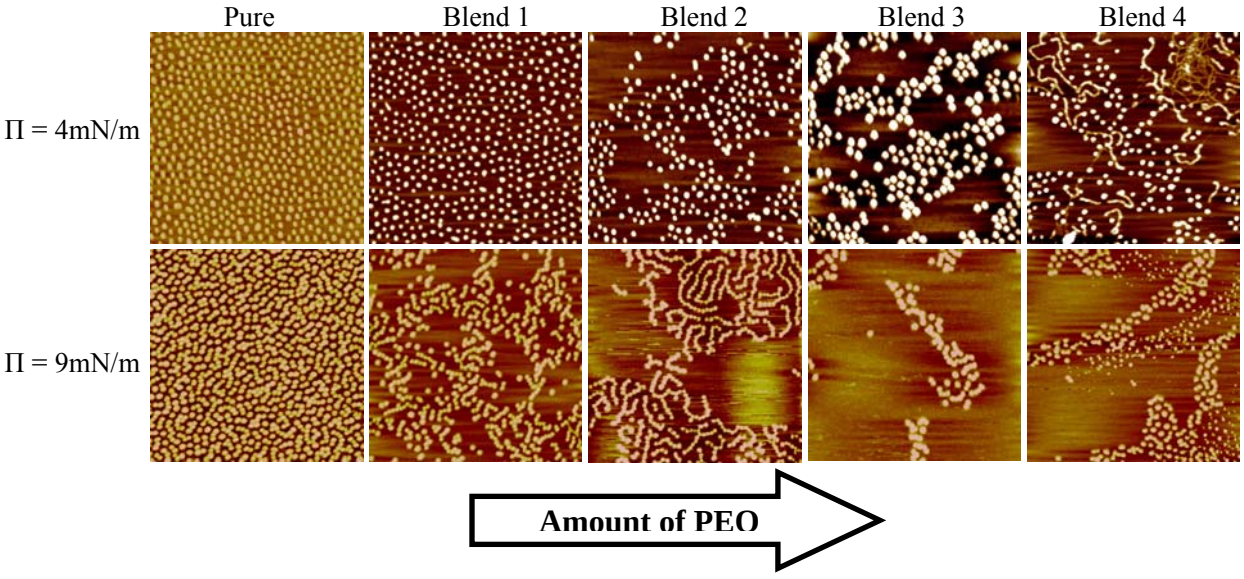

Figure 3-22. Height AFM images from tapping mode of the pure PS-*b*-PEO diblock copolymer and several blends for transfer pressures of 4 and 9 mN/m (scale 2×2μm). The height scale remains constant for the blends.

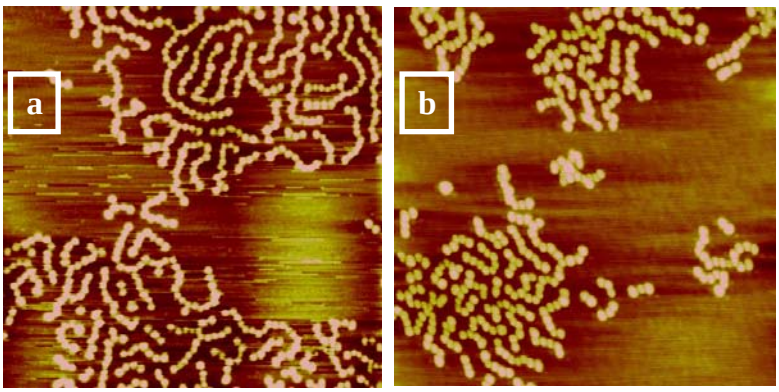

Figure 3-23. Height AFM images from tapping mode for Blend 2; (a) from successive spreading, and (b) from the mixed solution (scale 2×2μm)

Table 3-1. Characteristics of the PS-*b*-PEO sample investigated

MW (g/mol)	PEO wt%	PS wt%	Polydispersity	MW_{PEO}	MW_{PS}	N_{PEO}	N_{PS}
32,500	32	68	1.05	10,500	22,000	238	211

Table 3-2. The mass ratio of PS between the diblock copolymer and the homopolymer as well as the apparent number of styrene units have been calculated for each blend.

Blend #	1	2	3	4	5	6	7
Mass % of PS	70.2	72.3	75.8	78.6	80.7	84.0	86.3
Mole ratio of PS (homopolymer/copolymer)	0.138	0.275	0.551	0.826	1.102	1.653	2.204
$N_{PS,TOT}$	236	259	307	355	403	499	595

Table 3-3. Width of the pseudoplateau for each blend

Blend #	Pure	1	2	3	4	5	6	7
ΔA_P (nm^2)	22.8	23.0	22.2	21.1	22.3	22.5	20.5	21.1

Table 3-4. The mass ratio of PEO between the diblock copolymer and the homopolymer as well as the apparent number of styrene units have been calculated for each blend.

Blend #	1	2	3	4
Mass % of PEO	92.4	95.9	97.9	98.9
Mole ratio of PEO (homopolymer/copolymer)	0.025	0.05	0.101	0.202
$N_{PEO,TOT}$	295	352	467	697

Table 3-5. Pancake areas extrapolated from the π-A isotherms

Blend #	Pure	1	2	3	4
A_P (nm^2)	86	153	244	352	610

Table 3-6. Area for the second transition (described in Figure 2.5) extrapolated for each blend

Blend #	Pure	1	2	3	4
$A_{Transition\ 2}$ (nm^2)	46	72	112	149	268

Table 3-7. Molar ratio of PEO from the homopolymer and the diblock copolymer as well as the total number of EO units is given for each blend.

Blend #	Pure	1	2	3	4
n_{Homo}/n_{Block}	0	0.025	0.05	0.101	0.202
$N_{PEO,TOT}$	238	295	352	467	697

CHAPTER 4
INTERFACIAL BEHAVIOR OF STAR-SHAPED POLYSTYRENE-*BLOCK*-POLY(TERT-BUTYLACRYLATE) COPOLYMERS

4.1 Introduction

A system that has been of particular interest in our laboratories is one that consists of a hydrophilic block as well as a hydrophobic block. These types of copolymers are particularly interesting due to their ability to self-assemble when spread onto a water subphase. Many studies, including the previous chapter, have focused on polystyrene-*b*-poly(ethylene oxide) (PS-*b*-PEO) [32-44] copolymers due to the availability of PS and the biocompatibility of PEO, but very few have involved copolymers containing polyacrylates.

Homopolymers such has polyesters[106,107] and polyalkylesters spread easily at the air-water interface and have been widely studied. For example, Mengel *et al.* investigated the formation of multilayers of poly(tert-butylacrylate) using the LB film technique.[108] The isotherms obtained were in agreement with previous studies made on linear P*t*BA.[109,110] A plateau was observed for a pressure around 24mN/m indicating the presence of a transition from liquid-condensed (LC) to solid phase (S). Transferred onto silicon wafers, those types of polymers were also found to be very useful after modification forming multilayers of poly(acrylic acid) (PAA). The direct formation of Langmuir films using PAA homopolymers is impossible due to their high hydrophilicity.

Depending on the size and the composition of the chains, copolymers present different properties such as chain density and intermolecular interactions allowing them to adopt different geometries and form different morphologies. By varying the ratio between the hydrophobic and hydrophilic segments of the copolymers, researchers have been able to observe different morphologies of the films transferred from the air-water interface onto a solid substrate. Li *et al.* investigated the behavior of Langmuir films of linear PS-*b*-P*t*BA.[111] For mostly hydrophobic

copolymers, they observe multiple plateaus indicating the presence of more than one phase transition. This differs from the behavior of the P*t*BA homopolymer which only shows one transition corresponding to side-group reorientation towards the interface. They suggest that the other transitions correspond to some form of backbone condensation or organization.

4.2 Results and Discussion

The PS-*b*-P*t*BA diblock star copolymers given in Figure 4-1 were synthesized via atom transfer radical polymerization (ATRP) of styrene and tert-butylacrylate using the fifth generation dendritic initiator shown in Figure 4-2. The synthesis procedure has been described elsewhere.[112] The characteristics of the copolymers are given in Table 4-1 as well as their structures shown in Figure 4-2. The P*t*BA homopolymer was purchased from Polymer Source Inc. Its characteristics are given in Table 4-2. Regarding the copolymer, the calculated molecular weight values assumed the presence of 64 PS-*b*-P*t*BA branches. However, the absolute values obtained by differential viscometry and universal calibration showed that each star is composed of significantly less branches. The number of branches was obtained by dividing the absolute molecular weight (shown in Table 4-2) of each copolymer by the calculated molecular weight of one branch. Based on discussion with Dr. W. Ford and Young Hie Kim who synthesized the samples, we assumed that each arm is composed of 48 PS repeat units. After calculation, we then estimated that PS-*b*-P*t*BA(104) contains 37wt% PtBA; PS-*b*-P*t*BA(215), 47%; and PS-*b*-P*t*BA(445) is composed of 58% of PtBA (Table 4-1). It is important to note that those numbers are averages and that some of the stars may have a different number of branches as well as some linear chains might be present in the samples.

4.2.1 P*t*BA Homopolymer

Figure 4-3 shows the surface pressure-mean molecular area isotherm for the homopolymer. As described in previous investigations,[109,110] a phase transition is observed for a pressure around 24mN/m shown by the presence of a plateau on the isotherm plot.

The P*t*BA homopolymer is amphiphilic, forming stable films when compressed at the air-water interface. On the isotherm, three distinct regions can be detected: (1) all the P*t*BA chains are adsorbed onto the air-water interface, (2) represents a phase transition from a two-dimensional to a three-dimensional structure, and (3) accounts for the collapse region of the P*t*BA. As shown in Figure 4-3, two distinct areas can be extrapolated from the isotherm plot. We divided those values by the number of *t*BA units present in the homopolymer in order to simplify the comparison with other systems. For low pressure, A_p is equal to 30Å^2/tBA. This value is in agreement with the one given by Mudgil *et al.*[113] (35Å^2/tBA). In region 3, the extrapolation of the linear portion of the isotherm to π=0mN/m yields to the theoretical area A_0. Once again, the value observed for our P*t*BA homopolymer (5.4Å^2/tBA) is in conformity with the one observed in the literature (5Å^2/tBA).[111]

The P*t*BA homopolymer was transferred onto a mica substrate at three distinct pressures. The resulting images are given in Figure 4-4. The pressures were chosen in order to investigate the morphologies formed in the three distinct regions of the isotherm shown in Figure 4-5.

As expected, no morphology exists for a pressure of 15mN/m (Region 1). When compressed to a pressure corresponding to the plateau pressure (24mN/m), bright domains start to form (Region 2). Further compression leads to a film collapse observed in region (3).

A scheme of the characteristic Langmuir film structures for the different regions of the isotherms is presented in Figure 4-6. Region (1), as confirmed by the AFM images (several

images were taken in order to prove the reproducibility of the morphologies formed), shows a flat monolayer of P*t*BA completely adsorbed onto the air-water interface. Region (2) (morphology observed at the plateau) is composed of either single domains or small chains (dimers or trimers) of P*t*BA aggregates. These domains are visible due to desorption of the P*t*BA from the interface as the total available area is decreased. Each aggregate contains multiple polymer chains. In the LB film transferred for a surface pressure of 30mN/m (region 3), the bright domains represent 25% of the total area (assuming the darker area is composed of the adsorbed PtBA chains). If we assume that the bright domains observed in the AFM picture taken for a MMA corresponding to the middle of the plateau (Figure 4-4) represent half of the total desorbed PtBA observed in condensed region, then the aggregation number is about 12000. It is also important to note that the TR detected during the transfer (1.062) was also taken into account in the calculations. Region (2) represents the transition between the state where all the P*t*BA is adsorbed onto the interface and forms a homogeneous monolayer and that present in region (3) where the P*t*BA forms a three-dimensional network. This last structure explains the presence of the sharp increase in pressure and the dependence of the collapse on the polymer molecular weight. When transferred at a pressure of 30mN/m (Region 3), the appearance of bright domains is observed. These domains are believed to represent the P*t*BA that desorbs from the interface as the monolayer is compressed. The circular domains are characteristic and reproducible. They also tend to have a narrow distribution showing diameters of around 0.6μm as confirmed by the section view shown in Figure 4-7.

Additional experiments were done in order to determine the stability of the films formed at different surface pressures. Compression-expansion hysteresis experiments done for a maximum pressure of 50mN/m, which is located after the collapse pressure of the homopolymer (Figure 4-

8) also support our conclusions, showing a hysteresis as the monolayer was successively compressed and expanded. After complete expansion, the compression curves again overlap each other showing that the films formed can relax to their original monolayer. In contrast, for a maximum surface pressure of 20mN/m (below the plateau), the experiment shows no signs of hysteresis on expansion, proving the presence of a thermodynamically stable film for pressure values below the equilibrium spreading pressure of the P*t*BA segments (Figure 4-9). During the expansion, a decrease to a pressure lower than the one observed during the compression is observed. This can be explained by the fact that the desorbed P*t*BA chains undergo a faster desorption during the compression cycle than re-adsorption during the expansion cycle. Another possible explanation would be an artifact due to the wilhelmy plate. However, this is unlikely because there is no difference in multiple subsequent compression curves.

To observe the stability of the films formed at high surface pressures, an isochoric experiment was also performed. The film was compressed to a pressure of 50mN/m. Once this pressure was reached, the barriers were stopped and the pressure recorded over time. The plot in Figure 4-10 illustrates a rapid drop in pressure as soon as the compression stops, then the observed pressure slowly decreases to the equilibrium spreading pressure of the homopolymer (24mN/m). The films formed are thermodynamically unstable and quickly relax to the pressure observed for the plateau. The reason for the sharp surface pressure increase observed on the isotherm is still not clear; it could be from interactions between the collapsed and desorbed aggregates formed in region (2) or between eventual adsorbed P*t*BA segments.

4.2.2 PS-*b*-P*t*BA Star-Shaped Copolymers

4.2.2.1 Isotherm Experiments

Figure 4-11(a) shows the surface pressure-mean molecular area isotherms obtained for the three copolymers. Similar to the P*t*BA homopolymer, plateaus can be observed for a pressure of

about 24mN/m. Independent of the molecular weight of the copolymer, the plateau observed is horizontal, representing a first-order transition where the temperature and pressure stays constant while the single domains aggregate. This differs from polymers such as polystyrene-*b*-poly(ethylene oxide) (PS-*b*-PEO) presenting a pseudoplateau where a slight change in the surface pressure is detected upon compression.[32-44] As for the P*t*BA homopolymer, the plateau is detected for a surface pressure of 24mN/m. We know the desorption of P*t*BA chains from the interface has an effect on the length of the plateau; however, the effect of the PS domains remains unclear.

Our results are significantly different from those obtained by Lennox and co-workers for linear PS-*b*-P*t*BA diblock copolymers with relatively low P*t*BA wt %.[111] They showed that the presence of the PS block induces two additional phase transitions of the P*t*BA block below 20 mN/m and suggested that these transitions might originate from the peculiar surface aggregation into circular micelles. This difference in behavior can be explained by the significant difference in PS molecular weight between their sample (305 styrene repeat units) and our copolymers (each arm has 48 styrene repeat units).

The same three regions observed in the homopolymer are observed for the copolymers. An increase in the surface pressure is observed in the high mean molecular area going from a liquid expanded phase to a liquid condensed phase until a plateau suggesting a biphasic phase is reached at π=24mN/m. PS and P*t*BA are both hydrophobic homopolymers but contrary to PS, P*t*BA possesses slightly polar ester groups that allow its adsorption onto the water subphase. Upon further compression in the low molecular areas, the apparent surface pressure shows a sharp increase to values higher than 80mN/m. For this region, extrapolation of the linear portion of the isotherm to $\pi = 0\ \mathrm{mN/m}$ yields the theoretical area that a most compact surface film

would occupy at zero pressure (A_0). In previous studies on amphiphilic copolymers such as PS-*b*-PEO, no dependence of the collapse area on the PEO block length was observed. In our case, we can see the increase in collapse area as the size of the P*t*BA chains increases suggesting that the film collapse depends on both the hydrophilic and the hydrophobic block. Interestingly the films become more compact as the amount of P*t*BA increases. Likewise, Li *et al.* investigated the behavior of two different P*t*BA homopolymers, and observed more compact films when increasing the P*t*BA molecular weight.[111] This suggests that the area occupied by the longer chains includes a significantly smaller trapped area than the shorter chains. Throughout the plateau, the tert-butyl side groups go from a prone to a vertical conformation. Li *et al.* also studied the influence of the P*t*BA molecular weight on the behavior of PS-*b*-P*t*BA diblock copolymers.[111] They observed a linear dependence (y = 0.128x + 16.473) of the collapse area on the number of *t*BA repeat units. When the surface pressure is plotted versus the mean unit area (area available for 1 *t*BA repeat unit), a strong molecular weight dependence can be observed throughout the entire isotherm plot (Figure 4-11 (b)). In Figure 4-12, when A_0 per *t*BA repeat unit is plotted versus the number of *t*BA repeat units present in one arm, a linear dependence is detected (y = 0.0021 + 2.982). The value detected for PS-*b*-P*t*BA(104) is really close to the one given for the P*t*BA homopolymer (5.5 $Å^2$). As the P*t*BA molecular weight is increased, the star copolymers become more sterically hindered, forming less packed aggregates, yielding to a higher area per *t*BA unit. The areas per *t*BA unit observed by Li *et al*.[111] for several copolymers are significantly more larger (from 12 $Å^2$ to 70 $Å^2$) due to the amount of PS present in their copolymers: longer chains preventing the P*t*BA segments from packing more closely.

The area occupied by a styrene repeat unit is constant for the three copolymers and has an approximate value equal to 12$Å^2$/St (values are given in Table 4-3). This value is larger than the

one observed by Logan et al.[48] (8.9Å^2/St) for PS-*b*-PEO star copolymers. The significant variation between both values can be explained by the difference in interfacial behavior between PEO and P*t*BA blocks. For small molecular areas, the PEO chains stretch in the aqueous subphase while the P*t*BA desorbs from the interface. Therefore, in the case of the PS-b-PEO copolymers, the steric hindrance at the interface is lowered, allowing the PS domains to pack more closely.

4.2.2.2 AFM Imaging

AFM images were obtained for two transfer pressures as seen in Figure 4-14 We can see that the images obtained for a transfer pressure lower than the plateau value (24mN/m) only show the presence of single domains. The formation of adsorbed circular surface micelles without any collapsed domains can be observed. Even though their size decreases as the PtBA content increase, the size distribution of those surface micelles is rather monodisperse (verified by the image analysis software introduced in chapter 2) and independent on the molecular weight of P*t*BA in the sample suggesting those domains represent aggregates of PS chains. The domain sizes averaged 4200, 3500, and 3200nm^2 for the 3 systems. Li *et al.*[111] studied the behavior of linear PS-*b*-P*t*BA copolymers and observed domains that were approximately 10 times larger than the ones detected for our copolymers. However, this difference can easily be explained by the distinct architectures and the size of the PS blocks (305 styrene repeat units in their copolymers versus 48 for each arm of our star copolymers). It should be noted that the transfer ratios varied significantly between the values obtained for pressures below and above the plateau pressure. In fact for pressures equal to 24mN/m or less, all the transfer ratios were close to unity suggesting a homogeneous transfer of the Langmuir monolayer onto the mica substrate. However, when the monolayers were transferred for pressures above the plateau, the transfer ratios decreased dramatically (TR~0.5 for the 3 copolymers).

The hydrophilicity of the substrate and results from previous studies on PS-*b*-P*t*BA copolymers allow us to consider the more hydrophilic P*t*BA to be adsorbed onto the mica and the hydrophobic PS to occupy the higher layer. Therefore, the P*t*BA is represented by the darker (lower) areas whereas the PS exists as the brighter (higher) domains. The diameter of the bright circular domains observed in the AFM pictures is approximately 100nm and independent of the surface pressure. Each aggregate consists of multiple chains – for example, the aggregation number for the domains observed in Figure 4-14 in the case of the PS-*b*-PtBA(104) is equal to 132. Therefore, once a micelle has formed during the solvent spreading process, the micellar cores come closer to each other during compression. However, the aggregation number remains unchanged with the chains frozen within the glassy core of a particular micelle (the temperature of the experiment is well below the *T*g of the desorbed PS cores). It should be noted that the glass transition temperature (Tg) of a pure bulk PS (molecular weight comparable to the PS studied in this chapter) is 98°C.[141] In addition, Bliznyuk *et al.*[142] measured the surface glass transition for PS with molecular weights ranging from 3900 to 1,340,000g/mol. Using the model proposed by their group, the Tg of a PS of 5000g/mol (close to the PS molecular weight in one arm of the star copolymers) is approximately 50°C.

For low surface pressures, a decrease in the size of the circular micelles as well as an increase in the distance between them is observed when the size of the P*t*BA segments is increased (Figure 4-15). This observation is in accord with the interpretation of a P*t*BA layer located at the bottom of the film with PS domains on top of it as shown in the Figure 4-13. The decrease in the circular domain size can be due to the increase in repulsive forces between PS and P*t*BA when the fraction of P*t*BA becomes more significant.

For a pressure of 24mN/m several trials were made to observe the aggregation of the PS domains and the formation of lower domains representing the P*t*BA chains. In fact, as seen for the P*t*BA homopolymer throughout the plateau, the desorption of the P*t*BA chains can be observed leading to the chaining and further aggregation of the single and oligomeric PS domains observed at lower pressure. The formation of such aggregates is more easily seen on the copolymer containing the longest chains of P*t*BA (PS-*b*-P*t*BA(445)). When compressed to a pressure above the plateau (30mN/m), aggregation of these domains is observed for all copolymers. As shown in Figure 4-14, this aggregation becomes more significant as the number of *t*BA repeat units increases.

As demonstrated previously for the homopolymer, three regions can be detected in the isotherms as well as in the structures observed when the monolayer is transferred onto a solid substrate. Figure 4-16 gives a scheme of the general structures formed for different regions of the isotherms. Region (1) contains a homogeneous monolayer of amphiphilic P*t*BA with the hydrophobic PS forming single domains aggregated on top of it. Region (2) is similar to the structure observed for the P*t*BA homopolymer, the only difference being the presence of PS domains sitting on top. Finally region (3) is the analogous morphology to the one observed for the region (3) in the homopolymer. The domains of P*t*BA form a network, rendering the film very rigid and increasing the apparent surface pressure. The three-dimensional structure depicted for regions (2) and (3) can also be explained by the cross section shown in Figure 4-17 showing the different phases of the Langmuir-Blodgett film at high pressure (adsorbed P*t*BA, desorbed P*t*BA, and PS).The domains formed by the P*t*BA desorbed from the interface have a size comparable to those previously observed for the P*t*BA homopolymer (around 1μm) in Figures 4-4 and 4-6. This is explained in pictorial fashion in the scheme shown in Figure 4-18, representing

the three layers discussed in the previous paragraph. We can see the formation of large P*t*BA aggregates which are desorbing from the interface and possess smaller aggregates of PS sitting on top of them.

As discussed in the previous part, contrary to PS-*b*-PEO block copolymers, for PS-*b*-P*t*BA copolymers, the collapse area (A_0) depends on the P*t*BA block (Table 4-3). By calculating the area occupied by PS (A_{PS}) using equation 4-1 (where Γ is the aggregation number), we found A_{PS} to be constant for the 3 copolymers.

$$A_{PS} = \frac{Mean\ domain\ area}{\Gamma} \qquad 4\text{-}1$$

However, when A_{PtBA} (area occupied by the P*t*BA chains in the 3D structure) is plotted versus the number of *t*BA repeat units, a linear dependence is observed (y = 0.0482x + 37.049) (Figure 4-19). The linear dependence detected by Li *et al.* [111] exhibited a slope of 0.128. The significant difference between this value and the slope observed in the case of our copolymers could be explained by the difference in architecture (star-shaped versus linear copolymers), as well as the size of their PS segment which increases the steric hindrance.

4.2.2.3 Stability of the Langmuir Films

As shown in the compression-expansion hysteresis experiment (Figure 4-20) performed in the low MMA region, we were able to observe the formation of unstable films for pressures higher than 24mN/m. All the compression curves closely overlap, showing that the collapsed films are able to return to their original monolayer.

A drop in pressure is observed during the expansion cycle. This is due to the fact that the re-adsorption of the P*t*BA chains onto the air-water interface during the expansion cycle is slower than the desorption during the compression cycle. Additional compression-expansion hysteresis experiments performed for pressures below the plateau shown in Figure 4-21 allow us

to propose that the monolayers exist as thermodynamically stable films of PS-*b*-P*t*BA for pressures under 24mN/m. Figures 4-20 and 4-21 only show the results for the PS-*b*-P*t*BA(215). The behavior of the films being independent on the molecular weight of the P*t*BA block; the hysteresis experiments for the two other copolymers gave similar results.

To investigate the stability of the network formed at high pressures, transfers were performed after different stabilization times (from 15 minutes to 12 hours) for the copolymer PS-*b*-P*t*BA(215). The transfer ratios were recorded (Table 4-4) in order to determine if the films observed by AFM correspond to what is formed at the air-water interface. The transfer ratios being smaller than one even for a short stabilization time shows us the expansion of the film when transferred from the interface onto the solid substrate. This explains the AFM results observed in Figure 4-16, where the structure observed is not a complete network. The decrease of transfer ratio when increasing the annealing time supports once again, as shown in the compression-expansion hysteresis experiments, that the films formed at high pressures are thermodynamically unstable. Figure 4-22 shows the AFM images for the three copolymers transferred at a pressure of 30mN/m, which corresponds to region 3 of the isotherm. We can see that by increasing the stabilization time before transfer, the aggregation also increases, proving once again the instability of the monolayers formed at the air-water interface. A possible explanation for this phenomenon is the presence of attractive forces between the P*t*BA chains of different copolymers that at high surface pressures have the tendency to aggregate. Contrary to the PS-*b*-PEO copolymers studied in chapter 3, which showed a less well-defined transition from a two-dimensional system to a three-dimensional system, for the PS-*b*-P*t*BA copolymers, it is not clear to us whether the sharp surface pressure increase upon high compression in the isotherm is

due to interactions between the collapsed and desorbed aggregates formed in the plateau region or between eventual remaining adsorbed P*t*BA segments.

The presence of an increase in aggregation when increasing the stabilization time suggests the unstability of the Langmuir films above the plateau. In Figure 4-23, isochoric experiments are reported. The monolayers were compressed up to a pressure of 50mN/m and after the compression was stopped, values of the pressure were recorded over time. Once stopped, we observe a drastic drop in surface pressure toward the plateau pressure. This, once again, shows the unstable behavior of the film above the plateau. All three copolymers present the same behavior; the only observed difference is the presence of a larger pressure drop as the amount of P*t*BA in the copolymer increases. The surface pressure undergoes a sudden drop within the first seconds of the experiment before leveling off after a few minutes around 24mN/m. In any case, the isochoric experiments confirmed that the films formed above the plateau are not thermodynamically stable and relax within minutes down to the plateau surface pressure of 24mN/m, which can also be seen as the equilibrium spreading pressure (ESP) of the P*t*BA blocks. ESP analysis (not shown) was also performed by placing the solid copolymer sample onto the water subphase. The ESP value (24mN/m) observed was in agreement with the isochoric experiment.

4.3 Conclusions

In this chapter the behavior of several PS-*b*-P*t*BA star copolymers was investigated. The isotherm experiments showed the presence of a plateau for a surface pressure of 24mN/m. The copolymers studied, were composed of, on average 5 branches containing a constant PS core and different P*t*BA molecular weights. Even if the shape of the isotherms does not vary from the one of a P*t*BA homopolymer (already amphiphilic), a strong dependence on the molecular weight

was observed with an increase in the length of the plateau as we increase the number of *t*BA units.

AFM images were taken at pressures below and above the transition plateau. For the homopolymer, as expected, uniform flat films were observed before the transition. However, once the pressure reached the plateau pressure, aggregates were formed containing approximately 92000 PtBA chains, suggesting desorption of P*t*BA chains from the interface. When the PS-*b*-P*t*BA star copolymers were scanned, a strong molecular weight dependence of the length of the plateau as well as the collapse area was observed in correlation with the isotherm experiments. As the number of *t*BA repeat units increases, an increase in the aggregation was detected. For low surface pressures, the distance between the PS domains was greater as the P*t*BA molecular weight was increased, however, for high surface pressures, we saw the appearance of three different domains: adsorbed P*t*BA, desorbed P*t*BA, and PS domains. Estimations of the area occupied by the P*t*BA in the collapse area also showed the influence of the P*t*BA segment on A_0.

The Langmuir films formed above the plateau were found to be thermodynamically unstable as the aggregation increases with the stabilization time. Isochoric experiments were also performed and once the compression stopped, the monolayers relaxed to their equilibrium spreading pressure of 24mN/m. Below the plateau however, the copolymers formed elastic films, no hysteresis was observed during the compression-expansion experiments and the monolayer seems to relax to its initial state.

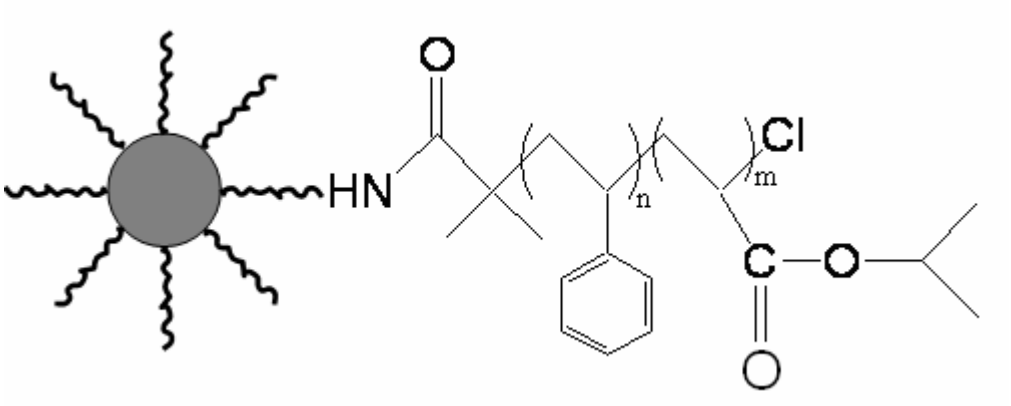

Figure 4-1. Schematic of the PS-b-P*t*BA copolymers with n=48 and m=104,215,445 (Adapted from Reference 87)

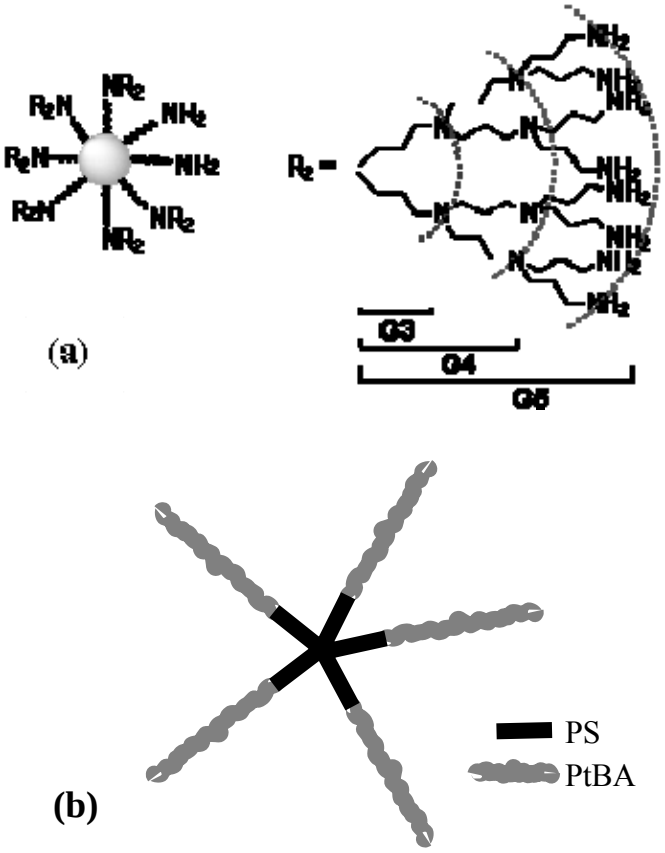

Figure 4-2. Schematic of dendritic initiator (a) (Adapted from Reference 87) and model of the PS-b-PtBA star copolymers (b)

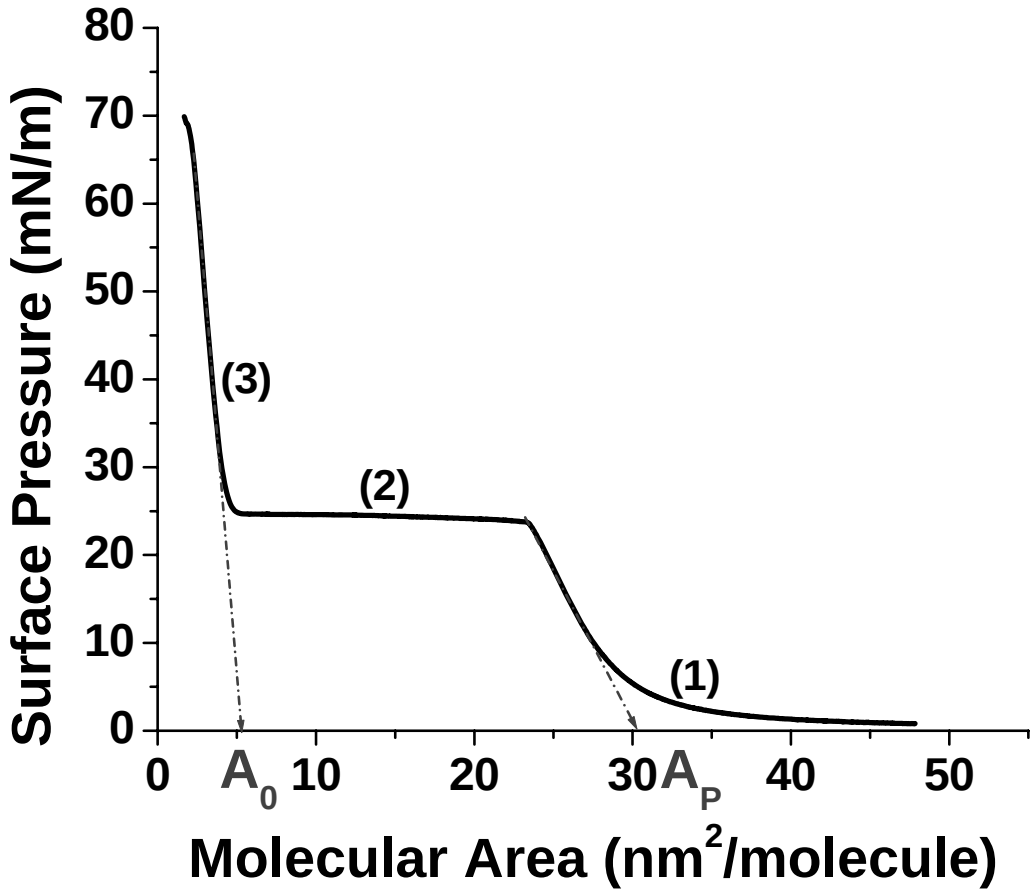

Figure 4-3. Surface pressure-MMA isotherm for a 13000g/mol P*t*BA homopolymer recorded for a compression speed of 5mm/min

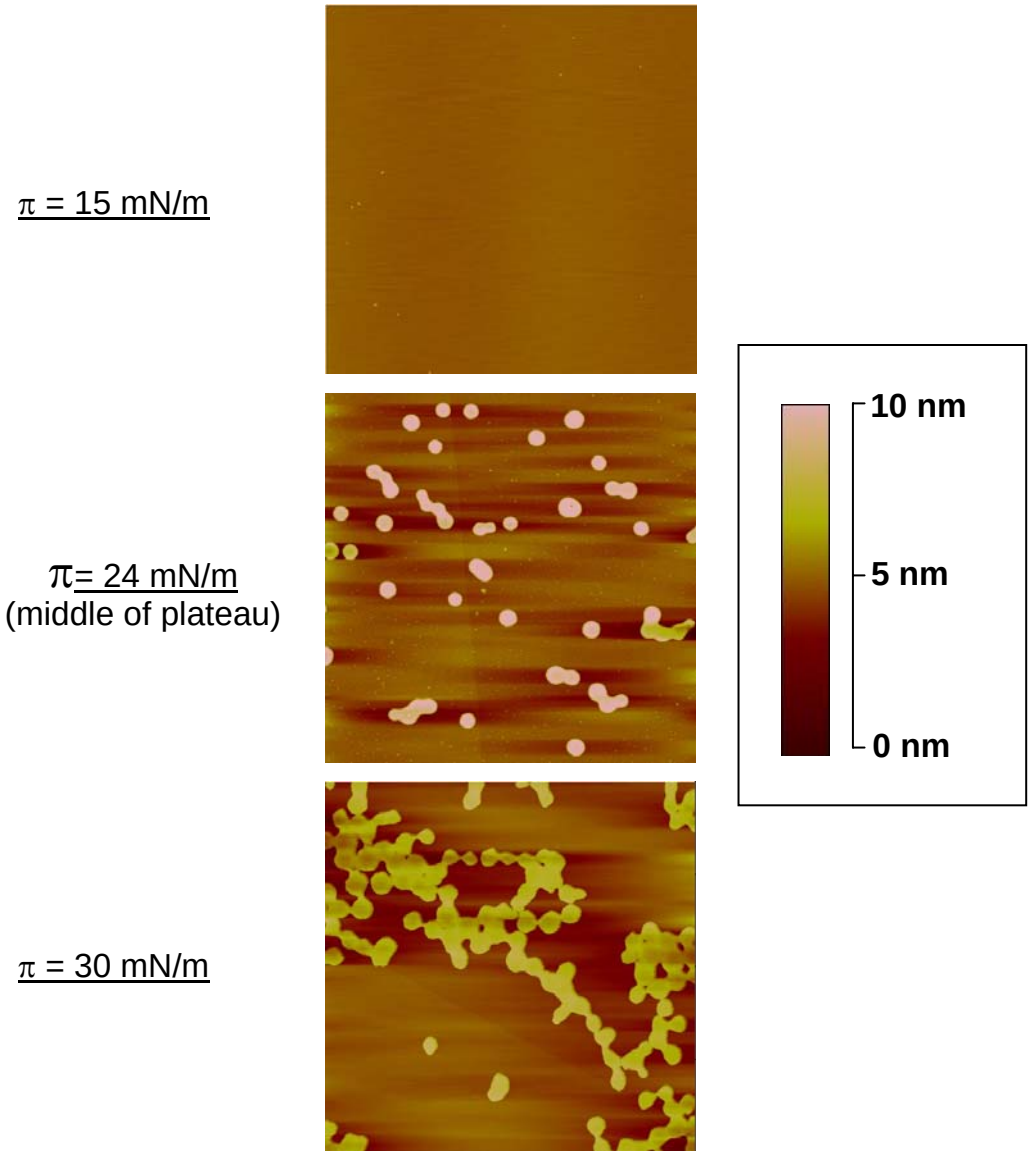

Figure 4-4. Height AFM images in tapping mode for the P*t*BA Homopolymer after transfer at three distinct surface pressures (Scale 10×10μm)

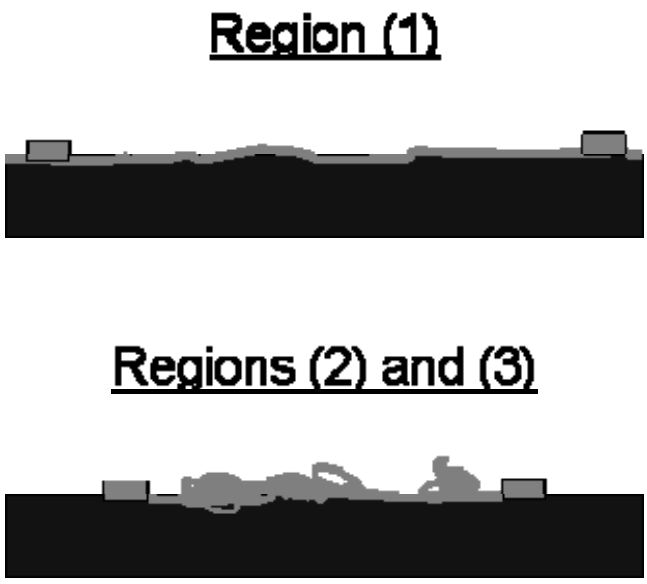

Figure 4-5. Proposed conformations for the P*t*BA homopolymer at the air-water interface. The different regions are labeled in Figure 4-3

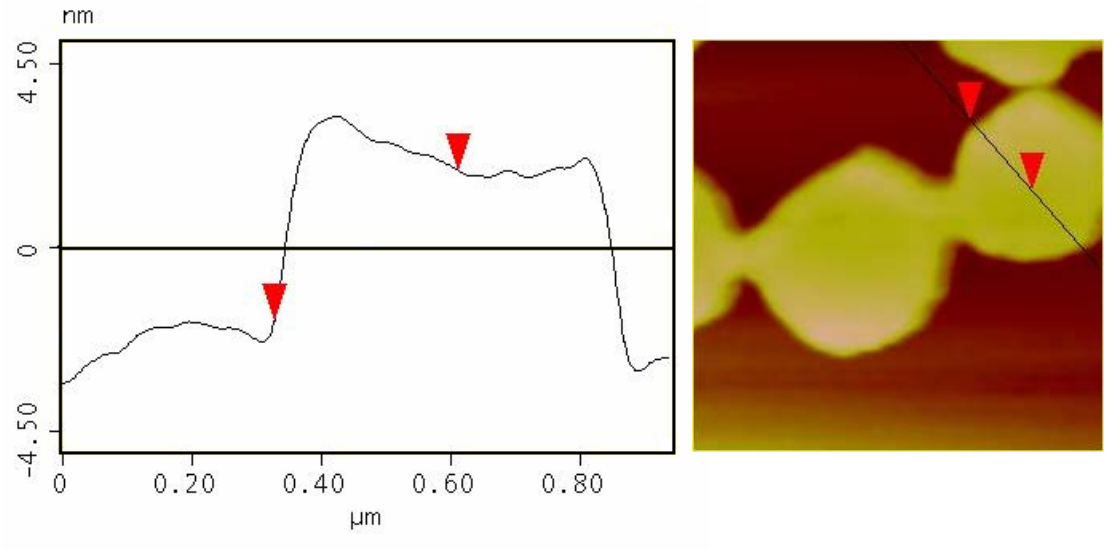

Figure 4-6. Section view of a circular domain formed when the P*t*BA monolayer is compressed above the plateau pressure (30mN/m) (image scale 1×1µm)

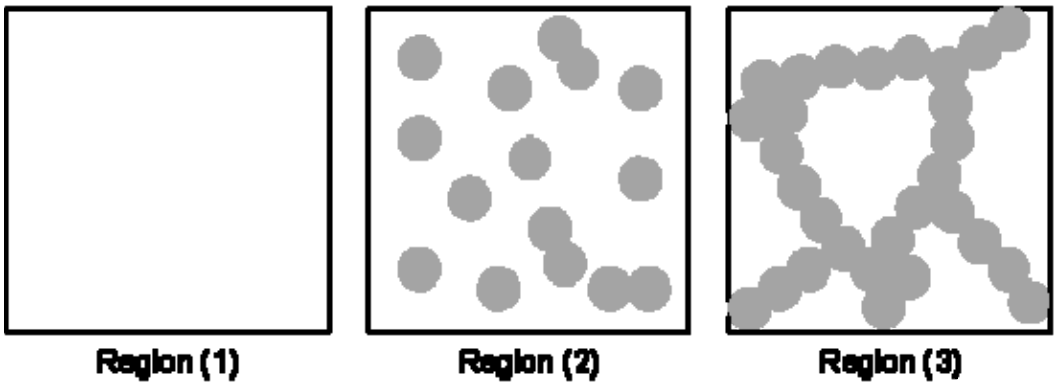

Figure 4-7. Scheme of the structures formed for 3 distinct regions of the isotherm when a monolayer of P*t*BA homopolymer is compressed at the air-water interface (Scale 10×10μm)

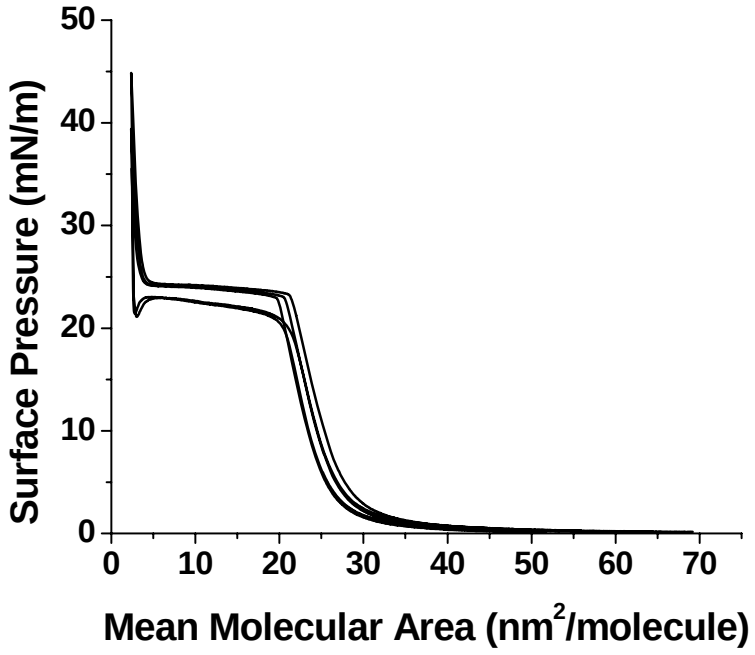

Figure 4-8. Compression-Expansion Hysteresis Experiment for the P*t*BA homopolymer compressed to a target pressure of 50mN/m (above the plateau). The compression and expansion rates were both 5mm/min.

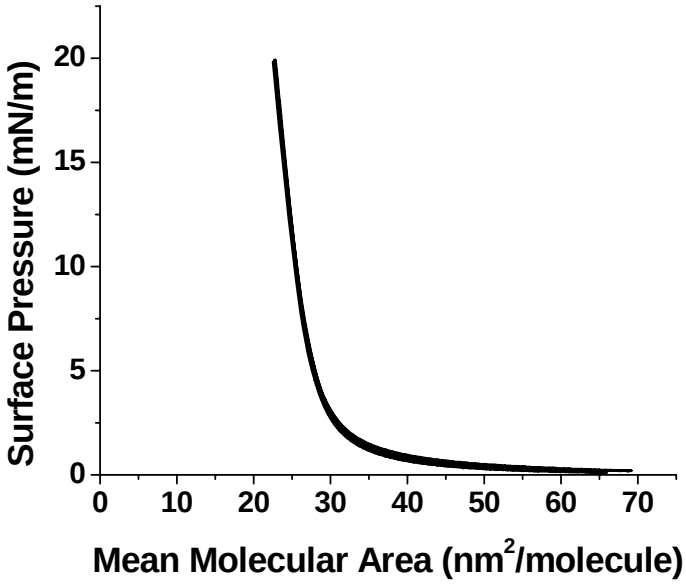

Figure 4-9. Compression-expansion hysteresis experiment for the P*t*BA homopolymer compressed to a target pressure of 20mN/m (below the plateau). The compression and expansion rates were both 5mm/min.

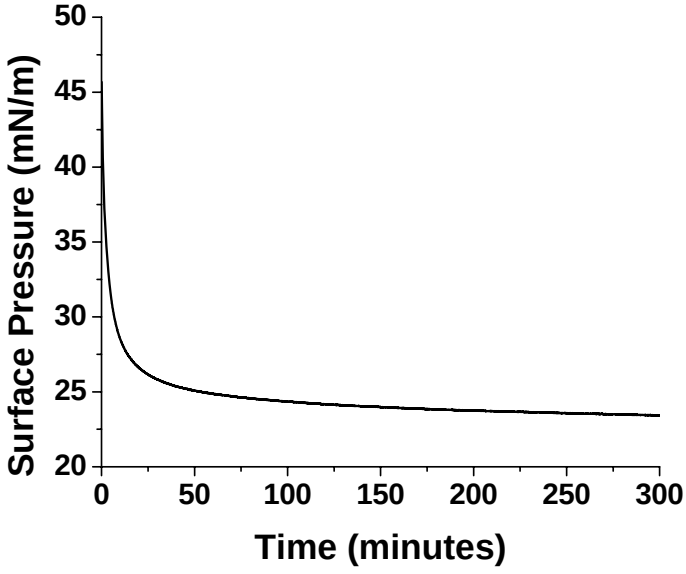

Figure 4-10. Isochoric experiment recorded for the P*t*BA homopolymer for a maximum pressure of 50mN/m. the compression speed was 5mm/min.

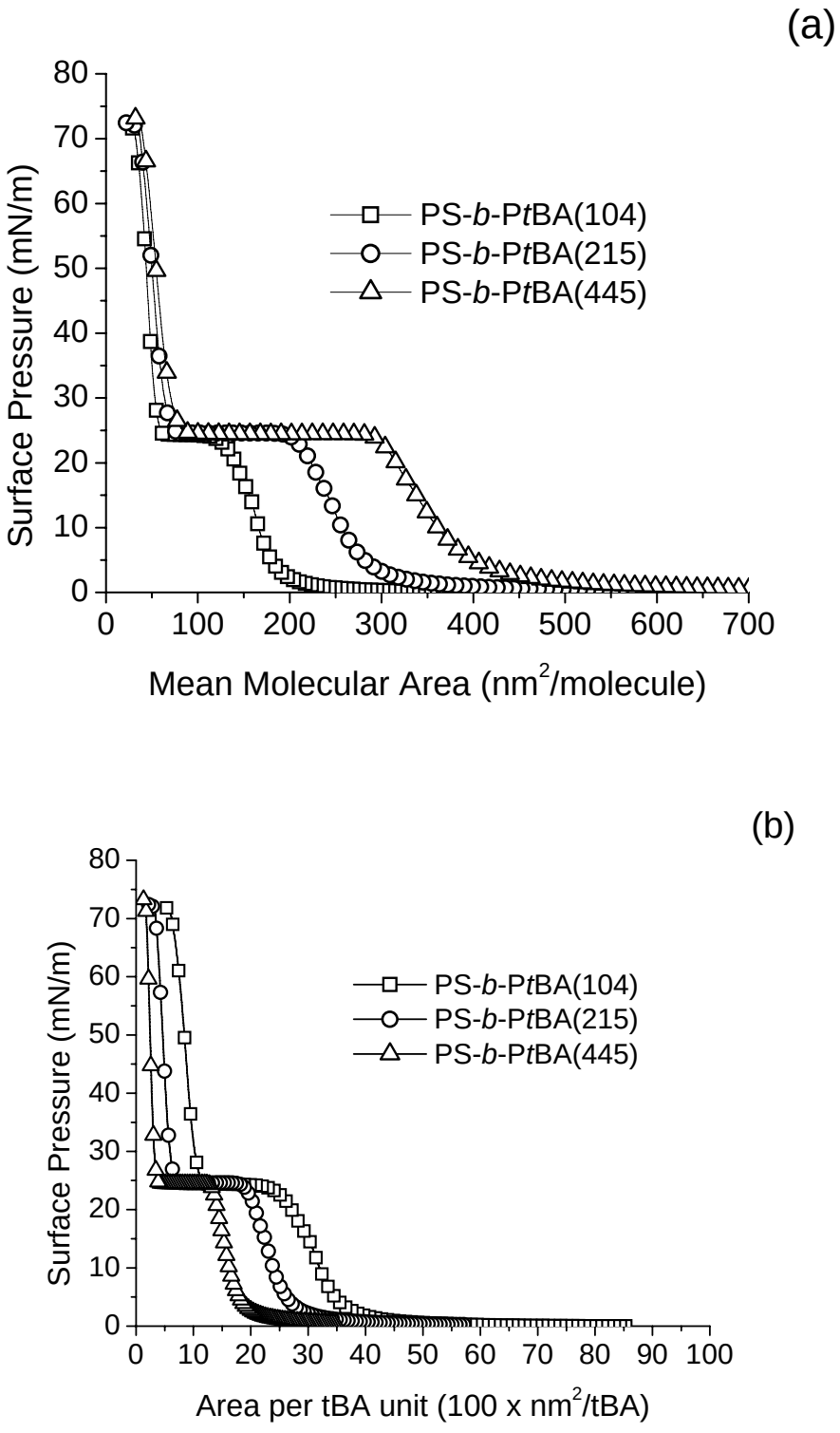

Figure 4-11. (a) Surface pressure-MMA isotherms plots of the 3 star-shaped copolymers (b) Isotherms of the 3 copolymers in terms of number of tBA repeat units. All the isotherm experiments were performed with a compression speed of 5mm/min.

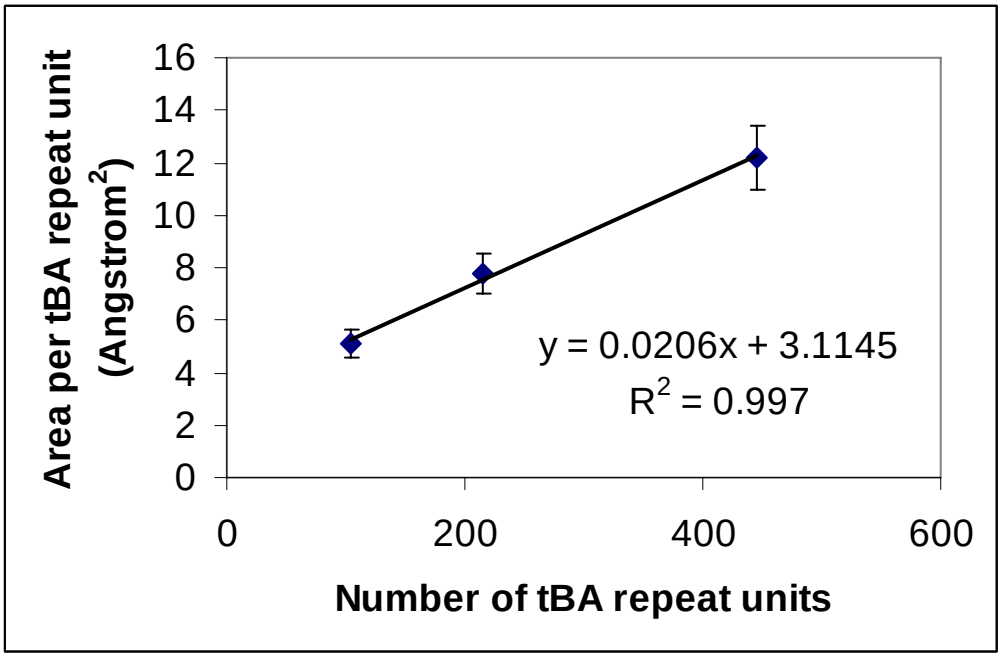

Figure 4-12. Plot of A_0 versus the number of *t*BA repeat units.

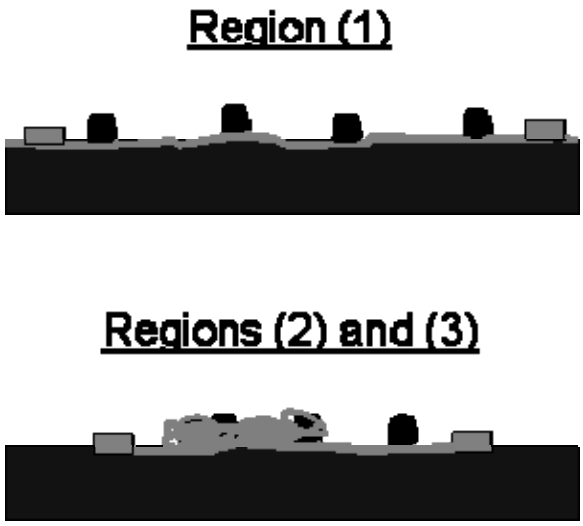

Figure 4-13. Proposed conformations for the PS-*b*-P*t*BA copolymers at the air-water interface. The different regions are defined in Figure 4-3.

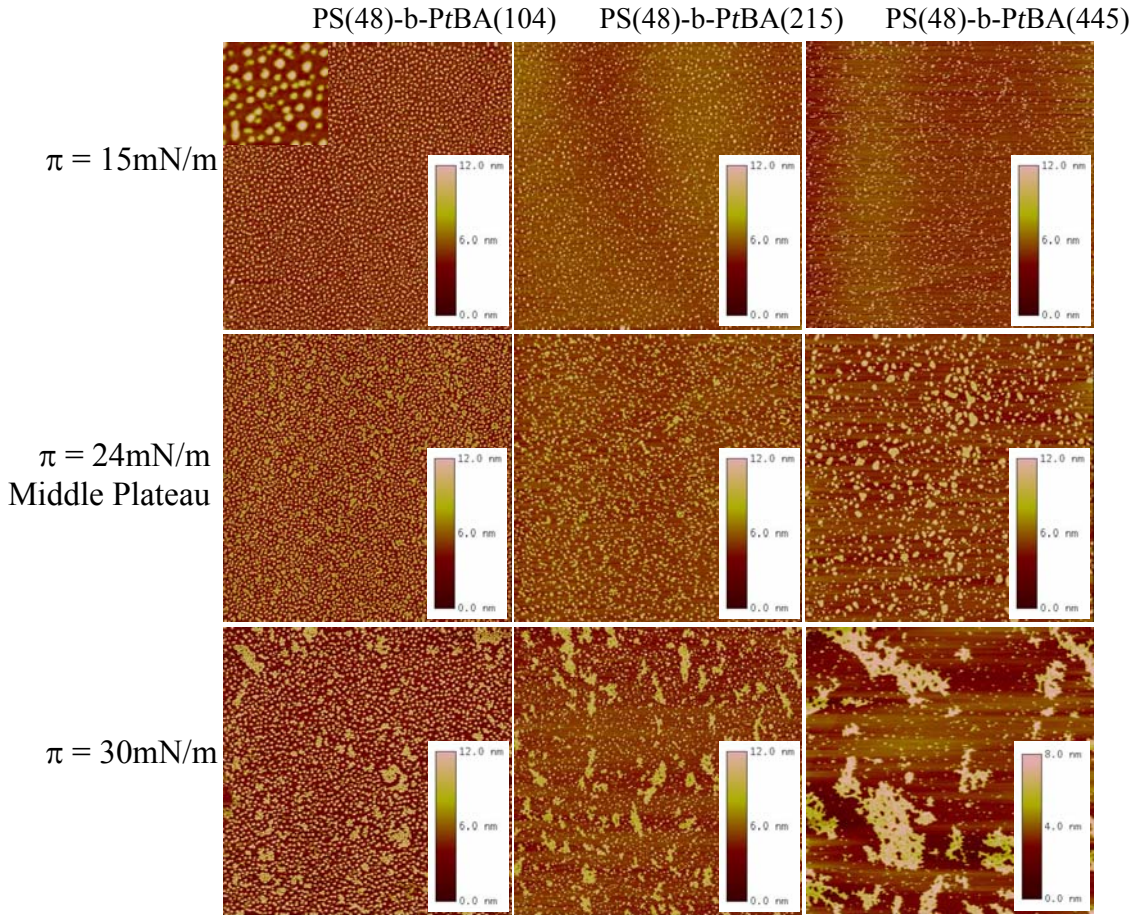

Figure 4-14. Height AFM images from tapping mode for the three copolymers. Transfer pressures were chosen to be in region (1) and region (3) of the isotherms. (Scale 10×10μm, inset scale 1×1μm)

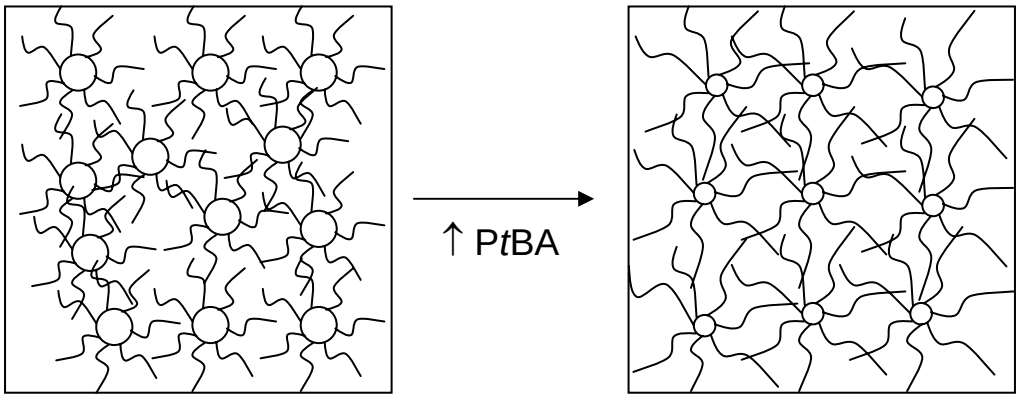

Figure 4-15. Scheme of AFM images for a transfer pressure of 15mN/m when increasing the size of the P*t*BA chains

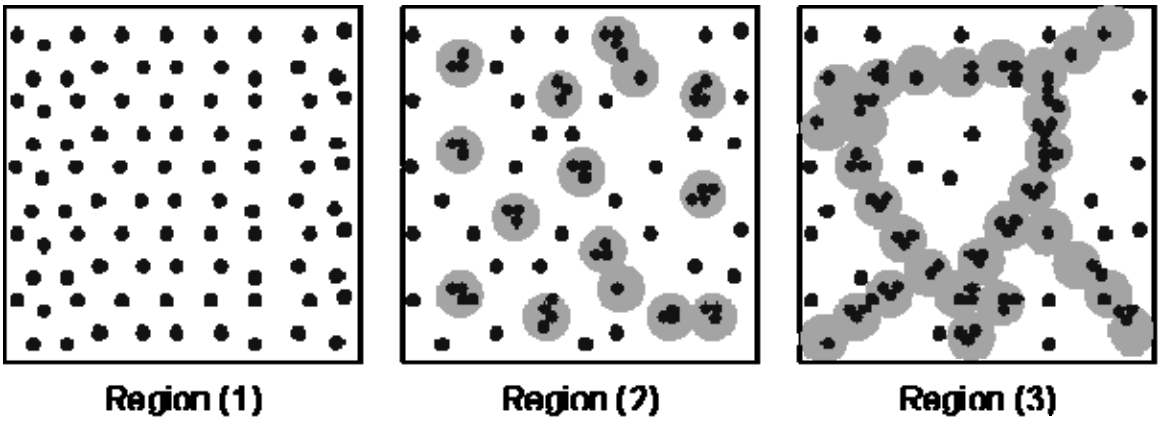

Figure 4-16. Schematic of the structures formed for 3 distinct regions of the isotherm when a monolayer of PS-b-P*t*BA copolymer is compressed at the air-water interface

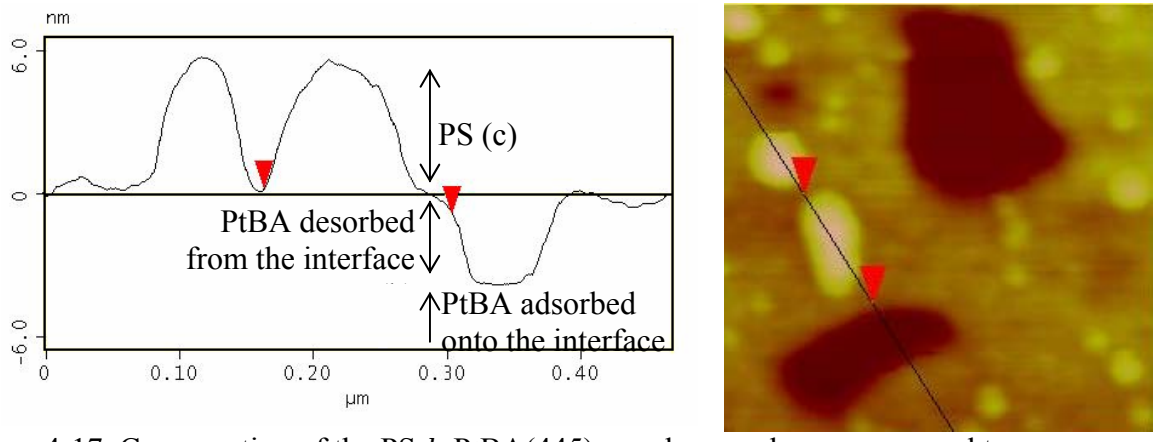

Figure 4-17. Cross section of the PS-*b*-P*t*BA(445) copolymer when compressed to a pressure of 30mN/m and studied in tapping mode

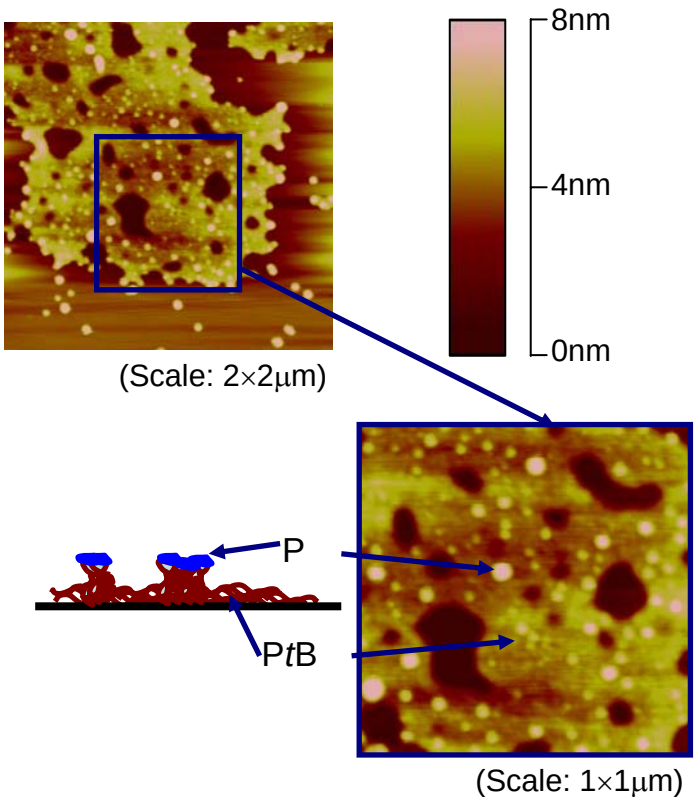

Figure 4-18. Close-up pictures and schematic of the three layers observed when the PS-*b*-P*t*BA(445) is compressed above the plateau pressure

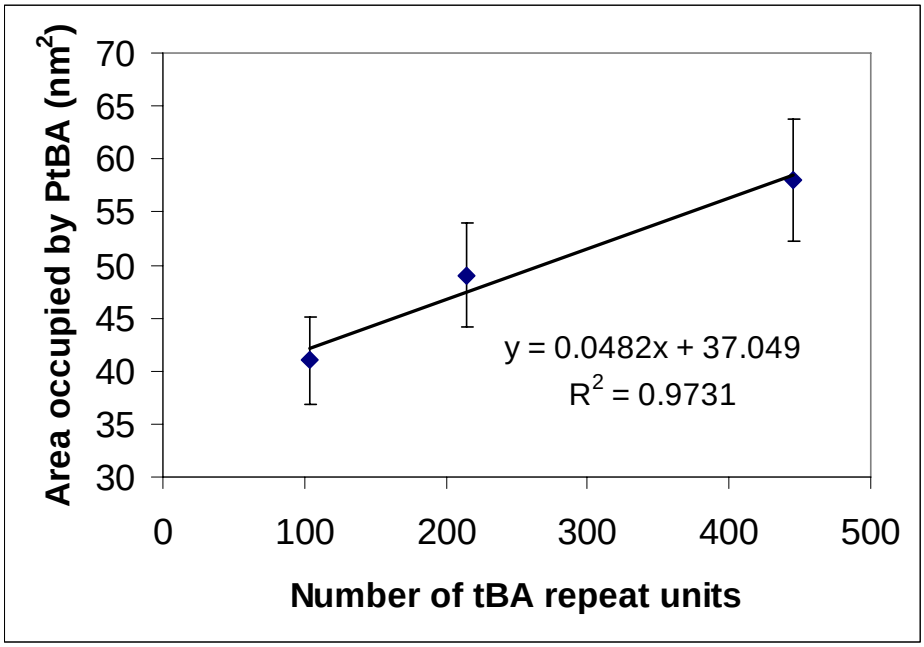

Figure 4-19. Plot of the Area occupied by the PtBA blocks (values in Table 4-3) versus the number of tBA repeat units

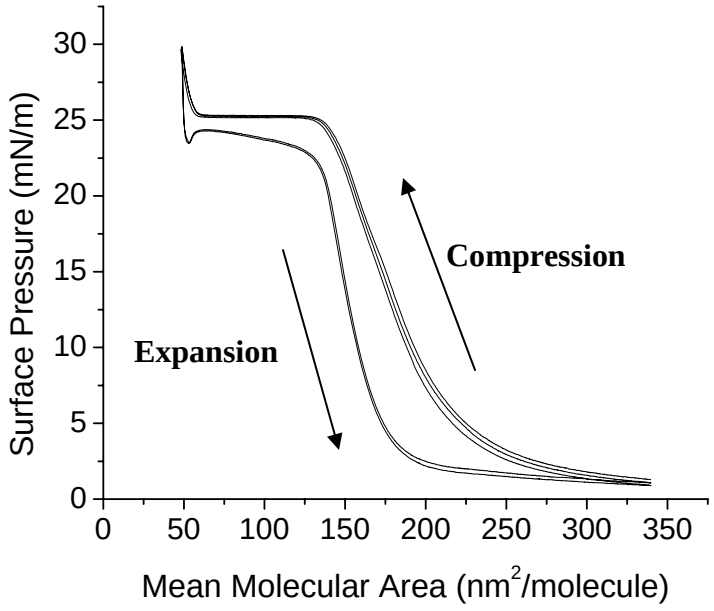

Figure 4-20. Compression-expansion hysteresis experiment for the PS-*b*-P*t*BA(215) copolymer compressed to a target pressure of 30mN/m (above the plateau). The compression and expansion rates were both 5mm/min.

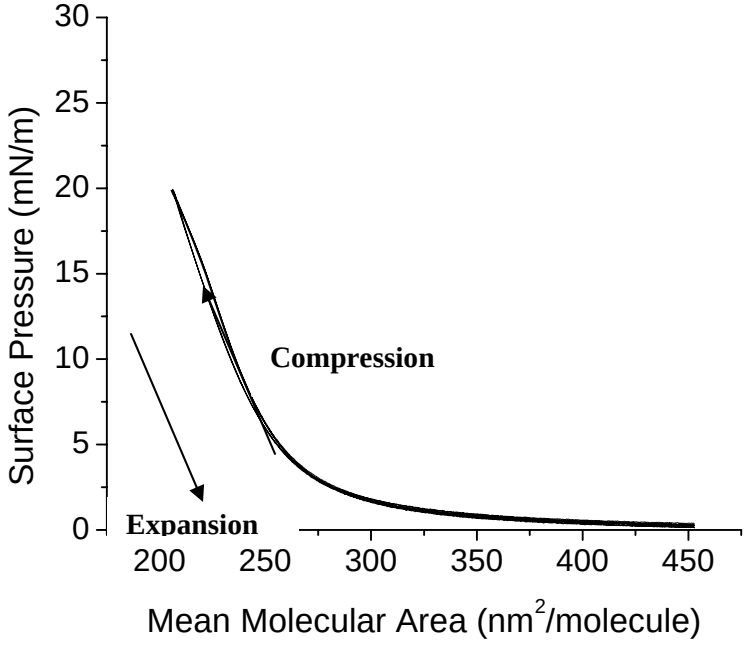

Figure 4-21. Compression-expansion hysteresis experiments for the PS-b-P*t*BA(215) copolymer compressed to a target pressure of 20mN/m (below the plateau). The compression and expansion rates were both 5mm/min.

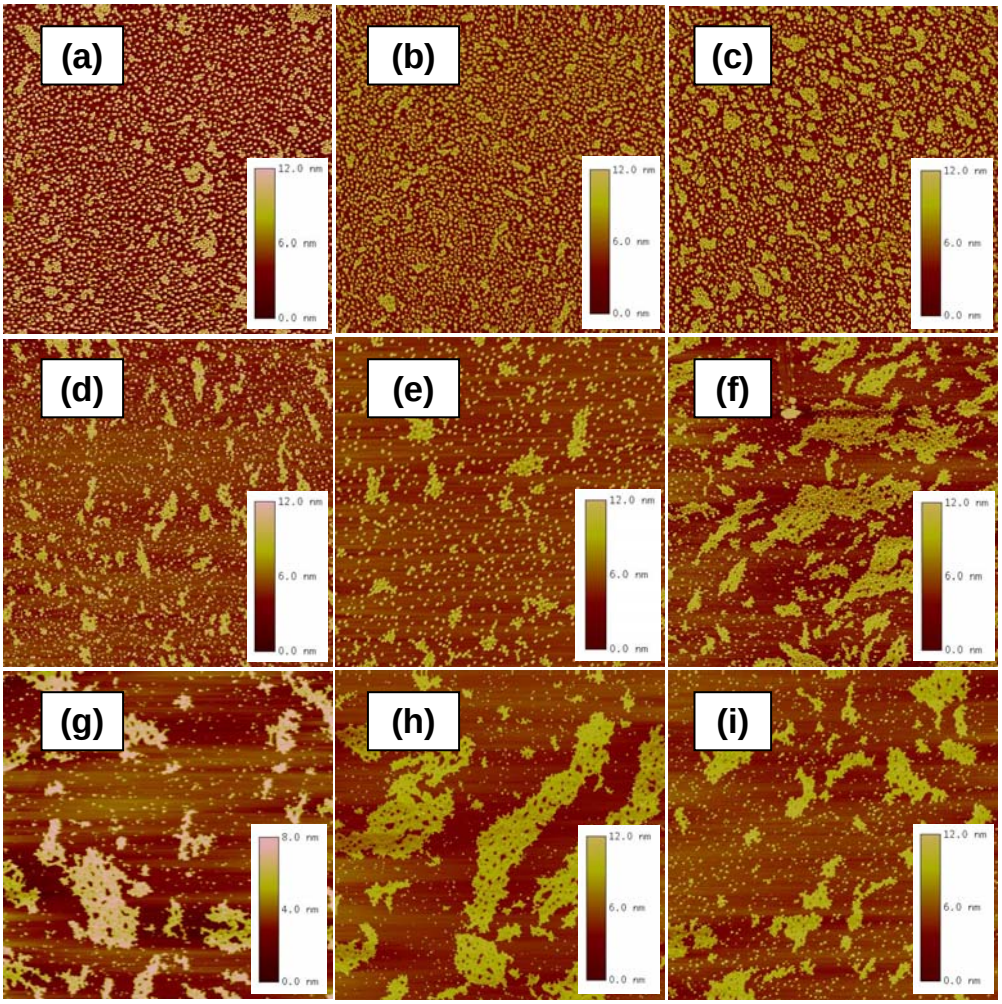

Figure 4-21. AFM images for a transfer pressure of 30 mN/m for different stabilization times. Stabilization times before transfer (minutes) for PS-*b*-P*t*BA(104): (a) 15, (b) 45 and (c) 90; PS-*b*-P*t*BA(215): (d) 15, (e) 45 and (f) 90; PS-*b*-P*t*BA(445): (g) 15, (h) 45 and (i) 90 (Scale 10×10μm)

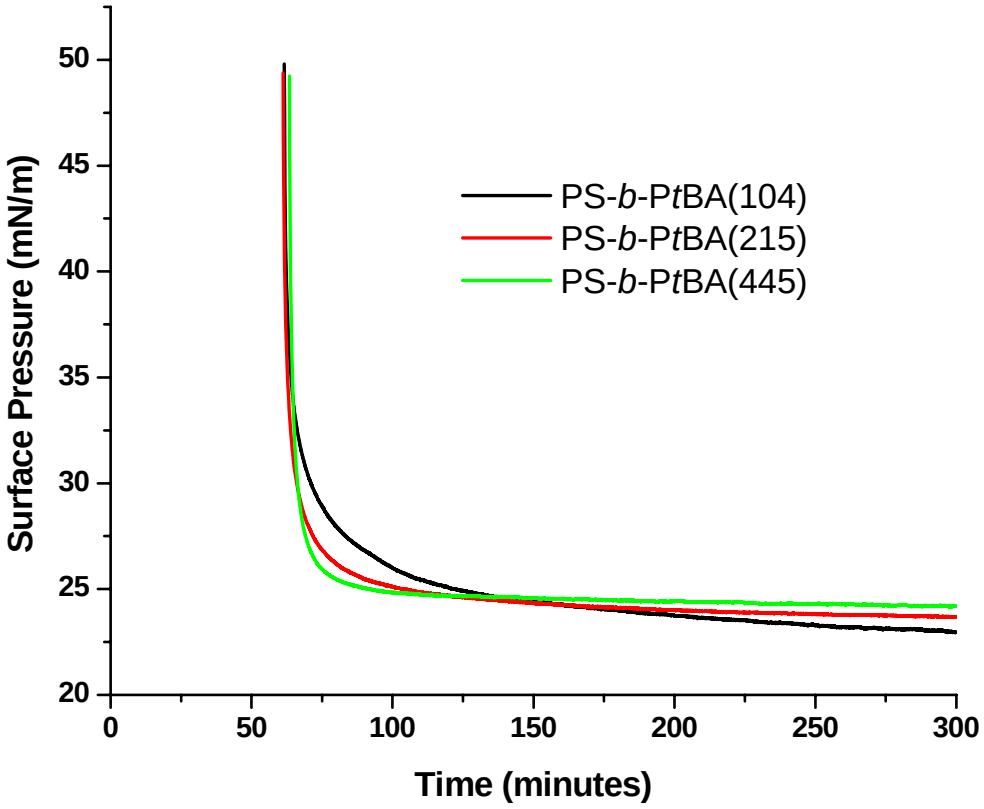

Figure 4-22. Isochoric experiments recorded for the three copolymers after compression to a target pressure of 50mN/m via a compression rate of 5mm/min.

Table 4-1. Characteristics of the Copolymers Used

Polymer	M_n* (g/mol)	wt% of PtBA	PDI*
PS-*b*-P*t*BA(104)	131,000	37	1.28
PS-*b*-P*t*BA(215)	155,000	47	1.33
PS-*b*-P*t*BA(445)	194,000	58	1.53

* M_n and PDI were determined using differential viscometry detection and universal calibration

Table 4-2. Characteristics of the Homopolymer Used

Polymer	# Tert-butylacrylate repeat units (m)	M_n (g/mol)
H101	101	13000

Table 4-3. Specific areas calculated for the 3 copolymers

Copolymer	Γ	A_0 (nm^2)	A_{PS} (nm^2)	A_{PtBA} (nm^2)
PS-*b*P*t*BA(104)	132	68	27	41
PS-*b*P*t*BA(215)	124	80	31	49
PS-*b*P*t*BA(445)	105	88	30	58

Table 4-4. Transfer ratios for different stabilization times before transferring the copolymer PS-*b*-P*t*BA(215) monolayer onto a mica substrate.

Stabilization Time (min)	15	45	90	720
Transfer Ratio	0.665	0.300	0.199	0.055

CHAPTER 5
SURFACE CHARACTERIZATION OF POLY(ETHYLENE OXIDE)-*BLOCK*-POLY(ε-CAPROLACTONE)

5.1 Introduction

Extensive work has been done on amphiphilic copolymers at the air-water interface but surprisingly studies on PCL-containing polymers are hard to find. On one hand PCL is an interesting polymer to use due to its biodegradability leading to non-toxic products.[114,115] On the other hand, low molecular weight PEO can be eliminated from the body by the renal system.[116] The addition of a highly flexible PEO chains at the end of a PCL segment can tailor some inherent properties of pure PCL such as high crystallinity, high hydrophobicity, and slow biodegradation.[117] Whereas very few investigations have been performed at the air/water interface, PEO-*b*-PCL copolymers have been investigated in solution and their micellar properties render them very useful as drug delivery vehicles.[115,118,119]

5.1.1 Crystallization of Semi-Crystalline Polymers

The crystalline state is characterized as a state exhibiting a melting temperature, T_m (first-order transition), and an X-ray scattering pattern with sharp reflections. T_m is controlled by properties such as hydrogen bonding, polarity, molecular weight, etc…

A crystal is in a lower free energy state than the liquid when the temperature is below the melting point for a large crystal of a very high molecular weight polymer. Figure 5-1 shows schematically the changes in the Gibbs free energy of liquid and a crystal with temperature.

For any spontaneous transformation, ΔG needs to have a negative value for a constant temperature and constant pressure process. At T_m^{∞} (melting point of an infinitely long crystal of finite molecular weight), a condition of equilibrium exists between the crystal and liquid as both phases have the same value of G and $\Delta G=0$.

The crystallization properties of block copolymers have been thoroughly investigated. The block copolymers studied are mostly composed of a semicrystalline block and an amorphous block. In such cases, the presence of a non-crystalline block enables the modification of the mechanical and structural properties of a crystalline polymer, through introduction of a rubbery or glassy component. There are a number of interesting features of these copolymers. Contrary to homopolymers, equilibrium chain folding can occur and crystallization is therefore controlled by the size of the non-crystallizable block.[120-136] Furthermore, in copolymers containing a crystallizable component, structural changes occurring due to microphase separation compete with those resulting from crystallization. Also, selective solvents for the amorphous block can lead to non-equilibrium morphologies because the crystallizable block can precipitate from solution and crystallize. As might be expected, the morphologies formed by the crystallization of block-copolymers therefore depend on both the molecular weight and the crystallization protocol (i.e. cooling rate). Contrary to homopolymers, where folding of chains occurs such that stems are always perpendicular to the lamellar interface, a parallel orientation has been observed for block copolymers crystallized from a lamellar melt phase, and a perpendicular folding has been seen in a cylindrical microstructure. Both orientations are shown in Figure 5-2.

While the case of block copolymers containing one crystalline block has been studied extensively, the behavior of block copolymers having two crystallizable blocks is still fairly unknown. It has been investigated for PCL-PEO-PCL triblocks and it was found that the crystals of PEO and PCL coexist independently and that there are no mixed crystals containing both PEO and PCL. In the copolymers, when the crystallizable block represents less than 25% of the minor component, its crystallinity decreases to zero. In the contrary, in a PEO/PCL binary blend, the two components crystallize separately even with less than 25% of the minor component.

As shown in Figure 5-3, in the blend PEO and PCL form independent crystallites whereas, in the block copolymer, chain connectivity leads to PEO and PCL lamellae occupying the same crystallite when comparable fractions of each are present. In that case, a significant reduction of the lamellae thickness as well as crystal imperfections was observed.

5.1.2 Crystallization of PCL at the Air-Water Interface

Li *et al.* studied the behavior of several PCL homopolymers at the air-water interface.[73,137,138] The crystallization processes were captured using BAM and showed an anisotropic crystal growth at slow compression rates. They observed an increase in the number of nuclei formed with increasing compression rates like the data shown in Figure 5-4.

Li *et al.* also studied the dependence [138] of PCL crystals on the molecular weight. They used PCL samples with number average molar masses (Mn) ranging from 3500 to 36000 $g.mol^{-1}$, and found out that the nucleation and growth of crystals as well as their morphologies and melting properties were dependent on the molar mass. Thomas Joncheray[139] studied the behavior of PCL homopolymers at the air-water. At low pressures the PCL chains were completely adsorbed onto the water subphase with characteristics of liquid expanded and liquid condensed phases. When an isotherm is recorded, below the collapse pressure, Ivanova *et al.*[140] determined that the PCL chain packing and orientation was dependent of the surface pressure. The isotherms recorded showed that the collapse pressure and chain packing was not dependent on the molecular weight of the PCL homopolymer used and that thermodynamically stable monolayers were formed for pressures below the collapse. While the films formed for such pressures are easily studied, the ones formed above the collapse pressure are more complicated to investigate due to phenomena such as desorption of molecules from the interface or formation of multilayers. In the case of the PCL, it was observed that the PCL chains aggregate on top of the water subphase. An interesting phenomenon was also surveyed; after the collapse point, a

decrease in surface pressure was detected corresponding to the crystallization of the PCL segments directly on the water. Compression-expansion hysteresis experiments also show the appearance of a pseudo-plateau during the expansion cycle as a result of the re-adsorption or melting of the PCL chains. AFM images of the PCL homopolymers transferred for a surface pressure before the crystallization on the water surface were taken and the formation of PCL crystals was observed. According to the isotherms, for such surface pressures, the PCL homopolymers are transferred into smooth and hydrated monolayers adsorbed onto the mica surface. It is assumed that upon drying, during and after transfer, part of the PCL chains crystallize, which likely results in a mica surface only partially covered with adsorbed or crystallized PCL chains.

5.2 Results and Discussion

The linear PEO-*b*-PCL diblock copolymer synthesized from a linear PEO macroinitiator (PEO2670, M_n = 2,670 g/mol, ~ 60 ethylene oxide repeat units) contains a PCL block with 35 ε-caprolactone repeat units (Figure 5-5 and Table 5-1). The PEO-*b*-PCL five-arm star-shaped copolymer consists of a hydrophilic PEO core with 9 ethylene oxide units/arm with hydrophobic PCL chains at the star periphery. Each star contains PCL block with 18 ε-caprolactone units/arm (Figure 5-6 and Table 5-1).

5.2.1 Isotherm Experiments

The isotherm of the linear PEO-*b*-PCL copolymer is given in Figure 5-7. Contrary to the isotherms observed for the PEO or PCL homopolymers,[138] pressures as high as 25mN/m can be reached. Better shown in the compressibility plot in Figure 5-8, a transition can be observed around 13.5mN/m. Thomas Joncheray[139] studied several PEO-*b*-PCL linear copolymers with a number of ε-caprolactone units ranging from 11 to 35 (the number of ethylene oxide units was

kept constant throughout the entire investigation). The maximum in monolayer compressibility for the high pressure transition increases as PCL chain length increases. This suggests the presence of a PCL-related phase transition. For PEO-*b*-PCL linear copolymers with a smaller amount of ε-caprolactone units, three different phase transitions can be observed for pressures of 6.5, 10.5, and 13.5mN/m. For the copolymer studied in this chapter (PEO_{60}-*b*-PCL_{35}), only the high pressure transition is observed. This transition is known to represent the crystallization of the PCL blocks.[138-140] It was suggested that the transition observed for a pressure of 6.5mN/m represents the dissolution of the PEO into the aqueous subphase. In our case, no transition is observed at low pressures indicating that when the PCL block size increases, the dissolution of PEO is made more difficult. Compression-expansion hysteresis plots of the PEO-*b*-PCL linear copolymer are shown in Figure 5-9. A broad melting transition is observed during the first expansion. This behavior was not observed for PCL homopolymer samples[138,139] and could be explained by the properties of the crystals formed during the first compression, such as size, shape or polydispersity. No plateau was observed during the compression or expansion cycle but we can detect a re-adsorption of the crystallized PCL chains for pressures under 5mN/m. Joncheray *et al.*[139] performed compression-expansion hysteresis experiments for several barrier speeds and the melting (re-adsorption) and crystallization (desorption) pressure values were found to be strongly barrier speed dependent. In the case where the barriers were moved infinitely slowly, the melting and crystallization pressure values would become identical.

The isotherm of the PEO-*b*-PCL star copolymer is shown in Figure 5-10. It exhibits three distinct regions corresponding to different conformations of the polymer chains. For high MMA, the surface pressure slowly increases until it reaches a pseudoplateau. For low MMA, a sharp increase in surface pressure is observed representing the formation of highly condensed films.

However, for the star copolymer studied, the intermediate MMA region shows an almost inexistent pseudoplateau. The compressibility plot shown in Figure 5-11 illustrates that absence even better by exhibiting no transition in the intermediate MMA range. This suggests that the PEO blocks are not adsorbed onto the interface but are more likely to be in the water subphase. Compression-expansion hysteresis experiments were performed for target pressures below (Figure 5-12) and above (Figure 5-13) the pseudoplateau pressure. For surface pressures below 9mN/m, the compression and expansion curves are superposable independent of the target pressure. This illustrates the reproducibility and stability of the films formed. Due to the size of the PCL blocks, the block copolymer is hydrophobic enough to avoid the irreversible dissolution of material in the aqueous subphase. The compression-expansion curves for a target pressure of 15mN/m are shown in Figure 5-13. A pseudoplateau is observed during the expansion cycles corresponding to the re-adsorption (melting) of the crystallized PCL chains.

In order to further interpret the crystallization behavior as well as the stability of the films formed, additional analysis using AFM and BAM is going to be discussed in the next part.

5.2.2 Brewster Angle Microscopy and Comparison to Previous AFM Imaging

Joncheray *et al.* studied the crystallization of PEO-*b*-PCL linear and star copolymers in the transferred LB monolayers and observed the formation of crystalline domains independent of the surface pressure, when investigated by AFM. While AFM gives some hint about the crystallization behavior of those polymers, BAM allowed us to observe the formation of crystals directly at the water subphase, subsequently eliminating variables such as affinity to substrate, transfer pressure, water evaporation and film thickness.

Figures 5-14 and 5-15 show the BAM images for the PEO-*b*-PCL linear and star copolymer respectively. Those images were taken at both intermediate and low MMA. Both star and linear copolymers do not seem to show any crystal formation for pressures below 10mN/m.

By AFM, several crystals were observed at low surface pressures, indicating the importance of sample preparation, differences in resolution of the two techniques, or differences in polymer behavior absorbed to a solid compared to the water surface. Generally, it also appears that more crystals are observed by AFM than what can be observed at the air-water interface. Nonetheless, above a specific pressure, crystals formed at the water surface exhibit the same morphologies as those observed by AFM (Figure 5-16). The only noticeable difference is the presence of more numerous crystals on the AFM images, suggesting again the influence of sample preparation before AFM imaging. As seen in chapter 2, the lateral resolution of the BAM is significantly lower than the one observed for AFM. Nonetheless, the BAM can detect features as small as 2μm which is 5 times smaller than the crystals showed in the AFM pictures.

A compression-expansion experiment was performed and the corresponding images are given in Figure 5-17. Analogous to the pressure results of the previous compression-expansion hysteresis isotherm plots, BAM reveals that the crystallized PCL chains melt and re-adsorb during the expansion cycle. When comparing the images for a surface pressure of 10mN/m, one can notice that some remaining crystals are still present during the second compression. As discussed earlier in the chapter, the melting (re-adsorption) and the crystallization (desorption) pressures are strongly dependent on the barrier speed. One can expect the images for different compressions to be identical for an infinitely slow barrier speed. The barrier speed dependence as well as the presence of hysteresis between the compression and expansion curves suggests the formation of thermodynamically unstable films for intermediate and high surface pressures. This metastability is shown in Figure 5-18 where the monolayer was compressed to a pressure of 18mN/m. The surface pressure was then kept constant and images were taken after several stabilization times. One can notice that for t = 0, no crystals are observed but as the stabilization

time increases, the amount of crystals increases, suggesting once again the presence of thermodynamically unstable films.

5.3 Conclusions

In this chapter, the interfacial behavior of a PEO-*b*-PCL linear copolymer and a PEO-*b*-PCL star copolymer were investigated. The morphologies formed were observed by BAM and compared to previous AFM results. The isotherm of the star-shaped block copolymer indicated the presence of a single phase transition characterized by a pseudoplateau that corresponds to the collapse and crystallization of the PCL chains above the water surface. Below that plateau, the PCL chains are completely adsorbed, anchoring the PEO chains to the interface. In this region, the compression-expansion hysteresis experiments as well as the structures observed by BAM showed the formation of thermodynamically stable monolayers.

Once the pseudoplateau is reached, the PCL chains crystallize at the interface. This phenomenon was highlighted by the BAM pictures. We were able to show that the PCL chains crystallize directly at the interface and not during the AFM sample preparation. The images observed by BAM were found to be strongly dependent on the stabilization time and a more important aggregation was observed over time. Compression-expansion experiments showed that the melting (re-adsorption) of the PCL chains was slower than their crystallization (desorption).

.

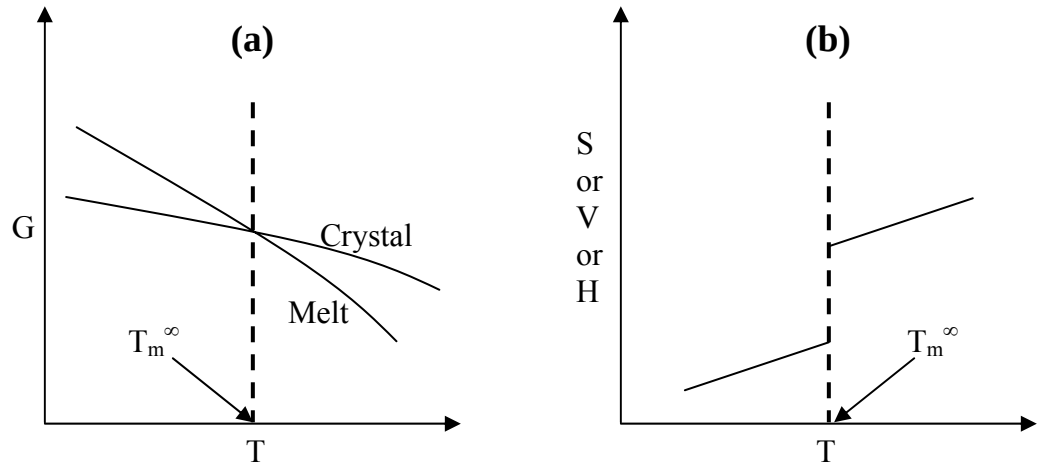

Figure 5-1. General behavior of thermodynamic variables at the equilibrium melting temperature T_m^∞ (a) Gibbs free energy (b) entropy, enthalpy and volume

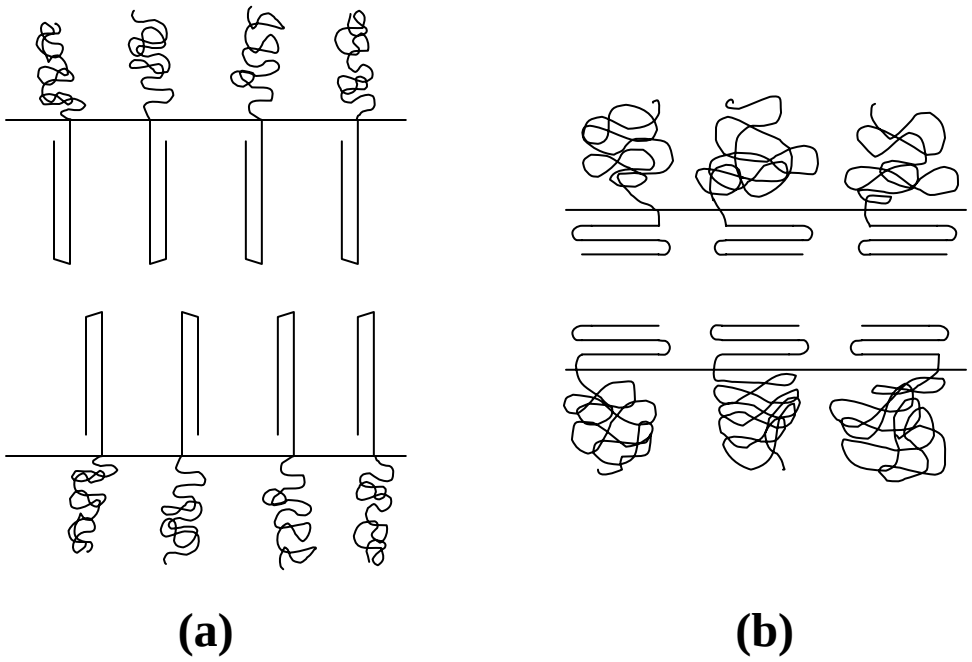

Figure 5-2. Schematic of perpendicular (a) and parallel (b) chain folding in semicrystalline block copolymers

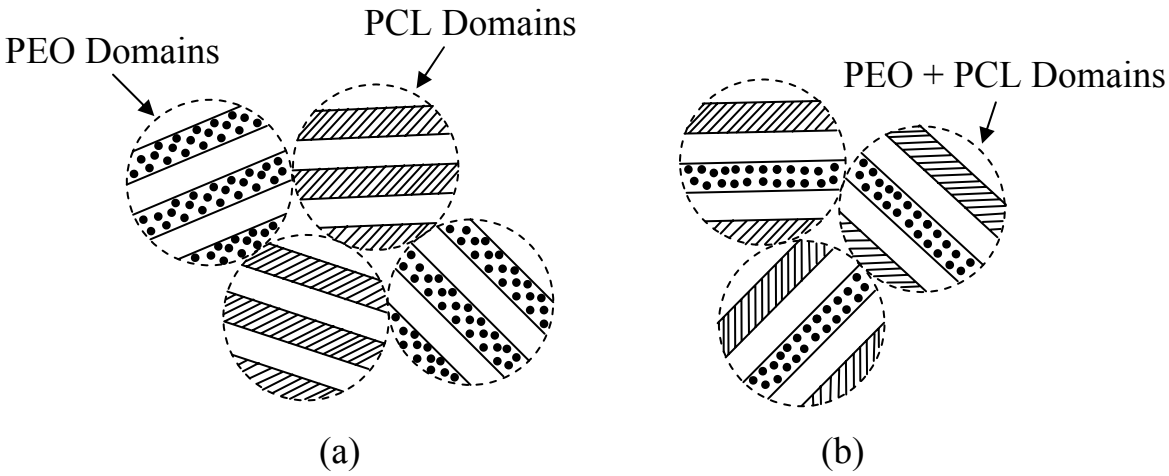

Figure 5-3. Schematic illustration of the morphology formed by blends and copolymers of two crystallizable polymers. (a) a PEO/PCL Blend and (b) a PCL-PEO-PCL triblock. In the blend, PEO and PCL are phase separated into domains in which each homopolymer crystallizes in a lamellar texture. In the copolymer, PEO and PCL blocks crystallize in the same domain due to chain connectivity

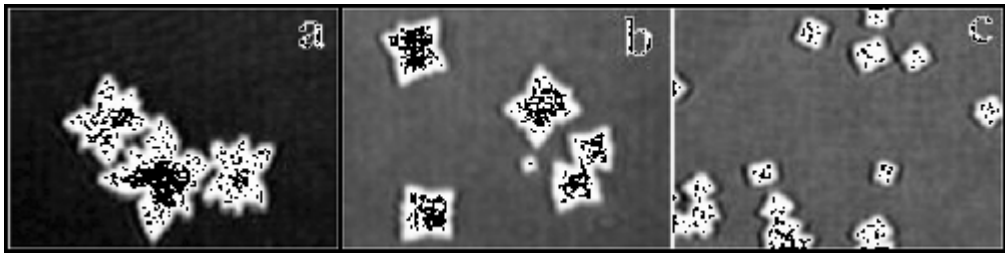

Figure 5-4. Compression rate dependence of crystal growth in Langmuir monolayers at 22.5 °C.[49] BAM images were obtained at compression rates of (a) 0.010, (b) 0.013, and (c) 0.026 $nm^2 \cdot monomer^{-1} \cdot min^{-1}$ for $A \sim 0.08$ $nm^2 \cdot monomer^{-1}$. All images are 1.28 × 0.96 mm^2 (Data borrowed from reference 137)

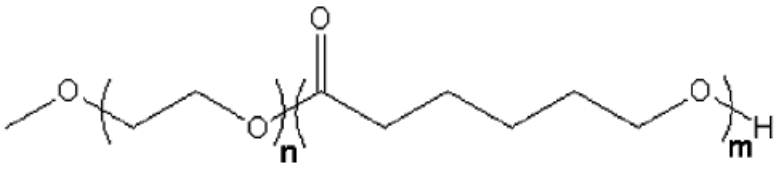

Figure 5-5. The linear PEO-*b*-PCL copolymer used in this study (n = 60, m = 35)

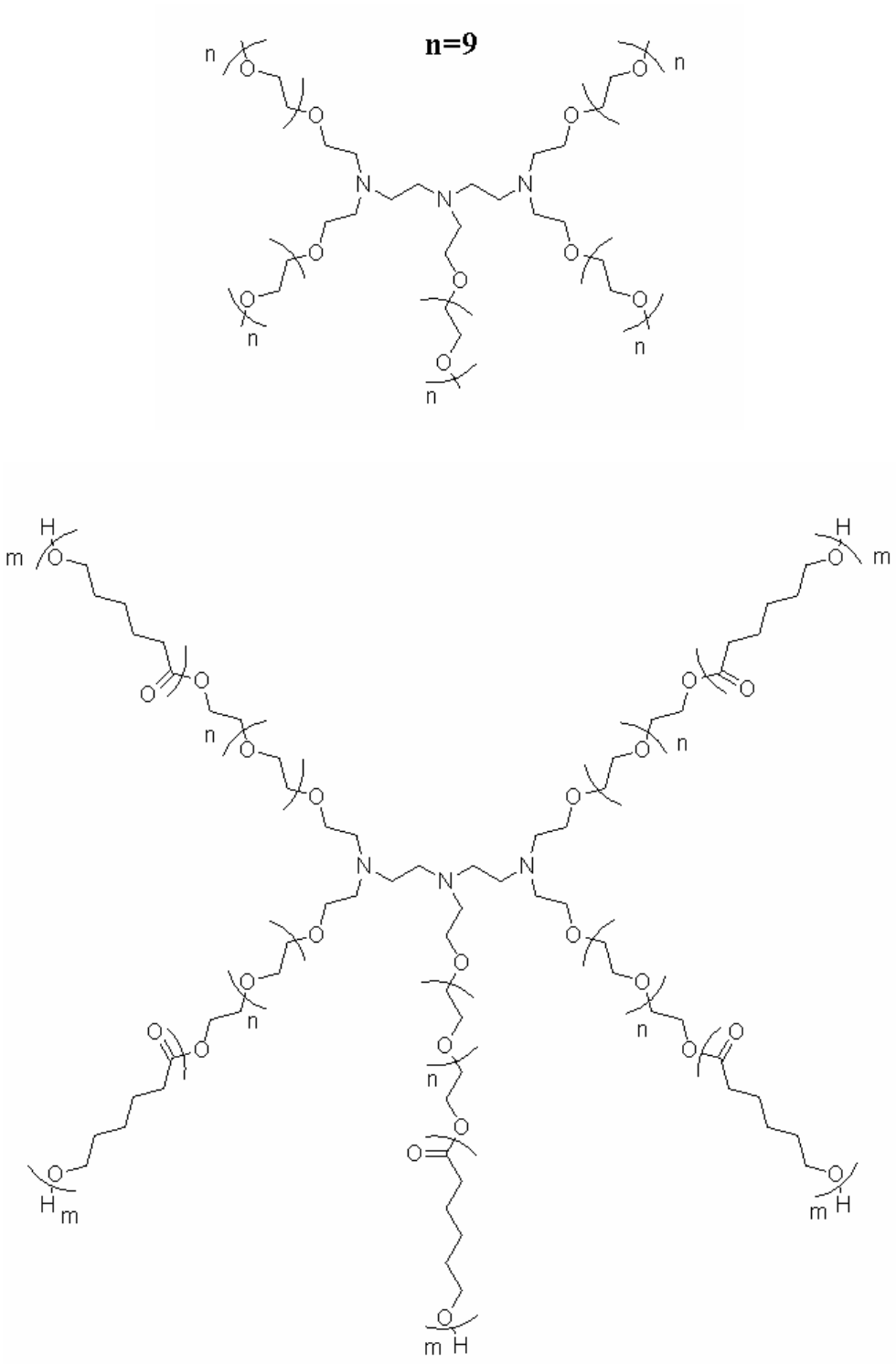

Figure 5-6. Schematic of the star-shaped PEO-*b*-PCL copolymer used in this study. Further characterization data are shown in table 5-1

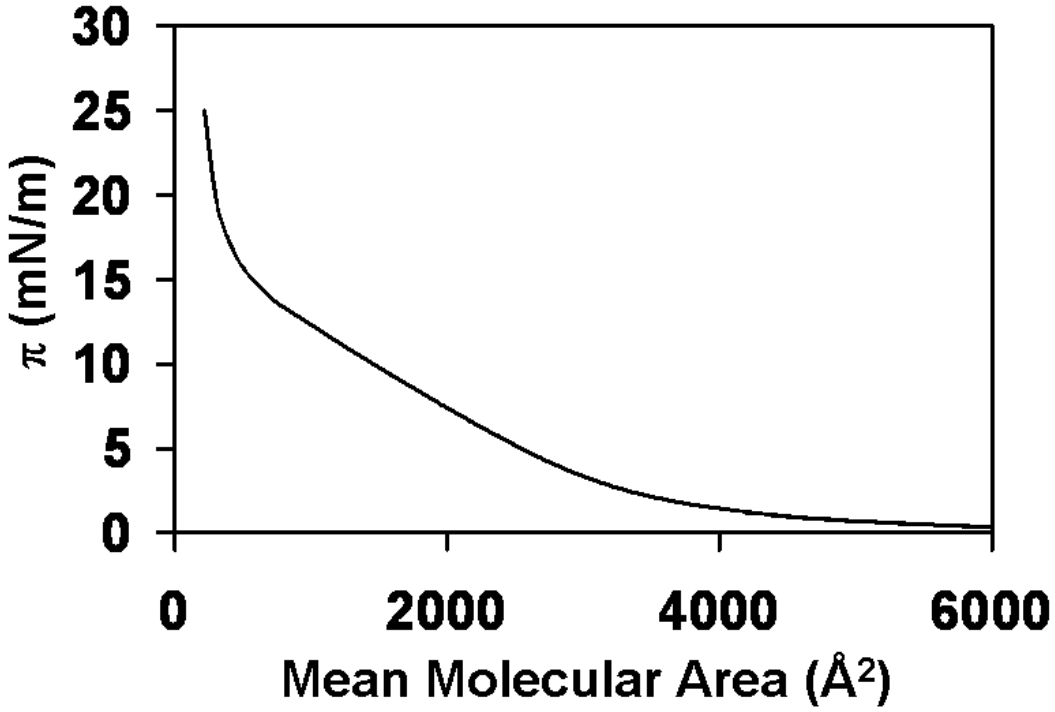

Figure 5-7. Surface pressure-MMA isotherm for the linear PEO_{60}-*b*-PCL_{35} linear copolymer for a compression rate of 5mm/min

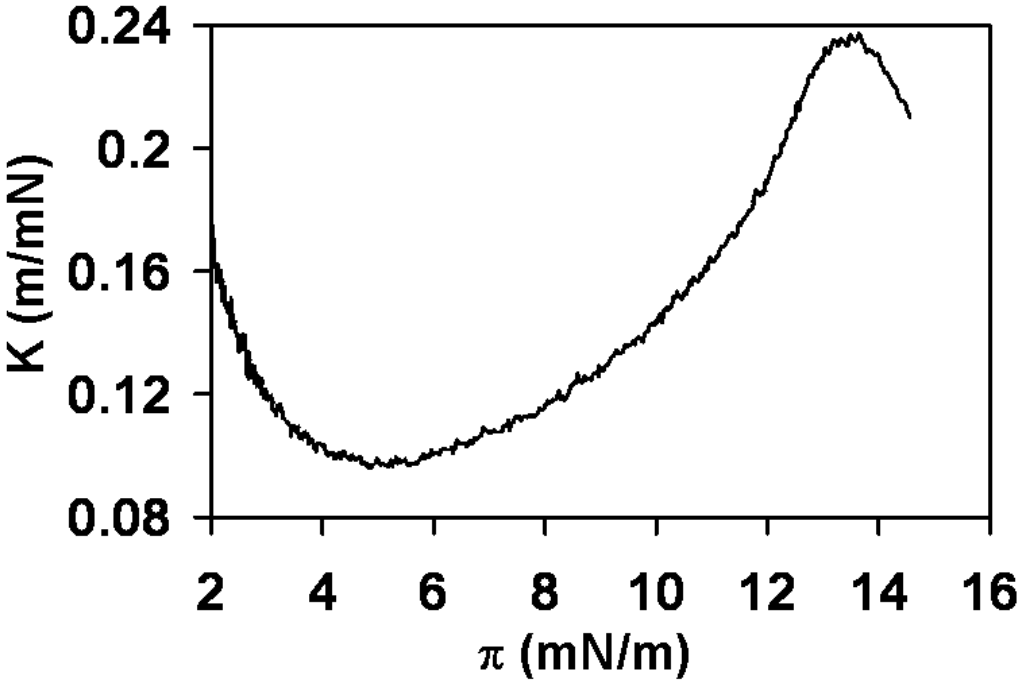

Figure 5-8. Compressibility plots of the PEO-*b*-PCL linear diblock copolymer versus surface pressure.

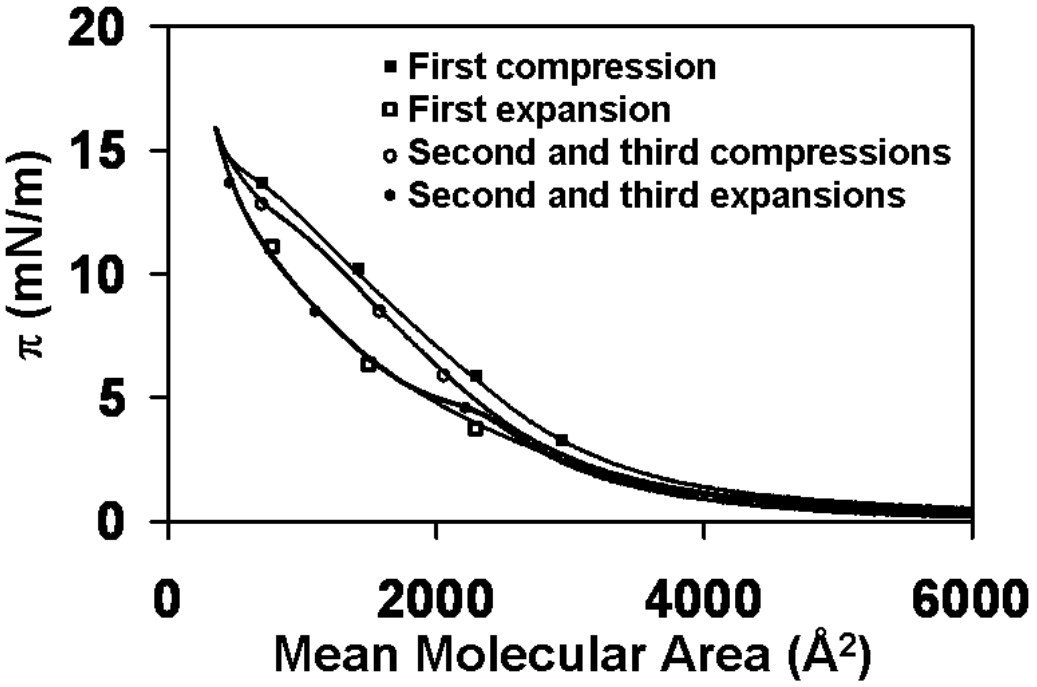

Figure 5-9. Compression-expansion hysteresis plot of the PEO-*b*-PCL linear copolymer compressed at a target pressure of 16 mN/m. The compression and expansion rates used in the experiments were both 5mm/min

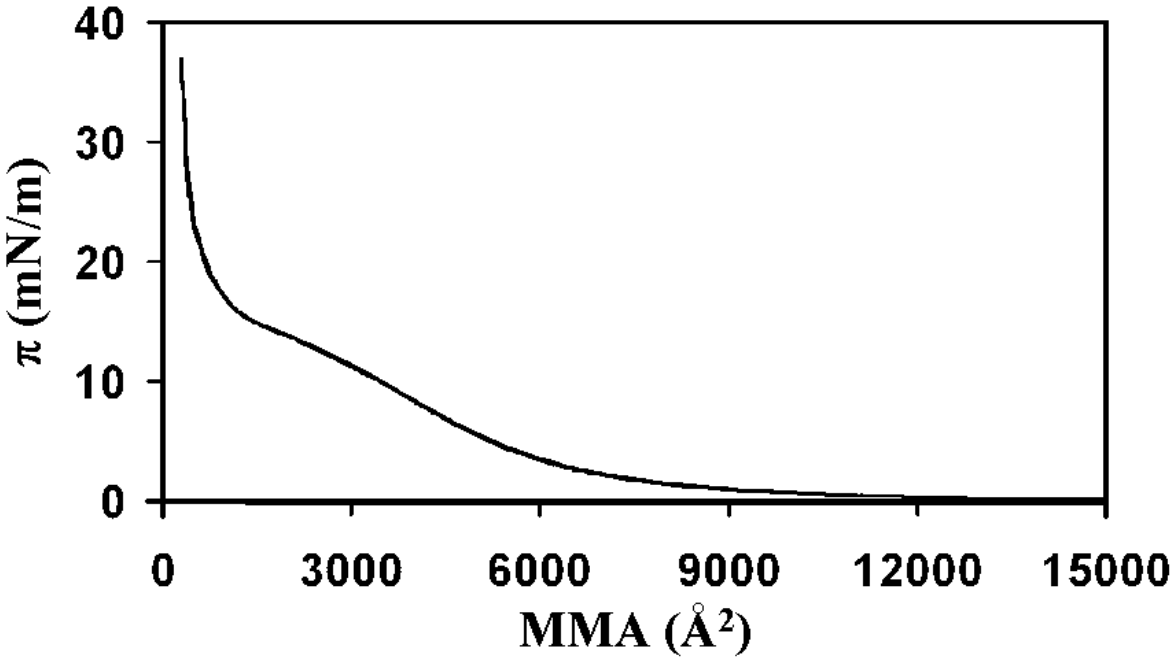

Figure 5-10. Surface pressure-MMA isotherm for the PEO-*b*-PCL star copolymer recorded for a speed of 5mm/min

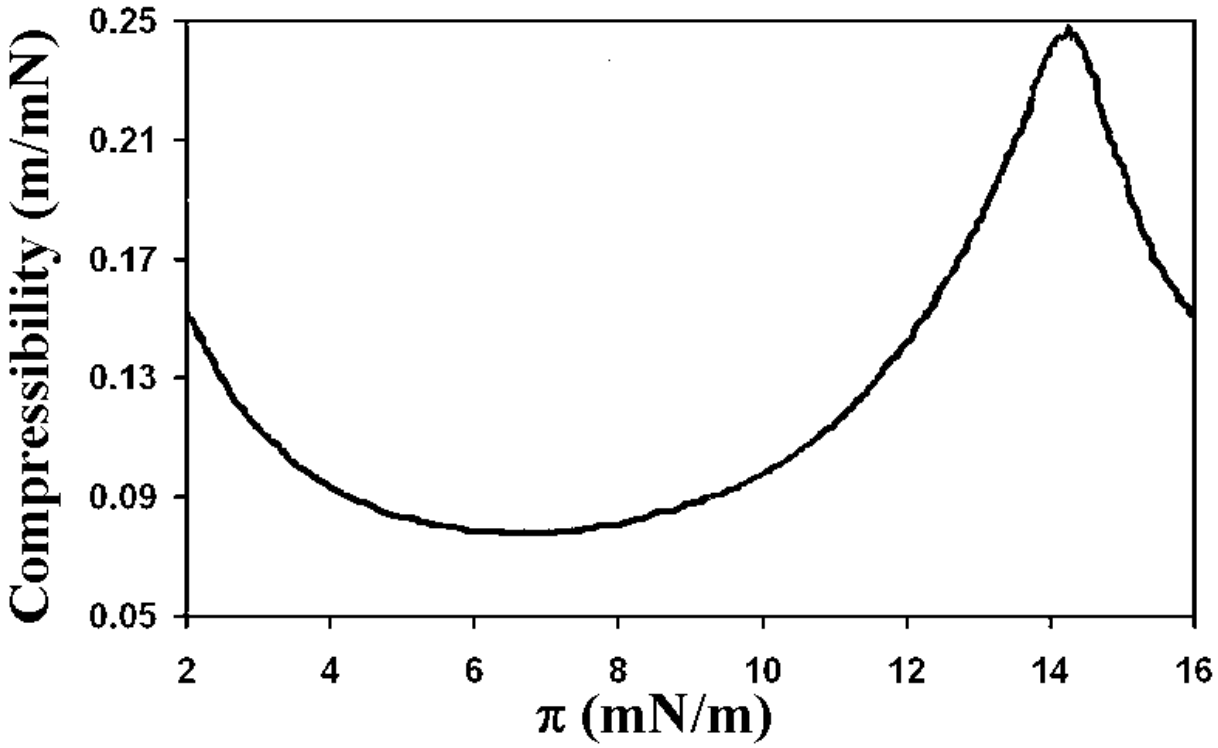

Figure 5-11. Compressibility plots of the PEO-*b*-PCL star diblock copolymer versus surface pressure.

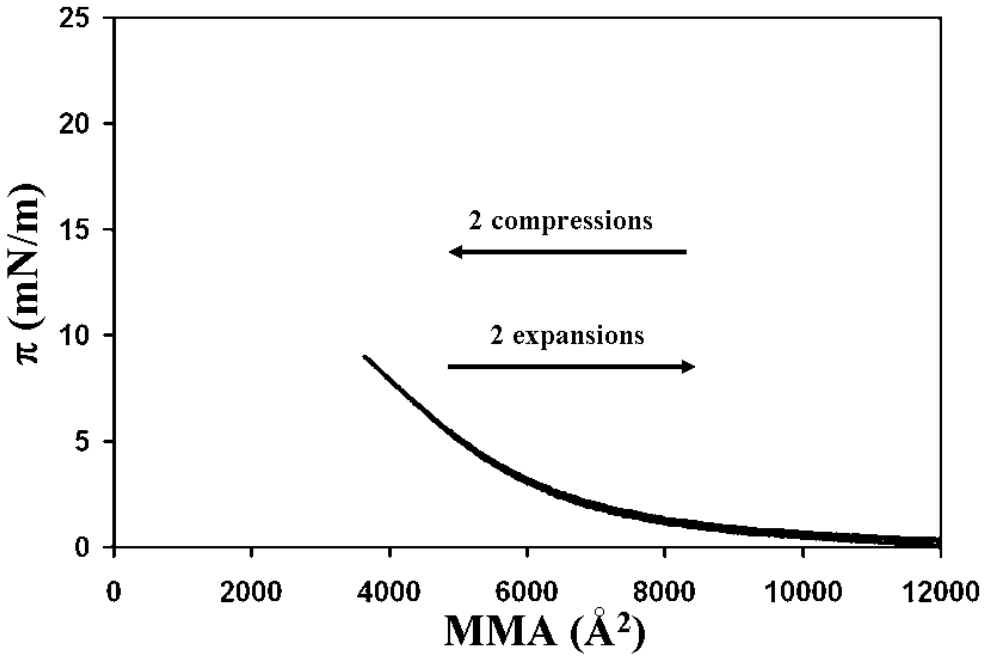

Figure 5-12. Compression-expansion hysteresis plot of the PEO-*b*-PCL star copolymer compressed at a target pressure of 9 mN/m. The compression and expansion rates used in the experiments were both 5mm/min

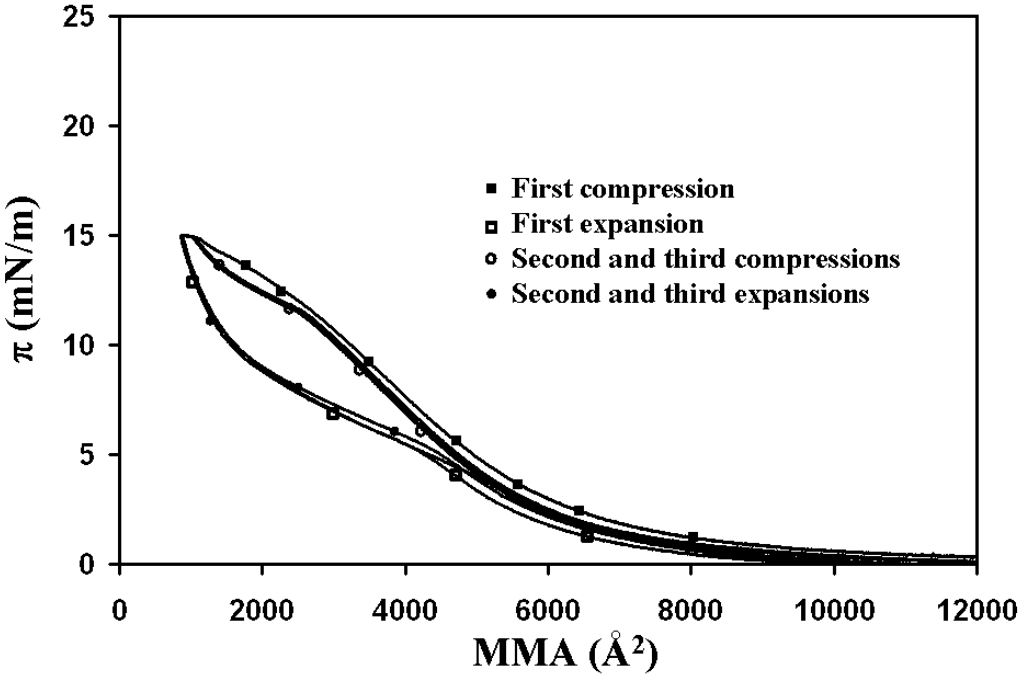

Figure 5-13. Compression-expansion hysteresis plot of the PEO-*b*-PCL star copolymer compressed at a target pressure of 15 mN/m. The compression and expansion rates used in the experiments were both 5mm/min

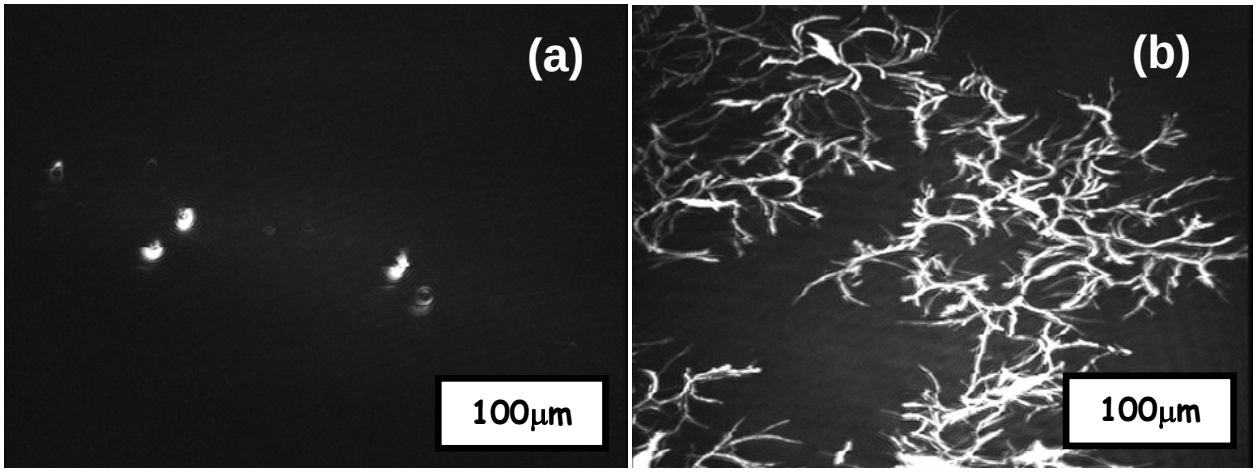

Figure 5-14. BAM Images of the PEO-*b*-PCL linear copolymer at a pressure for 10mN/m (a) and 15mN/m (b)

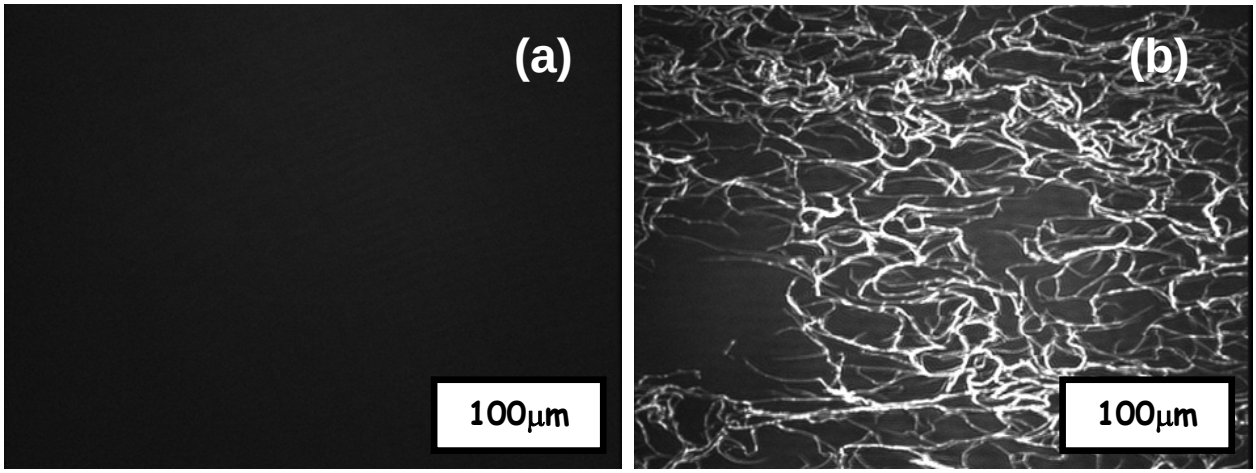

Figure 5-15. BAM Images of the PEO-*b*-PCL star copolymer for a pressure of 10mN/m (a) and 20mN/m (b)

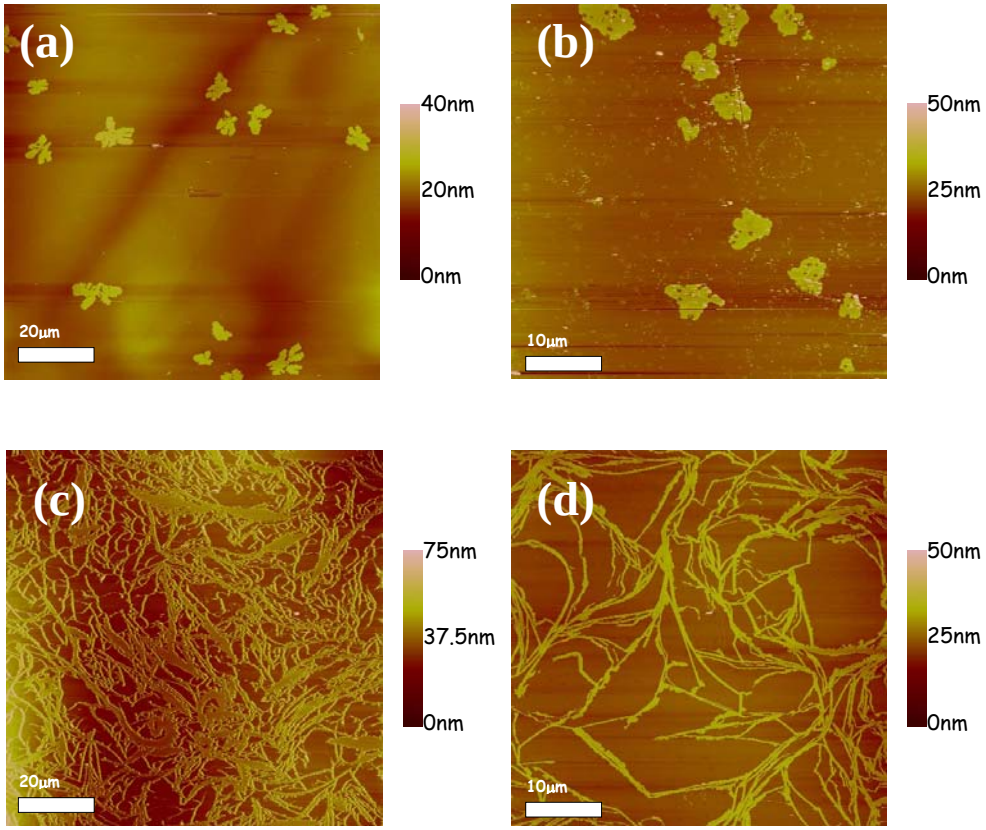

Figure 5-16.AFM Images for the linear PEO-*b*-PCL copolymer ((a) 10mN/m and (c) 15mN/m) and the PEO-*b*-PCL star copolymer ((b) 10mN/m and (d) 20mN/m)

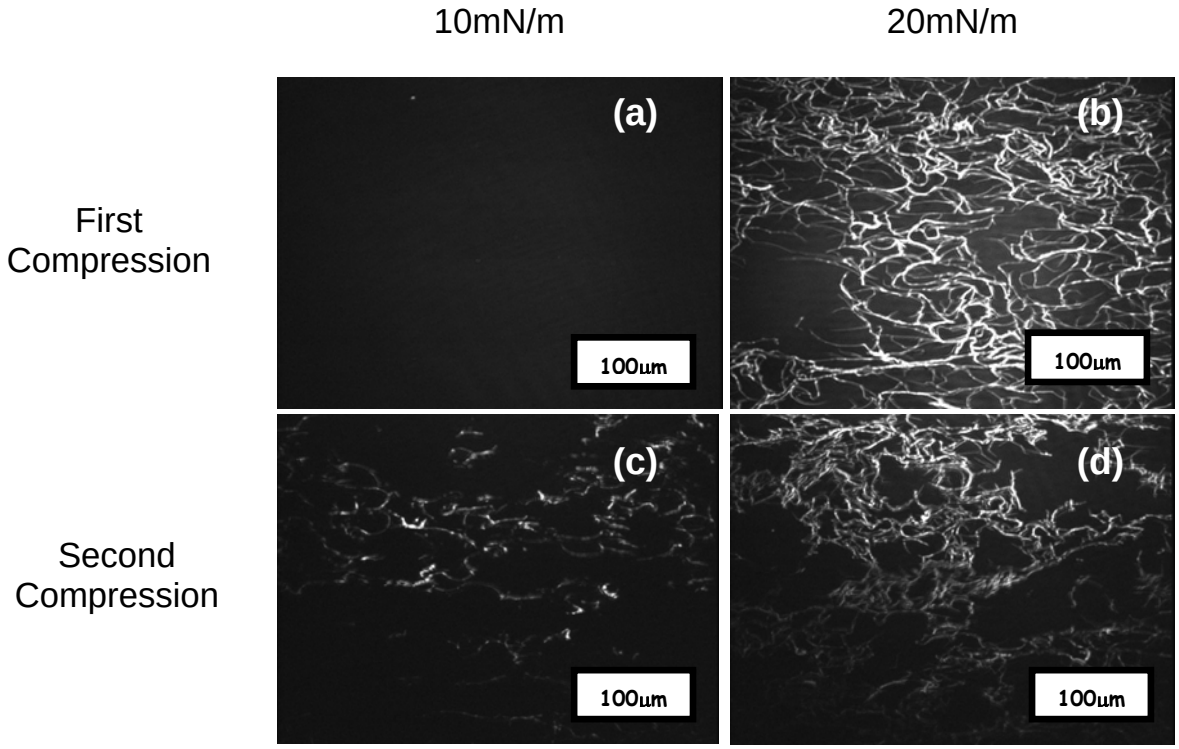

Figure 5-17. BAM Images of the PEO-*b*-PCL star copolymer for pressures of 10 and 20mN/m during the first (a and b) and the second compression cycle (c and d)

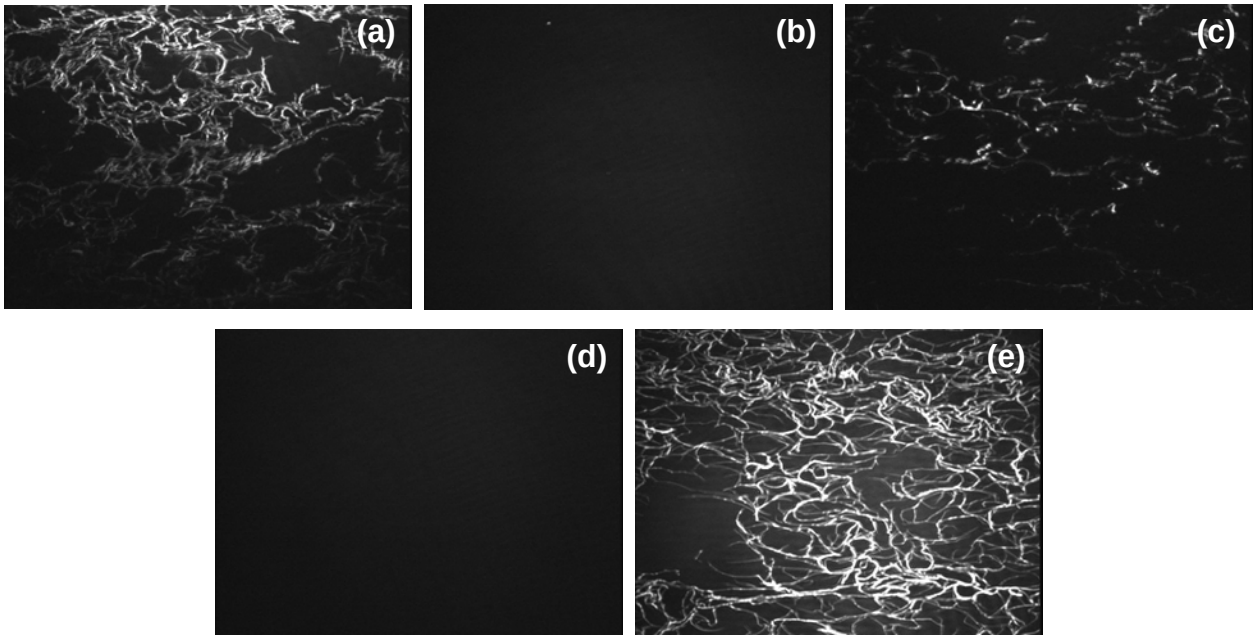

Figure 5-18. BAM images for a pressure of 18mN/m (a) and after waiting 15min (b), 20min (c), 35 min (d) and 55min (e)

Table 5-1. Characteristics of the linear and star-shaped copolymers

Name	PEO_{60}-*b*-PCL_{35}	Star
M_n [a] *(g/mol)*	6,680	13,110
PDI[a]	1.24	1.44
Avg no. of ethylene oxide units	60	9
Avg no. of ε-caprolactone units	35	18

[a] Determined by ^{1}H NMR
[b] Determined by GPC calibrated with linear polystyrene standards.

CHAPTER 6
CONCLUSION AND PERSPECTIVES

In this dissertation, the behavior of various amphiphilic copolymers was studied at the air-water interface using Langmuir-Blodgett methods as well as AFM and BAM.

6.1 Summary

6.1.1 Blends of a PS-*b*-PEO Copolymer with PS and PEO Homopolymers

As discussed previously, the addition of free homopolymer chains have an important effect on the architecture of the films formed (Figure 6-1). The isotherms displayed three different regions known as “pancake”, pseudoplateau, and “brush” areas. While the addition of PS seemed to affect the brush area of the isotherm, the addition of PEO showed a difference in the transition area (pseudoplateau). AFM was able to give us insights on the film architectures and showed the influence of each homopolymers on the chaining observed in the pure PS-*b*-PEO copolymer. On one hand the addition of PS increased the amount of chaining of the PS domains enhancing the hydrophobic properties of the monolayer, on the other hand the accumulation of PEO decreased the chaining present between the PS domains and favored the phase separation between clusters of micelles and layers of pure PEO. This chapter gave us fundamental information on copolymer blends at the air-water exhibiting more complex architectures without having to go through difficult synthesis techniques.

6.1.2 PS-*b*-PtBA Star Copolymers at the Air-Water Interface

Three star copolymers as well as a PtBA homopolymer were studied at the air-water interface. All the isotherms observed had a plateau at a pressure of 24mN/m suggesting the presence of a first order transition. A dependence on the PtBA molecular weight could be seen throughout the entire isotherm plot, however, the PS influence still unclear. After performing AFM experiments on the monolayers formed, we proposed the transition from a two-

dimensional PtBA completely adsorbed onto the interface to a three-dimensional PtBA that starts desorbing from the interface. An increase in the length of the PtBA chains affected both the region below and above the plateau. For pressures below the plateau, the addition of PtBA decreased the size of the copolymer domains as well as increased the distance between those domains. However, when transferred for pressures above 24mN/m, the aggregation observed in the monolayer increased with the amount of PtBA present in the copolymer. Compression-expansion hysteresis experiments showed the formation of thermodynamically stable films for pressures under 24mN/m. For pressures higher than 24mN/m, isochoric experiments were performed and exhibited a relaxation of the monolayer to its equilibrium spreading pressure.

6.1.3 PEO-*b*-PCL Copolymers at the Air-Water Interface

AFM results were compared to those obtained by BAM in order to better understand the crystallization behavior of the copolymers. The isotherms showed the presence of a pseudoplateau around 15mN/m. Below that pressure, the PCL chains are completely adsorbed onto the interface whereas they crystallize for pressures above the pseudoplateau pressure. BAM illustrated the influence of sample preparation when LB films were studied by AFM. In fact the films formed above the pseudoplateau were thermodynamically unstable and the aggregation was strongly time dependent. BAM pictures were taken for a pressure of 18mN/m after several stabilization times and the aggregation increased when upon annealing.

6.2 Correlation Between the Different Systems

PS- and PEO-containing systems were studied in order to determine the role played by each block on the copolymer self-assembling behavior.

Four PS-containing systems were investigated in this work: one completely hydrophobic (PS), PS-*b*-PEO diblock copolymer, PS-*b*-PtBA star copolymers, and blends. It is well-known that PS is hydrophobic and aggregates into irregular islands instead of spreading into monolayers

(Figure 6-2). We showed that by adding small quantities of an amphiphilic copolymer (PS-*b*-PEO), one was able to enhance and vary the interfacial properties of the PS homopolymer. The PS aggregates observed when in presence of the copolymer were also more regular than those observed when free PS homopolymer chains were spread at the interface. The films formed by the blends seem to have similar properties as those observed for a copolymer possessing the same total number of PS repeat units.

Two distinct PS-containing copolymers were used to investigate the effect of the hydrophilic block on the architectures formed. PS-*b*-PEO and PS-*b*-P*t*BA copolymers were studied with PEO being more hydrophilic than P*t*BA. For low surface pressures, comparable domains of PS can be detected for both systems ($\Gamma \sim 100$). PS-*b*-PEO copolymers have been widely studied at the air-water interface.[16-31] At low coverage, the interactions between the EO monomers and the interface is attractive. However, when the monolayer is compressed, the repulsive forces between the PS and the PEO blocks promote the desorption of some PEO from the interface into the water. Upon further compression the PEO is pushed into the water subphase as shown in Figure 6-2.[25] Contrary to the PEO-containing copolymer, the one containing P*t*BA as the hydrophilic group presented a completely different conformation. The P*t*BA is not as hydrophilic as the PEO and therefore cannot stretch into the water subphase. Instead, once the plateau pressure (24mN/m) is reached the P*t*BA started desorbing from the interface. For high surface pressures, a three-dimensional system was formed presenting 3 different regions: adsorbed PtBA, desorbed PtBA, and PS domains.

Depicted in Figure 6-3, three different PEO-containing systems were investigated in order to study the various films formed. High molecular weight PEO homopolymer form monolayers when spread at the air-water interface however, once the pseudoplateau pressure is reached, the

PEO dissolved in the water subphase. PS was used as an anchor to keep the PEO from dissolving, and a new region was detected on the isotherm. Contrary to PS, PCL homopolymers are already surface active and form films when spread at the air-water interface. Compare to the PS-*b*-PEO copolymer where the PS was just sitting on top of the PEO layer, the PCL crystallized directly at the interface forming new and interesting architectures. Even if the PCL homopolymers already formed monolayers when spread at the air-water interface, the PEO-*b*-PCL films could be compressed to higher surface pressures. In the pseudoplateau region, PCL homopolymers as well as PCL chains in the copolymers crystallized directly at the air-water interface. It was confirmed that above the pseudoplateau, all the PCL chains have collapsed and the sharp pressure represents the interactions between the hydrated PEO cores.

Those projects gave us interesting insights on the fundamental self-assembling behavior of PS- and PEO-containing amphiphilic copolymers. By using different hydrophilic and hydrophobic groups, we were able to monitor the formation of various architectures at the air-water interface. The control of conformations or orientations of the different blocks was easily achievable by monitoring the copolymer architectures, the amount of homopolymer added (in the case of the blends), or the surface pressure.

6.3 Future Work

Jeong *et al* [92-94], showed that the miscibility between PMMA homopolymer and PMMA block was higher in thin films than in the bulk. In that case spin coating was used to prepare the films. However, an interesting study for our blends would be to investigate the miscibility between PEO homopolymer and PEO block or PS homopolymer and PS block when spread onto a water subphase, compare to that observe in the bulk. This would allow us to get more fundamental information about the blend behavior and have a better control on the morphologies formed.

The condensed area, present for small molecular areas, demonstrates a dependence in PS in the case of the blends seen in chapter 3, as well as for star-shaped PS-*b*-PEO copolymers previously studied in our group[33]. For the PS-*b*-PtBA copolymers studied in chapter 4, a dependence of the condensed area on the PtBA molecular weight was observed. However, the effect of PS remains unclear. Studying copolymers with varying PS segments would provide more information on the influence of the hydrophobic block on the architectures formed and allow a better control on the architectures formed.

Further investigations would need to be done to determine the exact number of arms in each PS-*b*-PtBA star copolymer. One method would be to cleave the arms of the stars by base hydrolysis and then perform viscometry/universal calibration and light scattering experiments in order to detect the exact molecular weight as well as the mass distribution of the branches. Once we determine this value, we would be able to calculate the exact number of arms for each star and therefore have a better understanding of the aggregation properties at the air-water interface.

Mengel *et al.*[83] studied the chemical modification of P*t*BA films into PAA after transfer onto a solid substrate. The presence of PAA chains at the surface renders the film very useful for applications in molecular electronic and optical devices. This technique could be applied to our system in order to obtain PS-*b*-PAA films with well-defined architectures and surface chemistry. PS-*b*-PAA copolymers were shown to spread at the air-water interface. However, contrary to PS-*b*-PtBA copolymers, a strong pH-dependence is observed and the structures formed are not as well defined. By performing the chemical modification after transfer, we would be able to optimize the formation of those films and control the structures formed.

Various PCL molecular weights could also be investigated in the case of the PEO-*b*-PCL copolymers. Knowing the influence of the molecular weight on the crystallization process would

give insights on the transport properties of the polymer chains. The driving force of polymer crystallization is the degree of undercooling ($\Delta T = T_m^0 - T_x$), which is directly related to the crystallization temperature. Therefore, studies over a wide range of temperatures would provide information about the effect of temperature on the copolymer crystallization. An interesting investigation would be to study blends of PEO-b-PCL copolymers with PCL homopolymers of various molecular weights. This would give us information on the crystallization behavior and also know if the formation of crystals could be controlled by the amount of PCL present.

Finally, for most of the copolymers studied, the non stability of the films formed at high surface pressure was detected in the compression-expansion hysteresis or the isochoric experiments. Performing investigations for several compression rates would quantitatively describe the compression rate dependence of film formation at the air-water interface.

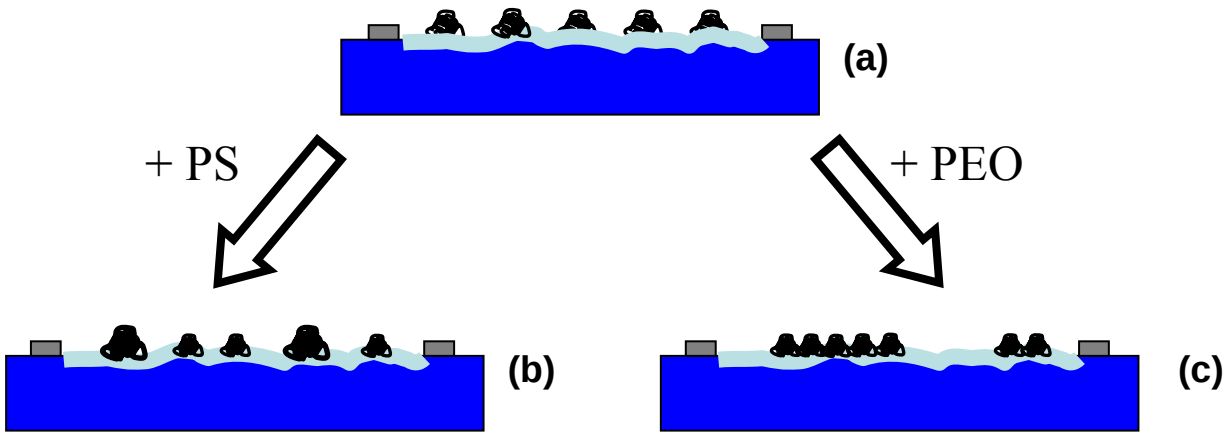

Figure 6-1. Morphologies observed at low surface pressures for (a) the pure PS-*b*-PEO copolymer, (b) the pure PS-*b*-PEO copolymer + PS homopolymer, and (c) the pure PS-*b*-PEO copolymer + PEO homopolymer (blue = PEO, black = PS)

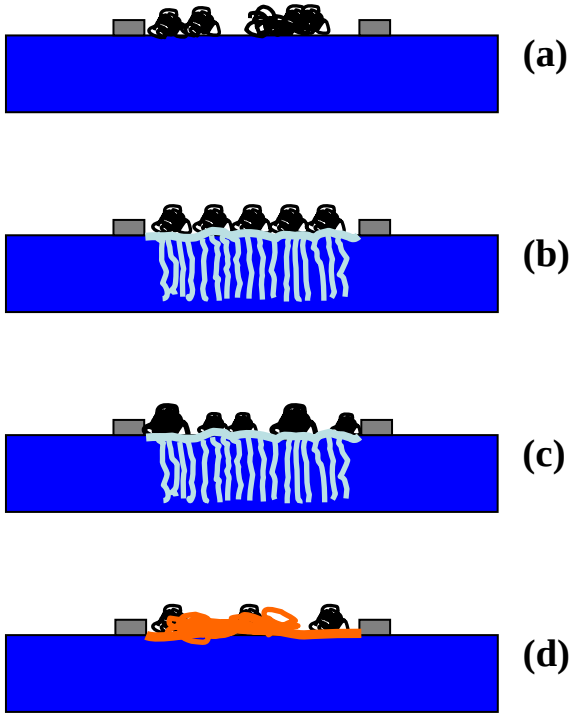

Figure 6-2. Morphologies observed at high surface pressure for (a) PS, (b) PS-*b*-PEO diblock copolymer, (c) PS + PS-*b*-PEO diblock copolymer, and (d) PS-*b*-PtBA copolymer (blue = PEO, black = PS, and orange = PtBA)

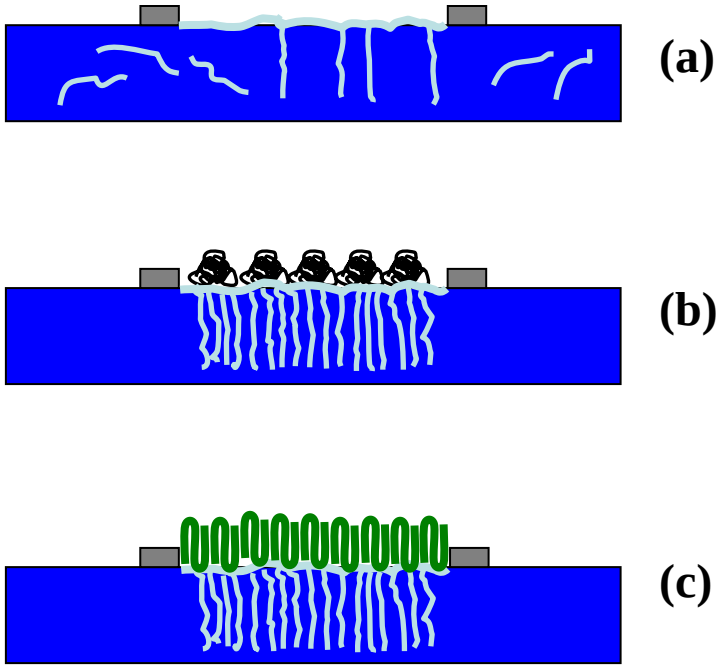

Figure 6-3. Morphologies observed at high surface pressure for (a) the PEO homopolymer, (b) PEO-*b*-PS diblock copolymer, and (c) the PEO-*b*-PCL copolymer (blue = PEO, black = PS, and green = PCL)

LIST OF REFERENCES

(1) Li, M.; Coenjarts, C. A.; Ober, C. K. *Adv. Polym. Sci.* **2005**, *190*, 183.

(2) Adhikari, R.; Michler, G. H.; Lebek, W.; Goerlitz, S.; Weidisch, R.; Knoll, K. *J. Appl. Polym. Sci.* **2002**, *85*, 701.

(3) Milner, S. T. *Macromolecules* **1994**, *27*, 2333.

(4) Lecommandoux, S.; Borsali, R.; Schappacher, M.; Deffieux, A.; Narayanan, T.; Rochas, C. *Macromolecules* **2004** *37*, 1843.

(5) Jagur-Grodzinski, J. *J. Polym. Sci. Part A: Polym. Chem.* **2002**, *40*, 2116.

(6) Matyjaszewski, K. *Mol. Cryst. Liq. Cryst.* **2004**, *415*, 23.

(7) Moad, G.; Chong, Y. K.; Postma, A.; Rizzardo, E.; Thang, S. H. *Polymer* **2005**, *46*, 8458.

(8) Park, M.; Harrison, C.; Chaikin, P. M.; Register, R. A.; Adamson, D. H. *Science* **1997**, *276*, 1401.

(9) Fink, Y.; Urbas, A. M.; Bawendi, M. G.; Joannopoulos, J. D.; Thomas, E. L. *J. Lightwave Technol.* **1999**, *17*, 1963.

(10) Kim, S. O.; Solak, H. H.; Stoykovich, M. P.; Ferrier, N. J.; de Pablo, J. J.; Nealey, P. F. *Nature* **2003**, *424*, 411.

(11) Abetz, V.; Simon, P. F. W. *Adv. Polym. Sci.* **2005**, *189*, 125.

(12) Matsen, M. W.; Bates, F. S. *J. Chem. Phys*. **1997**, *106*, 2436.

(13) Leibler, L. *Macromolecules* **1980**, *13*, 1602.

(14) Gohy, J. *Adv. Polym. Sci.* **2005**, *190*, 65.

(15) Hadjichristidis, N.; Pispas, S.; Floudas, G. *Block Copolymers: Synthetic Strategies, Physical Properties, and Applications*; John Wiley & Sons, Inc.: Hoboken, NJ, 2003.

(16) Vesselovsky, V. S.; Pertzov, V. N. *Zh. Fiz. Khim*. **1936**, *8*, 245.

(17) Torza, S.; Mason, S. G., Kolloid Z. *Z. Polym*. **1971**, *246*, 593.

(18) Good, R. J.; Koo, M. N. *J. Colloid Interface Sci*. **1979**, *71*, 283.

(19) Platikanov, D.; Nedyalkov, M.; Scheludko, A. *J. Colloid Interface Sci*. **1980**, *75*, 620.

(20) Platikanov, D.; Nedyalkov, M.; Nasteva, V. *J. Colloid Interface Sci*. **1980**, *75*, 620.

(21) Kralchevsky, P. A.; Nikolov, A. D.; Ivanov, I. B. *J. Colloid Interface Sci*. **1986**, *112*, 132.

(22) Gaydos, J.; Neumann, A. W. *J. Colloid Interface Sci*. **1987**, *120*, 76.

(23) Li, D.; Neumann, A. W. *Colloids Surf*. **1990**, *43*, 195.

(24) Drelich, J.; Miller, J. D.; Hupka, J. *J. Colloid Interface Sci*. **1993**, *155*, 379.

(25) Drelich, J.; Miller, J. D. *J. Colloid Interface Sci*. **1994**, *164*, 252.

(26) Duncan, D.; Li, D.; Gaydos, J.; Neumann, A. W. *J. Colloid Interface Sci*. **1995**, *169*, 256.

(27) Aveyard, R.; Clint, J. H. *J. Chem. Soc., Faraday Trans*. **1995**, *91*, 175.

(28) Gu, Y.; Li, D.; Cheng, P. *J. Colloid Interface Sci*. **1996**, *180*, 212.

(29) Chen, P.; Susnar, S. S.; Amirfazli, A.; Mak, C.; Neumann, A. W. *Langmuir* **1997**, *13*, 3035.

(30) Amirfazli, A.; Kwok, D.; Gaydos, J.; Neumann, A. W. *J. Colloid Interface Sci*. **1998**, *205*, 1.

(31) Seo, Y.; Paeng, K.; Park, S. *Macromolecules* **2001**, *34*, 8735.

(32) Niwa, M.; Hayashi, T.; Higashi, N. *Langmuir* **1990**, *6*, 263.

(33) Bijsterbosch, H. D.; de Haan, V. O.; de Graaf, A. W.; Mellema, M.; Leermakers, F. A. M.; Cohen Stuart, M. A.; van Well, A. A. *Langmuir* **1995**, *11*, 4467.

(34) Gonçalves da Silva, A. M.; Filipe, E. J. M.; d'Oliveira, J. M. R.; Martinho, J. M. G. *Langmuir* **1996**, *12*, 6547.

(35) Pagac, E. S.; Prieve, D. C.; Solomentsev, Y.; Tilton, R. D. *Langmuir* **1997**, *13*, 2993.

(36) Mortensen, K.; Brown, W.; Almdal, K.; Alami, E.; Jada, A. *Langmuir* **1997**, *13*, 3635.

(37) Dewhurst, P. F.; Lovell, M. R.; Richards, R. W.; Webster, J. R. P. *Macromolecules* **1998**, 31, 7851.

(38) Gragson, D. E.; Jensen, J. M.; Baker, S. M. *Langmuir* **1999**, *15*, 6127.

(39) Gonçalves da Silva, A. M.; Simões Gamboa, A. L.; Martinho, J. M. G. *Langmuir* **1998**, *14*, 5327.

(40) Fauré, M. C.; Bassereau, P.; Lee, L. T.; Menelle, A.; Lheveder, C. *Macromolecules* **1999**, *32*, 8538.

(41) Cox, J. K.; Yu, K.; Eisenberg, A.; Lennox, R. B. *Phys. Chem. Chem. Phys.* **1999**, *1*, 4417.

(42) Cox, J. K.; Yu, K.; Constantine, B.; Eisenberg, A.; Lennox, R. B. *Langmuir* **1999**, *15*, 7714.

(43) Devereaux, C. A.; Baker, S. M. *Macromolecules* **2002**, *35*, 1921.

(44) Rivillon, S.; Muñoz, M. G.; Monroy, F.; Ortega, F.; Rubio, R. G. *Macromolecules* **2003**, *36*, 4068.

(45) Shuler, R. L.; Zisman, W. A. *J. Phys. Chem.* **1970**, *74*, 1523.

(46) Kuzmenka, D. J.; Granick, S. *Macromolecules* **1988**, *21*, 779.

(47) Kumaki, J. *Macromolecules* **1988**, *21*, 749.

(48) Logan, J. L. *PhD Dissertation*; University of Florida: Gainesville, FL, **2005**.

(49) Francis, R.; Skolnik, A. M.; Carino, S. R.; Logan, J. L.; Underhill, R. S.;Angot, S.; Taton, D.; Gnanou, Y.; Duran, R. S. *Macromolecules* **2002**, *35*, 6483.

(50) Francis, R.; Taton, D.; Logan, J. L.; Masse, P.; Gnanou, Y.; Duran, R. S. *Macromolecules* **2003**, *36*, 8253.

(51) Logan, J. L.; Masse, P.; Dorvel, B.; Skolnik, A. M.; Sheiko, S. S.; Francis, R.; Taton, D.; Gnanou, Y.; Duran, R. S. *Langmuir* **2005**, *21*, 3424.

(52) Peleshanko, S.; Jeong, J.; Gunawidjaja, R.; Tsukruk, V. V. *Macromolecules* **2004**, *37*, 6511.

(53) Baines, F. L.; Billingham, N. C.; Armes, S. P. *Macromolecules* **1996**, *29*, 3416.

(54) Robinson, K. L.; Paz-Banez, V. P.; Wang, X. S.; Armes, S. P. *Macromolecules* **2001**, *34*, 5799.

(55) Cai, Y.; Burguière, C.; Armes S. P. *Chem. Commun.* **2004**, 802. (d) Liu, S.; Armes, S. P. *Angew. Chem., Int. Ed.* **2002**, *41*, 1413.

(56) Cameron, N. S.; Corbierre, M. K.; Eisenberg, A. *Can. J. Chem.* **1999**, *77*, 1311.

(57) Zhang, L.; Eisenberg, A. *J. Am. Chem. Soc.* **1996**, *118*, 3168.

(58) Zhang, L.; Shen, H.; Eisenberg, A. *Macromolecules* **1997**, *30*, 1001.

(59) Zhang, L.; Eisenberg, A. *Polym. Adv. Technol*. **1998**, *9*, 677.

(60) Wooley, K. L. *J. Polym. Sci., Part A: Polym. Chem.* **2000**, *38*, 1397.

(61) Ma, Y.; Cao, T.; Webber, S. E. *Macromolecules* **1998**, *31*, 1773.

(62) Ning, F.; Jiang, M.; Mu, M.; Duan, H.; Xie, J. *J. Polym. Sci., Part A: Polym. Chem.* **2002**, *40*, 1253.

(63) Voulgaris, D.; Tsitsilianis, C. *Macromol. Chem. Phys.* **2001**, *202*, 3284.

(64) Burguière, C.; Pascual, S.; Bui, C.; Vairon, J.-P.; Charleux, B.; Davis, K. A.; Matyjaszewski, K.; Bétremieux, I. *Macromolecules* **2001**, *34*, 4439.

(65) Teng, J.; Zubarev, E. R. *J. Am. Chem. Soc.* **2003**, *125*, 11840.

(66) Francis, R.; Lepoittevin, B.; Taton, D.; Gnanou, Y. *Macromolecules* **2002**, *35*, 9001.

(67) Joncheray, T. J.; Bernard, S. A.; Matmour, R.; Lepoittevin, B.; El-Khouri, R. J.; Taton, D.; Gnanou, Y.; Duran, R. S. *Langmuir* **2007,** ASAP Article.

(68) Matmour, R.; Lepoittevin, B.; Joncheray, T. J.; El-khouri, R. J.; Taton, D.; Duran, R. S.; Gnanou, Y. *Macromolecules* **2005**, *38*, 5459.

(69) Zhu, Y. B.; Gao, C. Y.; Liu, X. Y.; Shen, J. C. *Biomacromolecules* **2002**, *3*, 1312.

(70) Kweon, H. Y.; Yoo, M. K.; KyuPark, In; Kim, T. H.; Lee, H. C.; Lee, H. S.; Oh, J. S.; Akaike, T.; Cho, C. S. *Biomaterials* **2003**, *24*,801.

(71) Soo, P. L.; Luo, L. B.; Maysinger, D.; Eisenberg, A. *Langmuir* **2002**, *18*, 9996.

(72) Leiva, A.; Gargallo, L.; Radic, D. *J. Macromol. Sci., Part A: Pure Appl. Chem* **2004**, *41*, 577.

(73) Li, B.; Wu, Y.; Liu, M.; Esker, A. R. *Langmuir* **2006**, *22*, 4902.

(74) Baglioni, P.; Dei, L.; Gabrielli, G. *Colloid & Polymer Sci.***1986**, *264*, 241.

(75) Gabrielli, G.; Puggelli, M.; Gilarddoni, A. *Prog. Colloid Polym. Sci.* **1992**, *89*, 227.

(76) Baglioni, P.; Dei, L.; Ferroni, E.; Gabrielli, G. *Colloids Surf.* **1991**, *60*, 399.

(77) Puggelli, M.; Gabrielli, G.; Domini, C. *Prog. Colloid Polym. Sci.* **1989**, *79*, 52.

(78) Puggelli, M.; Gabrielli, G.; Domini, C. *Colloid Polym. Sci.* **1989**, *267*, 65.

(79) Gabrielli, G.; Puggelli, M.; Dei, L.; Domini, C. *Colloid Polym. Sci.* **1988**, *266*, 429.

(80) Puggelli, M.; Gabrielli, G. *Colloid Polym. Sci.* **1987**, *265*, 432.

(81) Caminati, G.; Gabrielli, G.; Puggelli, M.; Ferroni, E. *Colloid & Polymer Sci.* **1989**, *267*, 237.

(82) Thibodeaux, A. F.; Rädler, U.; Shashidhar, R.; Duran, R. S. *Macromolecules* **1994**, *27*, 784.

(83) Malzert, A.; Boury, F.; Saulnier, P.; Benoît, J. P.; Proust, J. E. *Langmuir* **2001**, *17*, 7837.

(84) Malzert, A.; Boury, F.; Saulnier, P.; Ivanova, Tz.; Panaïotov, I.; Benoît, J. P.; Proust, J. E. *J. Colloid Interface Sci.* **2003**, *259*, 398.

(85) Ivanova, Tz.; Saulnier, P.; Malzert, A.; Boury, F.; Proust, J. E.; Panaiotov, I. *Colloids and Surfaces, B: Biointerfaces* **2002**, *23*, 7.

(86) Hottle, J. R.; Kim, H.; Deng, J.; Farmer-Creely, C. E.; Viers, B. D.; Esker *Macromolecules* **2004**, *37*, 4900.

(87) Seo, Y.; Kim, K. S.; Galambos, A.; Lammertink, R. G. H. ; Vansco, G. J.; Sokolov, J.; Rafailovich, M. *Nano Lett.* **2004**, *4*, 483.

(88) Mayes, M.; Russell, T. P.; Satija, S. K.; Majkrzak, C. F. *Macromolecules* **1992**, *25*, 6523.

(89) Mayes, M.; Russell, T. P.; Deline, V. R.; Satija, S. K.; Majkrzak, C. F. *Macromolecules* **1994**, *27*, 7447.

(90) Smith, D.; Green, P. F.; Saunders, R. *Macromolecules* **1999**, *32*, 8392.

(91) Jeong, D.; Ryu, Y.; Kho, D. H.; Lee, D. H.; Kim, J. K.; Russell, T. P. *Macromolecules* **2003**, *36*, 3626.

(92) Jeong, D.; Ryu, Y.; Kim, J. K.; Kim, D. H.; Wu, X.; Russell, T. P. *Macromolecules* **2003**, *36*, 10126.

(93) Jeong, D.; Kim, H. C.; Rodriguez, R. L.; Tsai, I. Y.; Stafford, C. M.; Kim, J. K.; Hawker, C. J.; Russell, T. P. *Adv. Mater.* **2002**, *14*, 274.

(94) Jeong, D.; Ryu, Y.; Kho, D. H.; Kim, J. K.; Goldbach, J. T.; Kim, D. H.; Russell, T. P. *Adv. Mater.* **2004**, *16*, 533.

(95) Knoll, A.; Magerle, R.; Krausch, G. *Macromolecules* **2001**, *34*, 4159.

(96) Bodiguel, H.; Montes, H.; Fretigny, C. *Rev. Sci. Instrum.* **2004**, *75*, 2529.

(97) (a) Garcia, R.; Gómez, C. J.; Martinez, N. F.; Patil, S.; Dietz, C.; Magerle, R. *Phys. Rev. Lett.* **2006**, *97*, 16102. ; (b) Martinez, N. F.; Garcia, R. *Nanotechnology* **2006**, *17*, 167.

(98) Dorvel, B. R.; Keizer, H. M.; Fine, D.; Vuorinen, J.; Dodabalapur, A.; Duran, R. S. *Langmuir* **2007**, *23*, 7344.

(99) Langmuir, I. *J. Am. Chem. Soc.* **1917**, *39*, 1848.

(100) Langmuir, Irving; Blodgett, Katherine B. *Kolloid-Zeitschrift* **1935**, *73*, 258.

(101) Sheiko, S.S. *Advances in Polymer Science* **2000**, *151*, 61.

(102) Glass, J. E. *J. Phys. Chem.* **1968**, *72*, 4459.

(103) Digital Instruments *Nanoscope III Multimode Scanning Probe Microscope Instruction Manual*.: Santa Barbara, CA, **2000**.

(104) Sauer, B. B.; Yu, H. *Macromolecules* **1989**, *22*, 786.

(105) Potemkin, I. I.; Kramarenko, E. Y.; Khokhlov, A. R.; Winkler, R. G.; Reineker, P.; Eibeck, P.; Spatz, J. P.; Möller, M. *Langmuir* **1999**, *15*, 7290.

(106) Liu, Y.; Gong, A.; Liu, M.; Xi, F. *New J. Chem.* **2001**, *25*, 970.

(107) Nobes, G. A. R.; Holden, D. A.; Marchessault, R. H. *Polymer* **1994**, *35*, 435.

(108) Mengel, C.; Esker, A. R.; Meyer, W. H.; Wegner, G. *Langmuir* **2002,** *18*, 6365.

(109) Sutherland, J. E.; Miller, M. L. *Journal of Polymer Science, Polymer Letters Edition* **1969,** *7*, 871.

(110) Gabrielli, G.; Guarini, G. G. T. *Journal of Colloid and Interface Science* **1978,** *64*, 185.

(111) Li, S.; Clarke, C. J.; Eisenberg, A.; Lennox, R. B. *Thin Solid Films* **1999,** *354*, 136.

(112) Kim, Y. H.; Ford, W. T. *Polymer Preprints (American Chemical Society, Division of Polymer Chemistry)* **2005,** *46*, 169.

(113) Mudgil, P.; Dennis, G. R.; Millar, T. J. *Langmuir* **2006**, 7672.

(114) Gan, Z.; Jim, T. F.; Li, M.; Yuer, Z.; Wang, S.; Wu, C. *Macromolecules* **1999**, *32*, 590-594.

(115) Crisci, L.; Della Volpe, C.; Maglio, G.; Nese, G.; Palumbo, R.; Rachiero, G. P.; Vignola, M. C. *Macromol. Biosci.* **2003**, *3*, 749.

(116) Choi, Y. K.; Bae, Y. H.; Kim, S. W. *Macromolecules* **1998**, *31*, 8766.

(117) Deng, M.; Chen, X.; Piao, L.; Zhang, X.; Dai, Z.; Jing, X. *J. Polym. Sci., Part A: Polym. Chem.* **2004**, *42*, 950.

(118) Allen, C.; Han, J.; Yu, Y.; Maysinger, D.; Eisenberg, A. *J. Controlled Release* **2000**, *63*, 275.

(119) Storck, M.; Orend, K. H.; Schmitzrixen, T. *J. Vasc. Surg.* **1993**, *27*, 413.

(120) I.W. Hamley, The Physics of Block Copolymers, Oxford, New York (1998) [chapter 5].

(121) Ryan, A. J.; Fairclough, J. P. A.; Hamley, I. W.; Mai, S. M.; Booth, C. *Macromolecules* **1997**, *30*, 1723.

(122) Ryan, A.J.; Hamley, I.W.; Bras, W.; Bates, F.S. *Macromolecules* **1995**, *28*, 3860.

(123) Quiram, D.J.; Register, R.A.; Marchand, G.R. *Macromolecules* **1997**, *30*, 4551.

(124) Quiram, D.J.;Register, R.A.; Marchand, G.R.; Ryan, A.J. *Macromolecules* **1997**, *30*, 8338.

(125) Hamley, I.W.; Fairclough, J.P.A.; Terrill, N.J.; Ryan, A.J.; Lipic, P.M., Bates, F.S. *Macromolecules* **1996**, *29*, 8835.

(126) Nojima, S.; Kato, K.; Yamamoto, S.; Ashida, T. *Macromolecules* **1992**, *25*, 2237.

(127) Sakurai, K.; MacKnight, W.J.; Lohse, D.J.; Schulz, N.; Sissano, J.A. *Macromolecules* **1994**, *27*, 4941.

(128) Liu, L.Z.; Yeh, R.; Chu, B. *Macromolecules* **1996**, *29*, 5336.

(129) Rangarajan, P.; Register, R.A.; Fetters, L.J.; Bras, W.; Naylor, S.; Ryan, A.J. *Macromolecules* **1995**, *28*, 4932.

(130) Nojima, S.; Hashizume, K.; Rohadi, A.; Sasaki, S. *Polymer* **1997**, *38*, 2711.

(131) Chen, H.L.; Wu, J.C.; Lin, T.L.; Lin, J.S. *Macromolecules* **2001**, *34*, 6936.

(132) Shiomi, T.; Tsukada, H.; Takeshita, H.; Takenaka, K.; Tezuka, Y. *Polymer* **2001**, *42*, 5004.

(133) Shiomi, T.; Takeshita, H.; Kawaguchi, H.; Nagai, M.; Takenaka, K.; Miya, M. *Macromolecules* **2002**, *35*, 8056.

(134) Huang, P.; Zhu, L.; Guo, Y.; Ge, Q.; Jing, A.J.; Chen, W.Y. *Macromolecules* **2004**, *37*, 3689.

(135) Zhu, L.; Cheng, S.Z.D.; Calhoun, B.H.; Ge, Q.; Quirk, R.P.; Thomas, E.L. *J Am Chem Soc* **2000**, *122*, 5957.

(136) Takeshita, H.; Ishii, N.; Araki, C.; Miya, M.; Takenaka, K.; Shiomi, T.J. *J Polym Sci B* **2004**, *42*, 4199.

(137) Li, B.; Esker, A. R. *Langmuir* **2007**, *23*, 574.

(138) Li, B.; Esker, A. R. *Langmuir* **2007**, *23*, 2546.

(139) (a) Joncheray, T. J. *PhD Dissertation*; University of Florida: Gainesville, FL, **2006**. (b) Joncheray, T. J.; Bernard, S. A.; Matmour, R.; Lepoittevin, B.; El-Khouri, R. J.; Taton, D.; Gnanou, Y.; Duran, R. S. *Langmuir* **2007**; *23*; 2531.

(140) Ivanova, A.; Tadjer, A.; Radoev, B. *Int. J. Quantum. Chem.* **2002**, *89*, 397-404..

(141) Zeng, H.; Maeda, N.; Chen, N.; Tirell, M.; Israelachvili, J. *Macromolecules*, **2006**, *39*, 2350.

(142) Bliznyuk, V. N.; Assender, H. E.; Briggs, G. A. D. *Macromolecules*, **2002**, *35*, 6613.

BIOGRAPHICAL SKETCH

Sophie Bernard was born on February 25, 1979, in Bordeaux, France. She graduated from the University of Bordeaux in June 2001 with her B.S. degree in physical chemistry. She then worked as a research assistant under the direction of Dr. Yves Gnanou, in the Laboratoire de Chimie des Polymères Organiques, University of Bordeaux. She received her M.S. degree in physical chemistry of polymers from the University of Bordeaux in July 2002.

Since Sophie enrolled at the University of Florida in September 2002, she has been a graduate student under the direction of Dr. Randolph S. Duran.